Cristina Maria Bernardes Monteiro

Determination of argon and xenon absolute electroluminescence yields in Gas Proportional Scintillation Counters

University of Coimbra

2010

Cristina Maria Bernardes Monteiro

Determination of argon and xenon absolute electroluminescence yields in Gas Proportional Scintillation Counters

Dissertation submitted to
Faculdade de Ciências e Tecnologia da Universidade de Coimbra
for the degree of *Phylosophiae Doctor* in Technological Physics

Under the supervision of Prof. Dr. João Filipe Calapez de Albuquerque Veloso
and co-supervision of Prof. Dr. Carlos Manuel Bolota Alexandre Correia

University of Coimbra

2010

This work was supported by *Fundação para a Ciência e Tecnologia* and by the European Social Fund, through *Programa Operacional Potencial Humano (POHP)*, through the grant SFRH/BD/25569/2005.

To Cristiana

to Quim

To my parents

Acknowledgements

To Professor João Filipe Calapez de Albuquerque Veloso for the supervision of the present work and for all the support, suggestions and fruitful discussions along the years.

To Professor Carlos Manuel Bolota Alexandre Correia for having accepted the co-supervision of the present work and for all the encouragement provided.

To Professor Joaquim Marques Ferreira dos Santos for all the support, suggestions and fruitful discussions.

To Hugo Natal da Luz and Carlos Oliveira for the help in data taking and processing with the CAEN™ 1728b module and Radix program.

To Paulo Gomes for all the informatics support throughout the years.

To Fernando Amaro, who always seems to be there when we need a helping hand and, last but not least, for the friendship.

To Elisabete Freitas (Beta) for the long years of friendship.

To all my colleagues in the Lab, for all the support, collaboration and for the pleasant time we spent working together.

To all of those who, in any possible way, contributed to the fulfillment of this work.

To my parents, who always supported all my decisions ever since I was very young and for their unconditional love.

To Cristiana and Quim for the love and happiness they bring into my life.

List of Abbreviations

API	Advanced Photonix Inc.
ArDM	Argon Dark Matter
CI	Centro de Instrumentação
E/P	Reduced electric field, i.e. electric field divided by the pressure
EL	ElectroLuminescence
EXO	Enriched Xenon Observatory
FWHM	Full-width-at-half-maximum
G	Gain
G-APD	Geiger Avalanche PhotoDiode
GEM	Gas Electron Multiplier
GIAN	Grupo de Instrumentação Atómica e Nuclear
GLACIER	Giant Liquid Argon Charge Imaging ExpeRiment
GPM	Gas PhotoMultiplier
GPSC	Gas Proportional Scintillation Counter
ICARUS	Imaging Cosmic And Rare Underground Signals
LAAPD	Large Area Avalanche Photodiode
LEM	Large Electron Multiplier
LUX	Large Underground Xenon dark matter experiment
MDP	Minimum Detectable number of Photons
MICROMEGAS	MICROMEsh GAseous Structure
NEXT	Neutrino Experiment with a Xenon TPC
PC	Proportional Counter
PMT	PhotoMultiplier Tube
QE	Quantum Efficiency
RMD	Radiation Monitoring Devices Inc.
THGEM	THick Gas Electron Multiplier
TPC	Time Projection Chamber
VUV	Vacuum Ultra Violet
WIMP	Weak Interactive Massive Particle
XENON	XENON Dark Matter Experiment
ZEPLIN	ZonEd Proportional scintillation in LIquid Noble gases

TABLE OF CONTENTS

Determination of argon and xenon absolute electroluminescence yield in Gas Proportional Scintillation Counters

Cristina Maria Bernardes Monteiro

Physics Department

Faculty of Sciences and Technology - University of Coimbra

Abstract

Electroluminescence (EL), as the signal amplification method of primary ionisation signal, developed in the 70's in Gas Proportional Scintillation Counters (GPSC) with noble gas filling, has played an important role in applications to many fields such as X-ray astronomy, plasma physics, medical instrumentation and high-energy physics, up to rising of solid state detectors in the mid 90's. However, in the last decade EL amplification recovered importance in experiments for rare event detection, such as direct dark matter search and double beta decay. Low count rates and high background imply the need for high signal amplification with statistical fluctuations as low as possible.

EL studies are needed for correct detector simulation. While for xenon the literature reported several studies on absolute measurements of EL yield, both experimental and from simulation, yet with disperse results, for argon only one experimental result was reported and its results were ten times lower than the Monte Carlo values from studies performed in our group. The lack of coherent results raised the necessity to study the absolute EL yield in the noble gases xenon and argon thoroughly.

In the present work, absolute measurements have been performed for the EL yields of xenon and argon in a uniform electric field GPSC. The obtained results agree with those from Monte Carlo simulation, at room temperature, and with the most recent experimental results measured at cryogenic temperatures reported in the literature, for xenon. We have demonstrated, for the first time that the EL yield, at room temperature, is as high as predicted by the Monte Carlo simulation.

Furthermore, studies were performed on the absolute EL yield produced in the strong, variable electric fields of the electron avalanches produced in GEMs and THGEMs. The obtained results have shown that the EL yield values can be more than two orders of magnitude higher than those reached in the commonly used uniform field gaps. This fact can be important if photosensors others than PMTs, with less sensitivity and with area occupancy lower than 100%, are used because of less mass burden and lower radioactivity rates, such as APDs and G-APDs.

For the above mentioned studies a simple, straightforward method was used for absolute EL yield measurements, using LAAPDs simultaneously irradiated with EL pulses and X-rays. These X-rays are used as a reference for the absolute determination of the charge carriers produced in the LAAPD by the EL pulses. This technique has been successfully applied, during the last decade, for absolute measurements of primary scintillation yield from organic and inorganic crystals, being suitable for the measurements on EL carried out under the scope of this thesis.

Determinação do rendimento absoluto de electroluminescência para argon e o xenon em Contadores Gasosos de Cintilação Proportional

Cristina Maria Bernardes Monteiro

Departamento de Física

Faculdade de Ciências e Tecnologia da Universidade de Coimbra

Resumo

A electroluminescência (EL) em Contadores Gasosos de Cintilação Proporcional (CGCP) com enchimento a gases nobres foi desenvolvida na década de 70 como método de amplificação da ionização primária e desempenhou um papel relevante em aplicações a áreas tão diversas como a astronomia, a física dos plasmas, a instrumentação médica e a física das altas energias. Este protagonismo perdurou até meados da década de 90, época em que surgiram os detectores de estado sólido com qualidade e áreas de detecção melhoradas. A EL reconquistou interesse durante a última década em experiências dedicadas à detecção de eventos raros, como é o caso da procura da matéria negra e do decaimento beta duplo. As baixas taxas de contagem aliadas ao elevado nível de radiação de fundo, característicos destas experiências, definem a necessidade de uma grande amplificação do sinal, associada a baixas flutuações estatísticas, características intrínsecas à amplificação por EL.

A correcta simulação de detectores obriga a estudos de EL mais profundos. Na literatura são referidos diversos estudos, tanto experimentais como de simulação, de medições absolutas para o rendimento de EL em xénon, sendo que os resultados apresentavam

valores díspares. Para o árgon foi encontrado na literatura um único estudo experimental, cujos valores eram cerca de dez vezes inferiores aos de simulações de Monte Carlo efectuados no nosso grupo. A falta de resultados coerentes suscitou a necessidade de estudar o rendimento absoluto de EL nos gases nobres xénon e árgon.

No presente trabalho foram efectuadas medições absolutas para o rendimento de EL em xénon e árgon num CGCP de campo eléctrico uniforme. Os resultados obtidos estão em concordância, tanto com os de simulação de Monte Carlo para a temperatura ambiente como, para o xénon, com os resultados experimentais efectuados a temperaturas criogénicas mencionados na literatura. Mostrou-se, pela primeira vez, que o rendimento de EL à temperatura ambiente é tão elevado como o previsto por simulação de Monte Carlo.

Foram igualmente efectuados estudos para o rendimento da EL produzida nos campos eléctricos elevados e variáveis das avalanches de electrões produzidas em GEMs e THGEMs. Os resultados obtidos mostram que estes valores podem ser mais do que duas ordens de grandeza superiores aos obtidos na configuração de campo uniforme. Este facto pode ser importante quando forem utilizados fotosensores que não os PMTs, tais como os APDs ou G-APDs, com menor sensibilidade e/ou uma cobertura em termos de área inferior a 100%, mas que têm níveis de radioactividade menores.

Os estudos acima mencionados foram efectuados utilizando um método simples e directo para a medição do rendimento absoluto de EL, com recurso a LAAPDs irradiados em simultâneo com impulsos de EL e raios X. Estes últimos são utilizados como referência para a determinação absoluta dos portadores de carga produzidos no LAAPD pelos impulsos de EL.

CHAPTER 1

Introduction

The Atomic and Nuclear Instrumentation Group (GIAN) of the Instrumentation Centre (CI) has devoted several decades to the study of the production of electroluminescence (EL) as the signal amplification method in Gas Proportional Scintillation Counters (GPSC) with noble gas filling. This group reached vast experience in this research field, experimentally as well as in simulation using the Monte Carlo method, being the main studies performed with xenon and argon.

Electroluminescence, also known as secondary scintillation, has played an important role in the late 80's and begin 90's in Gas Proportional Scintillation Counters, in applications to many fields such as X-ray astronomy, plasma physics, medical instrumentation and

high-energy physics [c]. However, during the 90's, electroluminescence as well as Gas Proportional Scintillation Counters were thrust aside due to the emergence of solid state detectors, which quality improved increasingly.

At the end of the 90's and during the past decade, noble gas detectors based on electroluminescence production recovered significance, becoming even one of the first-line methods applied to direct dark matter search and neutrino detection experiments. Part of these experiments use xenon or argon as the preferred detection media in their double-phase – noble liquid /noble gas – detectors. Recently, xenon became also the gas of choice of two different large experiments aiming the detection of neutrinoless double beta decay and, again, the use of the electroluminescence process as the amplification method for the initial ionisation signal, with negligible statistical fluctuations, was a decisive key for that choice.

For xenon, the literature reported several studies on absolute measurements of the electroluminescence yield, both experimental and from simulation, that presented disperse results. For argon, only one experimental result was reported in the literature and its results were ten times lower than the Monte Carlo values from studies performed in GIAN. The lack of coherent results raised the necessity to study thoroughly the electroluminescence yield in the noble gases xenon and argon, of capital importance for detector simulation, especially in experiments where huge and, consequently, very expensive detector systems are needed.

In addition, those direct dark matter search and neutrino experiments that use or wish to use electroluminescence began to search for photosensors that could be an alternative to the traditionally used Photomultiplier Tubes (PMT), in view of their need to diminish the radioactive background as much as possible, because of the very low event rate inherent to these experiments. Since a possible solution meeting that requirement is photodiodes, their very low gains – up to few hundred compared to PMTs which values are typically of the order of 10^5, 10^6 – imply a much higher electroluminescence signal for proper detection. Avalanche-producing microstructures, like GEMs and THGEMs, present a very high charge gain and began to be considered as an option to incorporate the double-phase detectors. For that reason, it became appealing to study the electroluminescence production in those structures. On the other hand, photodiodes have been used to determine the (primary) scintillation yield of organic and inorganic scintillators, by using the direct X-ray interaction in the photodiode as reference for measuring the number of charge carriers produced in the photodiode. This method can be applied to the electroluminescence yield produced in noble gases.

The above studies were performed under the scope of this PhD project and are reported in the present thesis.

Chapter 2 aims to introduce the subject and to put the work into context among the ongoing international research. A brief summary on electroluminescence, on contemporary detectors based on

electroluminescence amplification and on Large Area Avalanche Photodiodes (LAAPD) for scintillation readout is presented in this chapter.

Chapter 3 presents the studies on electroluminescence performed for xenon at 1 bar in a uniform field configuration, using a Gas Proportional Scintillation Counter without drift region, equipped with a Large Area Avalanche Photodiode as the photosensor. With the LAAPD, a simple and straightforward method was used to obtain absolute measurements for the electroluminescence yield, making use of the ratio between the secondary scintillation peak in the GPSC and the peak from direct interaction of the X-rays in the LAAPD.

Similar studies to those reported in the former chapter, using the same method, are presented in **Chapter 4**, but for argon at 1 bar and, this time, using a parallel mesh Gas Proportional Scintillation Counter, also with an LAAPD as the photosensor. In addition, simulation studies were performed on the amount of scintillation produced around the wires of the mesh, for different electric field values, to evaluate its possible contribution to the total amount of measured electroluminescence.

The research performed on electroluminescence production with GEMs and THGEMs operating in pure xenon and pure argon for

pressures ranging from 1 up to 2.5 bar is described in **Chapter 5**. Results are presented for total gain, electroluminescence yield and energy resolution achieved in X-ray detection. Digital pulse processing was also applied to correlated pulse-height distributions, both from charge and from electroluminescence, to evaluate the possibility of improving the charge signals in terms of energy resolution and noise reduction.

In **Chapter 6** studies are presented on the characterisation of the response of the LAAPDs used throughout the work described in chapters 3, 4 and 6, in terms of the minimum detectable number of photons and the overall statistical fluctuations associated to photon detection. These studies complement former studies on characterization of these photodiodes for VUV detection, which had been done in GIAN throughout the past ten years.

Finally, **Chapter 7** summarizes the main conclusions of the results obtained in the previous chapters and presents an outlook of future work that will be performed or is already being carried out in the sequence of the studies presented in this thesis.

The studies performed in the scope of this thesis were carried out in the Atomic and Nuclear Instrumentation Group (GIAN) of the

Instrumentation Centre (CI) of the *Faculdade de Ciências e Tecnologia da Universidade de Coimbra*.

The studies described in this thesis resulted, thus far, in the following publications.

Publications in International Journals with refereeing

1. *Secondary scintillation yield from gaseous micropattern electron multipliers in direct Dark Matter detection*, C. M. B. Monteiro, A. S. Conceição, F. D. Amaro, J. M. Maia, A. C. S. S. M. Bento, L. F. R Ferreira, J. F. C. A. Veloso, J. M. F. dos Santos, A. Breskin, R. Chechik, ***Physics Letters B*** 677 (2009) 133-138.

2. *Secondary scintillation yield in pure argon*, C. M. B. Monteiro, J. A. M. Lopes, J. F. C. A. Veloso, J. M. F. dos Santos, ***Physics Letters B*** 668 (2008) 167-170.

3. *Secondary scintillation yield in pure xenon*, C. M. B. Monteiro, L. M. P. Fernandes, J. A. M. Lopes, L. C. C. Coelho, J. F. C. A. Veloso, J. M. F. dos Santos, K. Giboni, E. Aprile, ***Journal of Instrumentation*** 2 P05001 (2007).

4. *Detection of VUV photons with large-area avalanche photodiodes*, C.M.B. Monteiro, L.M.P. Fernandes, J.A.M. Lopes, J.F.C.A. Veloso, J.M.F. dos Santos, ***Applied Physics B-Lasers and Optics*** 81 (2005) 531-535.

CHAPTER 2

Gas Detectors and Noble Gas Electroluminescence

2. Electroluminescence in gaseous detectors

Electroluminescence has been used for the first time in the late 60's by the pioneering scientists Armando Policarpo and Carlos Conde [1,2]. Initially, detectors based on this signal amplification technique were interesting to be applied to the fields that were in progress in those days, namely X-ray spectrometry for astrophysics instrumentation, and were called Gas Proportional Scintillation Counters (GPSC) or Gas

Scintillation Proportional Counters (GSPC). Their detection media were noble gases, essentially xenon and argon and they reached their high point in the late 80's, begin 90's, being the most visible application X-ray astrophysics instrumentation, for instance to fly in balloons and satellites. At that time, the growing importance of solid state detectors, due to the considerable improvement in their manufacturing techniques, rendered the GPSC progressively outmoded to the level that, in the late 90's, our research group was one of the few in the world still working with GPSCs and using electroluminescence as the detector's signal amplification technique.

However, electroluminescence began to regain importance in the last decade with the appearance and rising importance of experiments dedicated to direct Dark Matter search, where several different techniques have been implemented and tried out in their detectors. Those reach from cryogenic detectors operating at temperatures below 100 mK such as CDMS [3], CRESST [4], EDELWEISS [5] and EURECA [6], to noble liquid detectors such as ZEPLIN, XENON, ArDM, WARP, LUX, DEAP and CLEAN, using liquid xenon at a temperature of 170 K, liquid argon at a temperature of 87 K or liquid neon at a temperature of 27 K as the detection media. From those, ArDM detects the ionisation charge signal with Large Electron Multipliers (LEMs), while ZEPLIN, XENON, WARP and LUX elected electroluminescence as the technique for the amplification of the primary ionisation in their next-generation double-phase detectors, detecting the corresponding scintillation signal with Photomultiplier Tubes (PMTs).

Recent data have shown that, among these detectors, XENON presents the highest sensitivity to WIMP detection [7,8].

Recently, the electroluminescence in xenon was also chosen as the signal amplification technique to be applied in xenon TPCs in international collaborations for the detection of neutrinoless double beta decay, namely EXO-gas and NEXT [9,10].

2.1. Electroluminescence as signal amplification technique

Electroluminescence is a process where thermalised electrons are accelerated in an external electric field, to produce secondary scintillation photons as a result of electron impact with the gas atoms and subsequent de-excitation, in opposition to the primary scintillation, which is produced by high energetic electrons generated in the interaction of ionising radiation with the gas medium.

In EL based detectors, the incoming radiation interacts preferably in a region of low intensity electric field, below the gas scintillation threshold. The primary electrons formed in the sequence of that interaction are guided, under the influence of that electric field, towards the scintillation region. In this latter, the electric field intensity is high and the primary electrons gain energy from the electric field to excite the gas atoms, which de-excite emitting secondary scintillation or EL

photons. These photons are collected with an adequate photosensor, like the PMT or the LAAPD, which produce a signal that is proportional to the detected number of electroluminescence photons.

The signal amplification technique based on electroluminescence can be used to considerable benefit over charge multiplication of primary electrons, the technique inherent to Proportional Counters (PC), not only because of the higher amplification gain, but also because the statistical fluctuations associated to the electroluminescence processes are much lower than those associated to the electron cloud formation, resulting in superior energy resolution. Consequently, if the electric field in the scintillation region is kept below the gas ionisation threshold, the electroluminescence based detectors present energy resolutions that are close to their intrinsic values [11].

Usually, molecular gases are avoided because of the high energy losses due to the presence of rotational and vibrational states, which absorb the electron energy in inelastic collisions before gas excitation can take place. This explains the use of pure noble gases and their mixtures as the first choice for electroluminescence detectors.

2.2. Electroluminescence in Noble Gases

The mechanism of light production in noble gases and their mixtures have been extensively described by various authors [12-19].

Under the intense electric field of the scintillation region, either in uniform fields with values below the ionisation threshold, or in the very intense and variable fields typical of electron avalanches, electrons gain from the field energy to excite the gas atoms by electron impact. Through inelastic collisions the atoms are brought to the first four excited atomic states $^3P_2$, $^3P_1$, $^3P_0$, $^1P_1$. The atomic states $^3P_2$ and $^3P_0$ are metastable with a long half life of about 100 μs, while the other two are resonant, decaying radiatively to the ground state. However, for pressures close to the atmospheric pressure the resonant states present a long half life, similar to that of the metastable states, due to high absorption and reemission of the resonant atomic radiation. This is the reason for the atomic emission of noble gases to be only observed at very low pressures, below 20 mbar.

For pressures above few tens of mbar, atomic emission is progressively replaced by molecular emission. Collisions of the excited atoms with atoms in the ground state, in a three-body collision process, lead to the formation of excited dimer states, $^3\Sigma_u$ and $^1\Sigma_u$. These states have very close energies but their lifetimes are a lot different, namely 4.2 and 3200 ns, respectively, for argon, and 6 and 110 ns, respectively, for xenon. The de-excitation of these molecular states give rise to two continua. The first continuum occurs from the de-excitation of $^3\Sigma_u$ and $^1\Sigma_u$ in high vibrational levels, $(^3\Sigma_u)^v$ and $(^1\Sigma_u)^v$, to the repulsive ground state, $^1\Sigma_g^+$. The second continuum is observed for the de-excitation of $^3\Sigma_u$ and $^1\Sigma_u$ in the lowest vibrational level, $(^3\Sigma_u)^{v=0}$ and $(^1\Sigma_u)^{v=0}$, to the ground state.

At pressures of a few hundred mbar, only the second continuum is visible. This is due to the relaxation of the excited vibrational states to the lowest vibrational state by collision with the atoms of the gas, before de-excitation. Therefore, at atmospheric pressure, the electroluminescence emission of argon and xenon correspond only to their second continua, a narrow peak of about 10 nm around 128 nm for argon and of about 14 nm around 172 nm for xenon.

The processes leading to emission in the second continuum occur through three-body collisions and can be schematized by

$$X^* + 2X \rightarrow X_2^* + X,$$

$$X_2^* \rightarrow 2X + h\upsilon.$$

One excited atom creates an excited excimer, X_2^*, which decays emitting one VUV photon, hυ.

An important aspect in electroluminescence production is related to the high number of elastic collisions that electrons undergo between two successive inelastic collisions, which are around 10^4 for electric fields around the gas ionisation threshold, and less than 10^4 in electron avalanches [20, 21]. This fact shows the crucial importance of gas purity. If there is a significant probability of collision with a molecular impurity before the electron reaches enough energy to excite the noble gas atom, it may lose its energy through the excitation of rotational and/or vibrational states of the impurity, without the occurrence of radiative emission, reducing this way the electroluminescence yield.

Xenon and argon present high excitation efficiencies, which reach values around 90% [21] and are due to the lack of rotational and vibrational energy-loss mechanisms. Electrons lose energy only by elastic collisions with the gas atoms. These losses are small due to the very small electron/atom mass ratio; however, the total amount of energy lost by the electrons is not negligible, even though small, because of the very high number of elastic collisions undergone by the electrons before they gain enough energy from the electric field to excite the gas atoms [21].

Similarly, the scintillation efficiency for xenon and argon is also high. The energy loss due to relaxation of the vibrationally excited dimers is a small fraction of the energy that electrons acquire from the electric field, and the overall scintillation efficiency reaches values of 80% for reduced electric fields of 4 kV cm^{-1} bar^{-1} [21,22].

As referred above, gas purification techniques are needed, because the amount of secondary scintillation produced is strongly dependent on the gas purity. A closed system is required with the inclusion of purifying elements, like getters, being this the most suitable for electroluminescence detectors.

2.3. The Gas Proportional Scintillation Counter

The Gas Proportional Scintillation Counter [1,2], is a radiation detector based on the production of electroluminescence photons from a

pure, noble gas and their mixtures, operating around or above atmospheric pressure. The electroluminescence process distinguishes the GPSC from both scintillators and Proportional Counters (PC). While the scintillators' operating principle is based on the collection of the primary scintillation following the radiation interaction inside the scintillator's gaseous, liquid or solid material, in the case of the PC it is the secondary electrons from primary charge multiplication in the filling gas that are collected, i.e. the secondary ionisation.

Commonly, a GPSC consists of three distinct parts, namely a chamber divided in two regions, the drift- or absorption region and the scintillation region, in addition to a suitable photosensor.

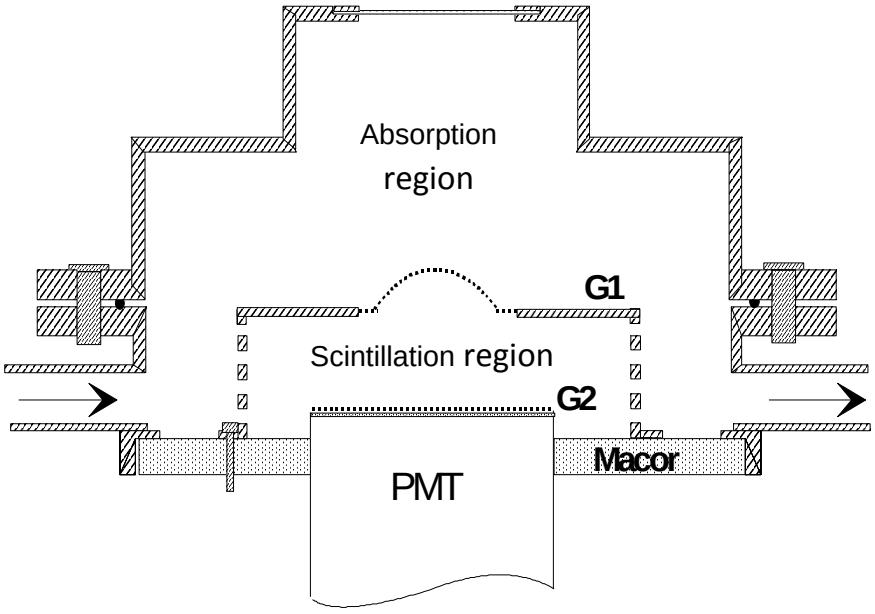

Figure 2.1 – Schematic of a Gas Proportional Scintillation Counter equipped with a Photomultiplier Tube.

The incident radiation is absorbed preferably in the drift region and the ionisation of the noble gas produces a primary electron cloud. The

weak electric field applied to the drift region, below the noble gas scintillation threshold, guarantees the absence of electroluminescence, whilst it is strong enough to minimise recombination and, hence, the loss of primary electrons. The purpose of this drift field is to guide the primary electrons to the scintillation region, which electric field value is set to values between the noble gas scintillation and ionisation thresholds. Upon transversing the scintillation region, the primary electrons gain enough kinetic energy from the electric scintillation field to excite the noble gas, by colliding with its atoms without, however, ionising them. In the de-excitation processes, the atoms of the noble gas emit electroluminescence in the form of vacuum ultraviolet (VUV) photons. Each primary electron leads to the production of a high number of electroluminescence photons, being the intensity of this scintillation pulse approximately proportional to the number of primary electrons produced in the absorption region and, hence, proportional to the energy of the radiation attaining the detector. A UV-sensitive photossensor collects the electroluminescence photons and converts them into an electric signal, which is proportional to the energy of the radiation that reached the detector.

This technique amplifies the absorbed energy through scintillation processes, rendering a superior energy resolution compared with a PC, which relies on charge amplification processes. Contrary to the latter, the scintillation amplification processes are characterized not only by a high efficiency in the conversion of the electric field energy into scintillation [20], but also by the associated statistical fluctuations which are negligible when compared to those produced in the

interaction of radiation [11]. Moreover, the number of statistical fluctuations introduced by the photossensor is usually lower than that resulting from charge multiplication processes. These reasons contribute to the enhanced performance of the GPSC when compared to the PC.

2.4. Double-phase detectors for direct Dark Matter Search

Noble gas, double-phase time projection chambers (TPC) present a unique capability. They provide, simultaneously, the information corresponding to both primary scintillation and ionization signals resulting from the absorption of an interacting particle inside the active detector volume, even if the ionisation signal is weak.

A noble gas double-phase TPC consists essentially of two different regions, namely a lower volume with an ultra-pure noble gas in the liquid state, the drift volume, and an upper volume with the same noble gas in the gas phase, the scintillation gap. Both liquid and gas volumes are surveyed by suitable photosensors, usually PMTs. Under the influence of a low electric field, the primary electrons are guided toward the liquid-gas interface, which limits the scintillation gap. The negative ground state energy of quasi-free electron in the liquid requires a strong electric field in the gas phase to extract electrons from the liquid into the gas. Once inside the gas of the scintillation gap,

electroluminescence photons are produced. The collected electroluminescence signal is proportional to the number of electrons extracted from the liquid into the gas phase and, hence, proportional to the primary ionisation in the liquid phase resulting from the interacting radiation.

The combination of both primary scintillation and ionisation signals provides a mean to efficiently discriminate interactions due to high-energy electrons and electromagnetic radiation from neutrons and WIMPs. In addition, it allows the improvement of the very low energy threshold as well as the excellent energy resolution required for these rare-event experiments.

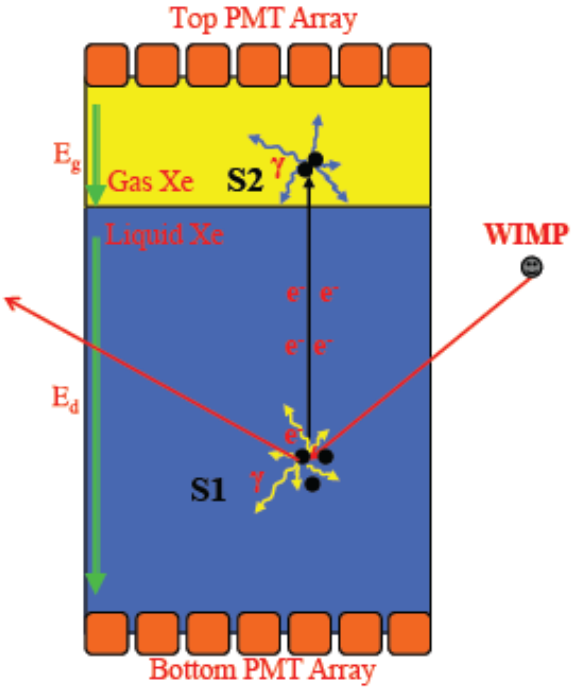

Figure 2.2 – Operating principle of a double-phase xenon TPC for direct dark matter search. The direction of the two electric fields, E_d (electric field in the drift gap) and E_g (electric field in the scintillation gap), are indicated by the arrows. [23].

2.5. Electroluminescence TPC for neutrinoless double beta decay

The NEXT (Neutrino Experiment with a Xenon TPC) project has as a goal the design and construction of a High Pressure Xenon Time Projection Chamber (TPC) to operate in the Canfranc Underground Laboratory (Huesca, Spain) with a source mass of 100 kg of enriched xenon, ^{136}Xe, for measuring its double-beta decay, both with neutrino and neutrinoless emission [24]. An energy resolution as best as possible is crucial not only to reduce the tail of the 2νββ spectrum from overlapping the region of interest of the 0νββ spectrum, but also to prevent the contamination of the region of interest by the most severe background from 2.6 MeV gamma rays from ^{206}Tl and 2.4 MeV gamma rays from ^{214}Bi, given the $Q_{\beta\beta}$ value of 2.48 MeV for the xenon ββ decay. On the other hand, the topological signal given by the tracking information aims to further reduce external backgrounds by identifying the unique signature of the 0νββ events, a double electron track in opposition to the single electron track resulting from gamma interactions. The optimization of these two features is essential for such experiment with very low event rates and high background levels.

A similar project is being carried out by the EXO-gas collaboration [9].

The advantage of a high pressure xenon TPC over liquid xenon TPCs is the tracking capability. In the case of liquid xenon the electron energies are deposited in a small region, while in the case of gaseous

xenon the energy is deposited along a track, which length is dependent on the gas pressure. In addition, the energy resolution is better in gaseous than in liquid xenon.

The need for the best possible energy resolution in NEXT and EXO dictates the use of electroluminescence as primary ionisation amplification method.

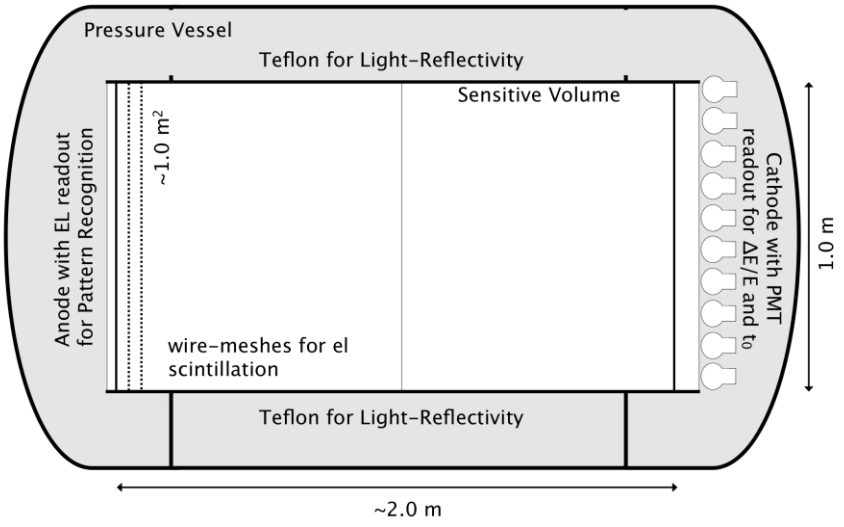

Figure 2.3 - Concept of NEXT: A TPC of about 2 m in length and 1 m in diameter [25].

2.6 The Large Area Avalanche Photodiode

In the present studies, a Large Area Avalanche Photodiode (LAAPD) is used to readout the electroluminescence from both xenon and argon gas.

During the last decade, significant advances in the development of LAAPDs triggered the study and the characterization of different commercially available LAAPDs (e.g. Hamamatsu [26-28], EG&G [27,29], API [30-33] and RMD [34,35]). Although applications to direct X-ray detection have been investigated [30, 37,38], LAAPDs have been used mainly as optical photosensors coupled to scintillation detectors for X-, γ-ray and particle detection, such as in the electromagnetic calorimeter of the CMS detector [26,27,36], in gas proportional scintillation counters [39,40], in PET [29,41-43] and atomic and nuclear physics [32-34,44] instrumentation. In addition, these devices can be applied to photon detection in other areas of optics.

It has been demonstrated that LAAPDs can replace PMTs with advantages, delivering similar performances. When compared to PMTs, LAAPDs are much more compact, present much less power consumption, a straightforward operation, can operate under intense magnetic fields [45] and have higher quantum efficiencies. On the other hand, the low gains and reduced active areas are the main drawback of LAAPDs. Low-energy X-ray detection techniques with LAAPDs were developed to measure the charge carriers produced in light measurements using X-rays as a reference, resulting in a straightforward process to evaluate the number of photons interacting in the photodiode.

Advanced Photonix, Inc. (API) has developed windowless LAAPDs with a spectral response that extends down to the vacuum-ultra-violet (VUV) region (~120 nm) [46], figure 2.4. The effective quantum

efficiency, here defined as the average number of primary electrons produced in the LAAPD per incident photon, is about 0.55 and 1.1 for 128-nm and 172-nm VUV photons [46], respectively, corresponding to spectral sensitivities of 50 and 150 mA/W. These values are much higher than the typical 10% of PMTs. In addition, PMTs need specific windows, suitable for VUV photons of those wavelengths, e.g. quartz for xenon and magnesium fluoride for argon electroluminescence.

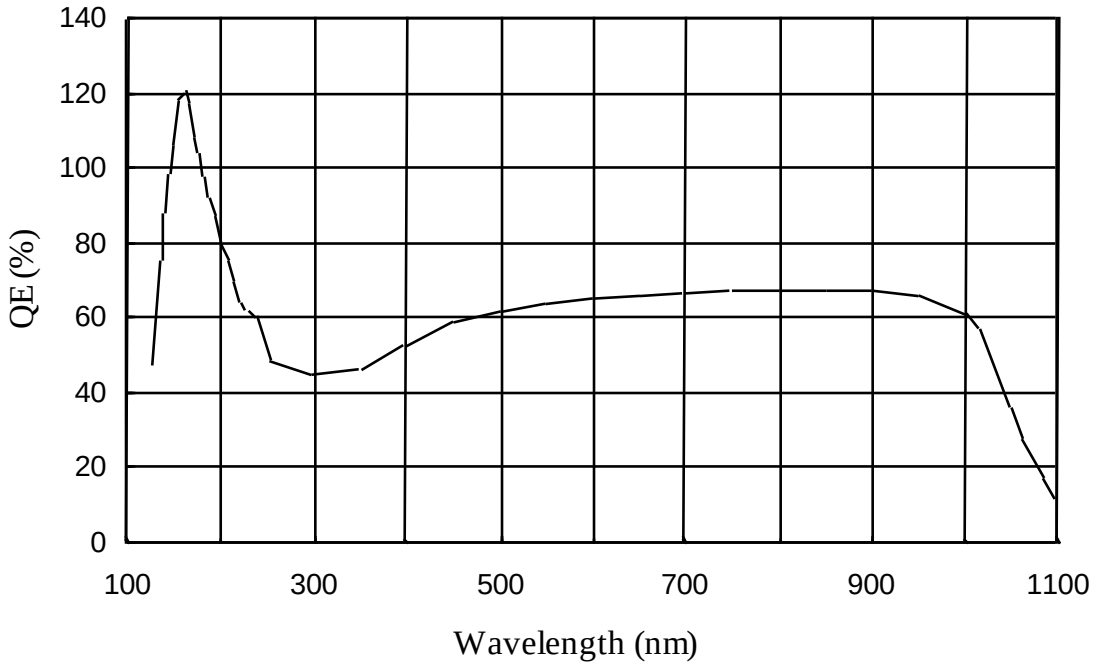

Figure 2.4 – Large Area Avalanche Photodiodes' quantum efficiency as a function of wavelength [45].

Enhanced quantum efficiency of LAAPDs from Advanced Photonix Inc. is the result of maximizing the quantum yield and transmittance while reducing recombination through the selection of an optimized thickness of silicon dioxide as the antireflection layer. The high-quality

silicon surface also reduces losses from recombination of charge carriers [46].

A review on the characteristics of API LAAPDs for X-ray and VUV detection is presented in [47].

2.6.1. Operation principle

Large area avalanche photodiodes are compact devices, manufactured in silicon, having as main characteristic a *p*-*n* junction, where the electric field can reach values high enough to allow ionisation by collision, with subsequent avalanche multiplication [9 and references therein].

Like any other solid state detector, LAAPDs consist of two different layers, the *p* or *p*+ layer and the *n* or *n*+ layer; both are doped with a very low concentration of impurities, as is shown in figure 2.5. When a high inverse electric field is applied to the LAAPD, a high quantity of free charge carriers remain only in a small region of the *p* layer, the so-called drift region. In this region, the electric field intensity is low, increasing towards the *p*-*n* junction, and being at its maximum around the junction. Since the absorption of either X-rays or VUV photons in photodiodes occurs preferably by photoelectric effect, each photon incident in the drift region or on the p-layer creates electron-hole pairs. Those electrons are, then, accelerated towards the *p*-*n* junction where

they undergo multiplication by avalanche formation due to the very intense electric field located around the junction. Typical gains of a few hundred are common and increase exponentially with the applied biasing voltage.

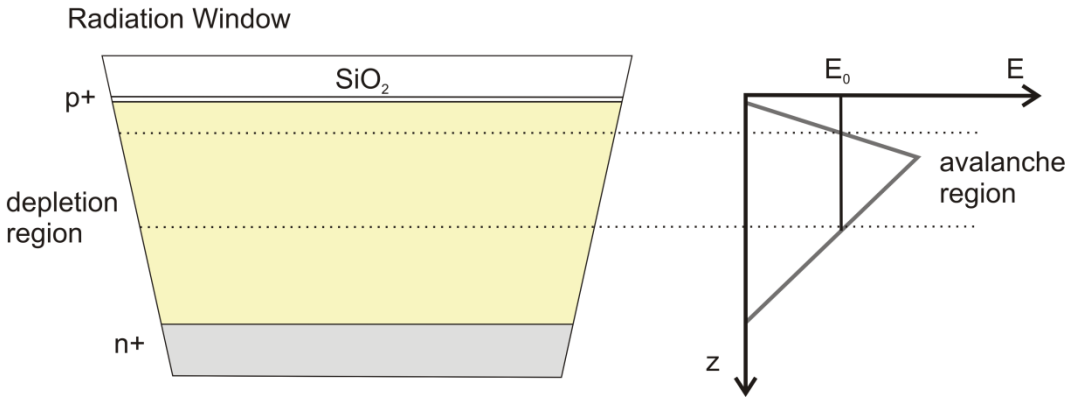

Figure 2.5 – Schematic of an avalanche photodiode with the typical shape of its internal electric field [45].

2.7 References

[1] A.J.P.L. Policarpo, M.A.F. Alves and C.A.N.Conde, *The argon-nitrogen proportional scintillation counter*, *Nucl. Instrum. Meth.*, 55 (1967) 105.

[2] C.A.N. Conde and A.J.P.L. Policarpo, *A gas proportional scintillation counter*, *Nucl. Instrum. Meth.*, 53 (1967) 7-12.

[3] Z. Ahmed, D. S. Akerib, S. Arrenberg, C. N. Bailey, D. Balakishiyeva, et al., *Dark Matter Search Results from the CDMS II Experiment - The CDMS II Collaboration*, *Science* Vol. 327 (2010) 1619 – 1621.

[4] G. Angloher, M. Bauer, I. Bavykina, A. Bento, A. Brown, et al., *Commissioning Run of the CRESST-II Dark Matter Search*, *Astroparticle Physics* 31 (2009) 270-276.

[5] E. Armengaud, C. Augier, A. Benoit, L. Berge, O. Besida, et al., *First results of the EDELWEISS-II WIMP search using Ge cryogenic detectors with interleaved electrodes*, E. Armengaud et al. - *Phys. Lett. B* 687 (2010) 294-298.

[6] H Kraus et al., *EURECA — the European future of cryogenic dark matter searches*, *J. Phys.: Conf. Ser.* 39 (2006)139-141.

[7] J. Angle, et al. (XENON10 Collaboration), *Limits on spin-dependent WIMP-nucleon cross sections from the XENON10 experiment*, *Phys. Rev. Lett.* 101, 091301 (2008).

[8] E. Aprile, et al. (XENON10 Collaboration), *First Dark Matter Results from the XENON100 Experiment*, *Phys. Rev. Lett.* (2010), in press.

[9] Sinclair D. 2005 SNOLAB and ECO report to the IV SNOLAB Workshop, SNOLAB, August 15-17, 2005.

[10] F.Grañena et al. (NEXT Collaboration), NEXT Letter of Intent, Laboratorio Subterráneo de Canfranc EXP-05

[11] J.M.F. dos Santos, J.A.M. Lopes, J.F.C.A. Veloso, P.C.P.S. Simões, T.H.V.T. Dias, et al., *On the portability of gas proportional scintillation counters for x-ray spectrometry*, *X-Ray Spectrometry*, 30 (2001) 373-381.

[12] A. Gedanken, J. Jortner, B. Raz and A. Szoke, *Electronic energy transfer phenomena in rare gases*, *J. Chem. Phys.* 57 (1972) 3456.

[13] A.J.P.L. Policarpo, *The gas proportional scintillation counter*, *Space Sci. Instr.* 3 (1977)77.

[14] A.J.P.L. Policarpo, *Light production and gaseous detectors*, *Phys. Scripta* 23 (1981)539.

[15] M.S.S.C.P. Leite , *Radioluminescence of rare gases*, *Portugal. Phys.* 11 (1980) 53

[16] T. Takahashi, S. Himi, M. Suzuki, J-Z Ruan and S. Kubota, *Emission spectra from Ar-Xe, Ar-Kr, Ar-N2, Ar-CH4, Ar-CO2 and Xe-N2 gas scintillation proportional counters*, *Nucl. Instr. Meth.* 205 (1983) 591.

[17] J. Galy, K. Aouame, A.Birot, H. Brunet and P. Millet, *Energy transfers in Ar-Xe and Ne-Xe mixtures excited by alpha particles: II. Kinetic study*, *J. Phys. B* 26 (1993) 477.

[18] M.A.G.R.L. Feio, *Electroluminescência e contadores gasosos de cintilação proportional - GSPC*, *Tese de Doutoramento*, Faculdade de Ciências e Tecnologia da Universidade de Coimbra, 1983.

[19] M. M. F. R. Fraga, *Emissões Luminosas e Desenvolvimento de Avalanches em Detectores Gasosos*, *Tese de Doutoramento*, Faculdade de Ciências e Tecnologia da Universidade de Coimbra,1994.

[20] Dias T.H.V.T., Stauffer A.D. e Conde C.A.N., *Unidimensional Monte Carlo simulation of electron drift velocities and electroluminescence in argon, krypton and xenon, J. Phys. D: Appl. Phys.*, 19 (1986) 527-545.

[21] F.P. Santos, T.H.V.T. Dias, A.D. Stauffer and C.A.N. Conde, *Tridimensional Monte Carlo Calculation of the VUV electroluminescence and other electron transport parameters in xenon, J. Phys. D: Appl. Phys.,* vol.27 (1994) 42-48.

[22] T.H.V.T. Dias, F.P. Santos, A.D. Stauffer and C.A.N. Conde, *Monte Carlo simulation of x-ray absorption and electron drift in gaseous xenon*, *Phys. Rev. A* 48 (1993) 2887.

[23] E. Aprile, et al. (XENON10 Collaboration), *Design and Performance of the XENON10 Dark Matter Experiment*, Accepted for publication to *Astroparticle Phys.* (2010).

[24] J. Díaz, N. Yahlali, M. Ball, J. A. S. Barata, et al., *The NEXT experiment*, *Journal of Physics: Conference Series* 179 (2009) 012005.

[25] Markus Ball on Behalf of the NEXT Collaboration, *NEXT: A Neutrinoless Double Beta Decay Experiment*, 2009 *IEEE NSS Conf. Rec (2009) 1034.*

[26] K. Deiters, Y. Musienko, S. Nicol, B. Patel, D. Renker, et al. *Properties of the most recent avalanche photodiodes for the CMS electromagnetic calorimeter*, Nucl. Instrum. Methods A 442, 193 (2000).

[27] A. Karar, Y. Musienko, J. Ch. Vanel, *Characterization of avalanche photodiodes for calorimetry applications*, Nucl. Instrum. Methods A 428, 413 (1999).

[28] R Bugalho, B Carrico, CS Ferreira, M Frade, M Ferreira, *Characterization of avalanche photodiode arrays for the ClearPEM and ClearPEM-Sonic scanners*, J. Inst. 4 (2009) P09009.

[29] R. Lecomte, C. Pepin, D. Rouleau, H. Dautet, R.J. McIntyre, et al., *Radiation detection measurements with a new "Buried Junction" silicon avalanche photodiode*, Nucl. Instrum. Methods A 423, 92 (1999).

[30] M. Moszynski, M. Szawlowsky, M. Kapusta, M. Balcerzyk, *Large area avalanche photodiodes in scintillation and X-rays detection*, Nucl. Instrum. Methods A 485, 504 (2002).

[31] VN Solovov, F Neves, V Chepel, MI Lopes, RF Marques, AJPL Policarpo, *Low-temperature performance of a large area avalanche photodiode*, Nucl. Instrum. Meth. A 504 (2003) 53.

[32] M. Moszynski, M. Szawlowsky, M. Kapusta, M. Balcerzyk, *Avalanche photodiodes in scintillation detection*, Nucl. Instrum. Methods A 497, 226 (2003).

[33] R. Neilson, F. LePorta, A. Pocara, K. Kumarb, A. Odian, et al., *Characterization of large area APDs for the EXO-200 detector*, Nucl. Instrum. Meth. A 608 (2009) 68.

[34] R. Farrel, F. Olschner, K. Shah, M.R. Squillante, *Advances in semiconductor photodetectors for scintillators*, Nucl. Instrum. Methods A 387, 194 (1997).

[35] R. Farrel, K. Shah, K. Vanderpuye, R. Graziaso, R. Myers, G. Entine, *APD arrays and large-area APDs via a new planar process*, Nucl. Instrum. Methods A 442, 171 (2000).

[36] J.P. Pansart, *Avalanche photodiodes for particle detection*, Nucl. Instrum. Methods A 387 (1997) 186.

[37] L.M.P. Fernandes, J.A.M. Lopes, J.M.F. dos Santos, C.A.N. Conde, *Application of a Large Area Avalanche Photodiode in Energy Dispersive X-Ray Fluorescence Analysis*, X-ray Spectrom. 30, (2001) 164.

[38] L.M.P. Fernandes, A. Antognini, M. Boucher, C.A.N.Conde, O. Huot, et al., *Application of large-area avalanche photodiodes to X-ray spectrometry of muonic atoms*, Spectrochimica Acta B 58, 2255 (2003).

[39] J.A.M. Lopes, J.M.F. Dos Santos, R.E. Morgado, C.A.N. Conde, *A xenon gas proportional scintillation counter with a UV-sensitive, large-area avalanche photodiode*, IEEE Trans. Nucl. Sci. 48, 312 (2001).

[40] C.M.B. Monteiro, J.A.M. Lopes, P.C.P.S. Simões, J.M.F. dos Santos, C.A.N.Conde, *An Argon Gas Proportional Scintillation Counter With UV Avalanche Photodiode Scintillation Readout*, IEEE Trans. Nucl. Sci. 48, 1081 (2001).

[41] B. Pichler, G. Böning, E. Lorenz, R. Mirzoyan, W. Pimpl, et al., *Studies with a prototype high resolution PET scanner based on LSO-APD modules*, IEEE Trans. Nucl. Sci. 45, 1298 (1998).

[42] A. Ruru Chen, A. Fremout, S. Tavernier, P. Bruyndonckx, D. Clément, J.-F. Loude, C. Morel, *Readout of scintillator light with avalanche photodiodes for positron emission tomography*, Nucl. Instrum. Methods A 433, 637 (1999).

[43] R Bugalho, B Carrico, CS Ferreira, M Frade, M Ferreira et al., *Experimental characterization of the Clear-PEM scanner spectrometric performance*, J. Inst. 4 (2009) P10011.

[44] T Nebel, FD Amaro, A Antognini, F Biraben, JMR Cardoso, et al., *Status of the muonic hydrogen Lamb-shift experiment*, Can. J. Phys. 85 (2007) 469.

[45] LMP Fernandes, A Antognini, M Boucher, et al., *Behaviour of large-area avalanche photodiodes under intense magnetic fields for VUV- visible- and X-ray photon detection*, Nucl. Instrum. Meth. A 498, 362 (2003).

[46] B. Zhou, M. Szawlowski, *An explanation on the APD spectral quantum efficiency in the deep UV range,* Interoffice Memo, Advanced Photonix Inc., 1240 Avenida Acaso, Camarillo, CA 93012, EUA, 1999.

[47] L.M.P. Fernandes, F.D. Amaro, A. Antognini, J.M.R. Cardoso, C.A.N. Conde, et al., *Characterization of large area avalanche photodiodes in X-ray and VUV-light detection*, J. Inst. 2 (2007) P08005.

CHAPTER 3

Xenon Electroluminescence in Uniform Electric Field

3. Motivation

Gas proportional scintillation counters (GPSC) using xenon as the fill gas, or scintillator, have been widely used as X-ray and low-energy γ-ray detectors [1,2]. More recently, dual-phase detectors with xenon filling have been developed for Dark Matter search, for the direct detection of Weak Interacting Massive Particles (WIMP) [3-5]. In both cases, electrons resulting from the radiation interaction are guided to a specific region inside the detector, the scintillation gap, where the value

of the electric field is such that electrons can acquire enough energy to excite the noble gas atoms through inelastic collisions, leading to the production of secondary scintillation, the so-called electroluminescence. The most common type of collision that occurs is the elastic collision. Between two successive inelastic collisions, the electrons undergo a very large number of elastic collisions, above 10^4 [6], while they acquire enough energy from the electric field to excite the atoms. Nevertheless, the amount of energy lost by the electron in this large number of elastic collisions is small, given the very large difference in masses between the electron and the xenon atom. The excitation efficiency, i.e. the fraction of energy, attained from the electric field by the electron, that is spent in exciting the xenon atoms, reaches values around 95% for reduced electric fields, E/p - the electric field divided by the gas pressure - of 4 kV cm^{-1} bar^{-1} [6,7]. On the other hand, for low reduced electric fields this energy loss is not negligible, since the number of elastic collisions increases significantly. The excitation efficiency presents a fast decrease for values of E/p below 2 kV cm^{-1} bar^{-1} [6,7], being zero below a characteristic E/p threshold. Below this threshold, electrons never get enough energy to excite the xenon atoms.

The mechanisms of electroluminescence production are well known [6,8-10]. For pure xenon, the wavelength of the emission depends on the gas pressure. Below 10 mbar, the emission is mainly of atomic nature, with two peaks centred in 130 nm and 147 nm, approximately. For higher pressures, the formation of excited dimers Xe_2^* is favoured through three body collisions, and molecular emission becomes increasingly more important. These emissions are centred in 147 nm for

the first continuum and in 172 nm for the second continuum. The first continuum corresponds to the VUV radiative decay of the vibrationally excited, $(Xe_2^*)^v$, excimer state, while the second continuum corresponds to the VUV radiative decay of the vibrationally relaxed, $(Xe_2^*)^{v=0}$, excimer state. Above 400 mbar, the second continuum is dominant and the electroluminescence presents only a narrow peak, of about 10 nm FWHM, centred in 172 nm [9]. The energy loss due to the relaxation of vibrationally excited dimers is still a small fraction of the energy that the electrons attain from the electric field and the overall scintillation efficiency reaches values of 80% for reduced electric fields of 4 kV cm^{-1} bar^{-1} [6,7].

Concerning the electroluminescence yield, defined as the number of secondary scintillation photons produced per drifting electron per unit path length, the data available in the literature are not in agreement. While the data obtained at room temperature using Monte Carlo simulation [7] and Boltzman calculations [11] are in perfect agreement with each other [7], the values obtained experimentally [12-16] are much lower than the former and differ significantly from each other, as can be seen from figure 3.4, further on. On the other hand, the results for saturated gas at cryogenic temperatures [15,16], in equilibrium with the liquid phase, are in agreement with each other, as well as with the simulation results calculated for room temperature.

The electroluminescence yield, along with its dependence on the electric field, is an important parameter for detector simulation. Nevertheless, absolute measurements are difficult to perform and

usually rely on comparison/calibration performed with experimental set-ups and/or settings other than those used to measure the secondary scintillation itself, e.g. [16].

In this chapter, a straightforward method has been applied, making use of only one experimental set-up to carry out absolute electroluminescence yield measurements. A VUV-sensitive large area avalanche photodiode (LAAPD) was used to detect, simultaneously, the secondary scintillation of a xenon (GPSC) and the original X-rays. The X-rays were used as the reference for determining the absolute number of VUV-photons impinging the LAAPD. This method has been largely employed to measure the primary scintillation yield of inorganic crystals, like in [17 and references therein]. The electroluminescence yield was measured as a function of electric field in the scintillation gap and compared with the other experimental and calculated results found in the literature.

3.1. Experimental Setup

In these studies, a xenon-filled GPSC was used, instrumented with a silicon LAAPD [18]. The GPSC is schematically depicted in figure 3.1 and was already used in [19,20].

It is a driftless prototype with a 1.1-cm deep scintillation region. The LAAPD is positioned just below the electron-collection grid, G, which is made of stainless steel wire, 80 μm in diameter with 900-μm

spacing; this grid has an optical transparency, T, of 84%. The radiation window is maintained at negative high-voltage, HV, while grid G, LAAPD and detector enclosures are maintained at ground potential. The electric field in the scintillation region is defined by HV. The radiation window is a 12.5-μm thick, 10 mm in diameter aluminized Mylar film. A Macor ceramic is used between the detector body and the radiation window holder, for electrical insulation. Both Mylar window and Macor are glued to the stainless steel by means of a low vapour pressure epoxy (TRA-CON 2116). The detector upper and lower parts and the LAAPD enclosure are vacuum-tight by compression of indium gaskets.

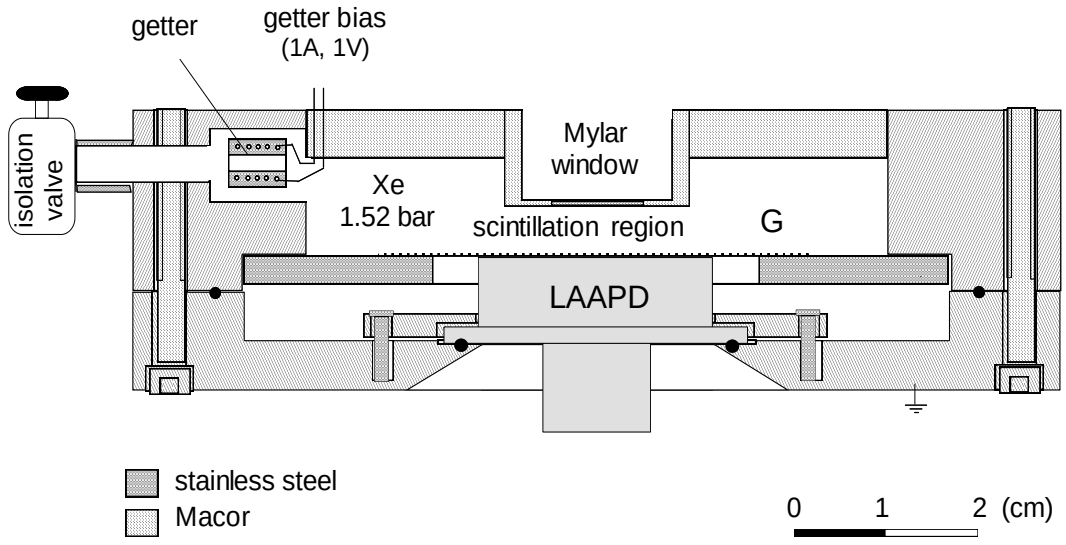

Figure 3.1 – Schematic of the driftless GPSC instrumented with an LAAPD, used in the present work.

The detector is pumped down to pressures in the 10^{-6} mbar range, and filled with high purity xenon (Air Liquide, N45) at a pressure of 1.52 bar. After being sealed, the gas purity in the detector is maintained by a

small non-evaporable getter (SAES ST172/HI/7-6/150C), which is placed inside the xenon envelope and kept at a temperature of about 200ºC. These simple, high-vacuum detector assembling techniques have been developed and used in GIAN for more than one decade and have proven to be capable of keeping the xenon in sealed detectors at high purity levels, inducing high scintillation efficiencies, which is confirmed by the best energy resolutions obtained with GPSCs [1].

For this study, a 1-mm collimated 5.9-keV X-ray beam from a ^{55}Fe X-ray source was used, filtered with a Cr-film to remove the 6.4-keV Mn K_β-fluorescence line. X-rays entering the scintillation region through the radiation window are absorbed in the xenon gas by photoelectric effect, generating a primary electron cloud. The electrons are accelerated in the electric field established by HV. Each primary electron produces a large number of VUV photons.

However, in a driftless GPSC this number of VUV photons is dependent on the distance covered by the primary electron in the scintillation region and, hence, on the X-ray interaction depth. Nevertheless, for low-energy X-rays with absorption depths much smaller than the scintillation region thickness, the effect of the different X-ray interaction depths on the distance covered by the primary electron cloud in the scintillation region and, thus, on the amount of scintillation light produced, is small and the proportionality between incident X-ray energy, average number of primary electrons and average number of scintillation photons is maintained.

The scintillation photons absorbed in the sensitive area of the LAAPD produce electron–hole pairs in the silicon, which are multiplied through the avalanche process. Concurrent with the acquisition of the scintillation signals resulting from the absorption of X-rays in xenon, a transmitted fraction of the incident X-rays is detected directly by the LAAPD. The dead layer of the LAAPD surface is much smaller than the penetration depth of 6-keV X-rays in silicon, resulting in negligible associated effects. The number of electron–hole pairs produced through direct absorption of X-rays in the LAAPD is determined from the energy of the X-ray and the w-value in silicon, i.e. the mean energy required to produce a pair of charge carriers. The LAAPD reverse bias voltage determines the multiplication gain in the avalanche process.

In the driftless design, the primary scintillation produced by the X-ray interaction is detected together with the electroluminescence. However, the number of primary photons is more than three orders of magnitude lower than the number of photons resulting from electroluminescence, as can be seen further on.

As referred, for each 5.9-keV X-ray interaction in the driftless detector volume, the total number of secondary scintillation photons produced by the drifting primary electron cloud depends on how deep in the scintillation region the X-ray is absorbed. Nevertheless, the average number of VUV photons is well defined, since the respective pulse-height distribution has a Gaussian shape with a tail towards the low energy region. Although the driftless GPSC results in degraded energy resolution for scintillation events, it allows a higher transmission of the

5.9-keV X-rays through xenon and, therefore, more direct X-ray interactions in the LAAPD, which is convenient for this study. In our case, approximately 0.2% of the 5.9-keV X-rays are transmitted through 1.1 cm of xenon.

The charge pulses collected in the LAAPD are integrated in a 1.5 VpC^{-1} charge-sensitive preamplifier (Canberra 2004), followed by linear amplification (Hewlett Packard 5582A) with a 2-μs shaping time. Pulse-height analysis is performed with a 1024-channel analyser (Nucleus PCA-II). The peaks in the pulse-height distribution are fit to a Gaussian function superimposed on a linear background. The pulse amplitude for each type of event is determined from the centroid of the fitted Gaussian.

3.2. Experimental Results

Figure 3.2 depicts a typical pulse-height distribution obtained with the driftless GPSC equipped with an LAAPD for scintillation readout.

The salient features of the pulse-height distribution include not only the 5.9-keV X-ray full-energy peak from the absorption in the xenon volume of the GPSC, but also the xenon L_α- and L_β-escape peaks from 5.9-keV X-ray absorption in the xenon volume of the GPSC, the 5.9-keV X-ray peak from direct absorption in the LAAPD, the 4.1- and

4.8-keV xenon L_α- and L_β-fluorescence peaks from absorption in the LAAPD, and the system electronic noise.

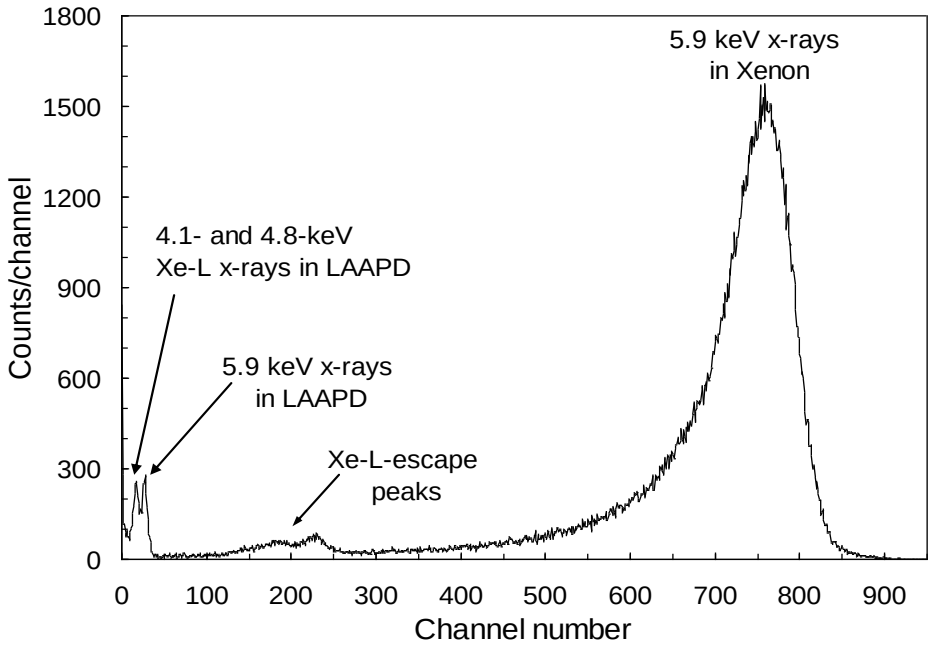

Figure 3.2 - Pulse-height distribution from a xenon driftless GPSC instrumented with a large area avalanche photodiode, for 5.9-keV X-rays. An E/p of 5.4 $kVcm^{-1}bar^{-1}$ was used in the scintillation region.

While the amplitude of the scintillation peak depends on both scintillation region and LAAPD biasing, the amplitude of the events resulting from direct X-ray interaction in the LAAPD depends only on the LAAPD biasing. The latter events are present even for a zero or reverse electric field in the scintillation region. On the other hand, when the detector is vacuum-pumped, only the peak resulting from the direct interaction of 5.9-keV X-rays in the LAAPD is present. Therefore, both pulse-height distributions enable a direct comparison of the pulse amplitudes resulting from both the 5.9-keV X-ray full-absorption in the

gas, i.e. from the xenon scintillation, and the 5.9-keV X-ray direct absorption in the LAAPD. This allows a direct quantification of the VUV-photons impinging the LAAPD, given the quantum efficiency of the device.

Figure 3.3 depicts the GPSC relative amplitude as a function of reduced electric field, E/p, in the scintillation region. The results follow the typical behaviour of electroluminescence in noble gases, i.e. an approximately linear dependence on the reduced electric field in the scintillation region, with the scintillation threshold at an E/p value of about 0.8 $kVcm^{-1}bar^{-1}$ for xenon (e.g. Ref. [28] and references therein). Above a reduced electric field of 4.5 $kVcm^{-1}bar^{-1}$, the xenon ionisation threshold, the relative amplitude variation departs from the linear behaviour, reflecting the exponential growth in the number of electrons produced in the scintillation region by the drifting electron cloud [29].

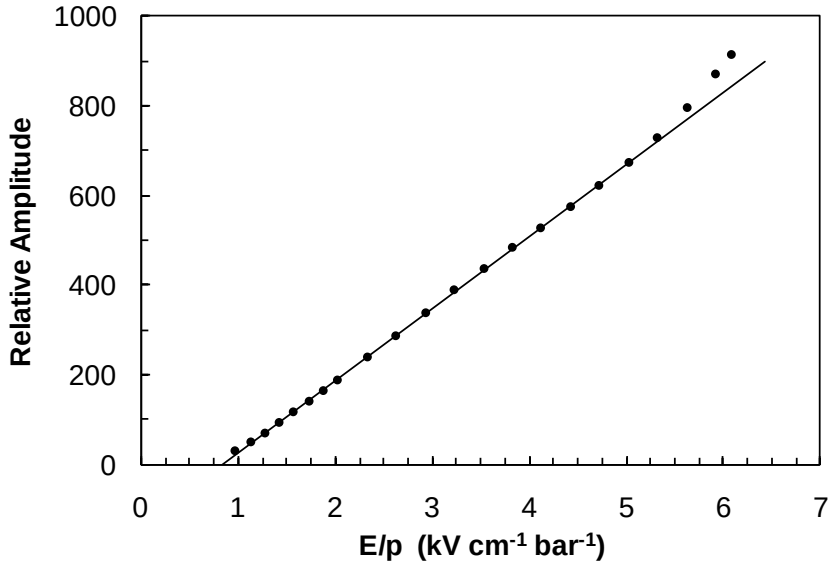

Figure 3.3 – Detector relative pulse amplitude as a function of reduced electric field in the scintillation region, for 5.9-keV X-rays from a ^{55}Fe radioactive source and for xenon.

3.3. Absolute Measurement of Electroluminescence Yield

For a reduced electric field of 4.1 kVcm^{-1}bar^{-1}, the ratio between the pulse amplitudes resulting from the full-absorption of the 5.9-keV X-rays in xenon and the 5.9-keV X-rays absorbed in the LAAPD, as obtained from the corresponding pulse-height distribution, is $A_{UV}/A_{XR} = 19.9 \pm 0.1$ for low LAAPD gains, where gain non-linearity in the photodiode is less than 1% [19]. As the w-value in silicon is 3.62 eV [24], the average number of free electrons produced in the LAAPD by the full absorption of the 5.9-keV X-rays is

$$N_{XR} = \frac{5895\,eV}{3.62\ eV} \cong 1.63 \times 10^3 \text{ electrons} \qquad (3.1).$$

Thus, the number of free electrons produced in the LAAPD by the electroluminescence pulse from full absorption of the 5.9-keV X-rays in xenon is

$$N_{EL} = \frac{A_{UV}}{A_{XR}} \times N_{XR} \cong 3.24 \times 10^4 \text{ electrons} \qquad (3.2).$$

Hence, the average number of VUV photons impinging the photodiode for the scintillation pulses due to the 5.9-keV X-ray full-absorption in the gas is

$$N_{UV,APD} = \frac{N_{EL}}{QE} \cong 2.95 \times 10^4 \text{ photons} \qquad (3.3)$$

According to Advanced Photonix, Inc., the LAAPD manufacturing technology is well established, and quite good reproducibility is obtained. Therefore, it is expected that the observed behaviour for individual LAAPDs is representative for any of these devices [21]. A value of QE = 1.1 for the number of charge carriers produced in the LAAPD per incident 172-nm VUV photon was provided by the manufacturer [22] for the LAAPDs we acquired [23]. However, at present the manufacturer provides different values for the quantum efficiency of the LAAPDs currently manufactured which, in the VUV region [18], are somewhat higher than formerly. An uncertainty of about 0.1 was assumed for the LAAPD quantum efficiency [32]. This uncertainty is the major source of error in the measurements of the present studies.

The average solid angle, Ω, subtended by the photosensor active area for the primary electron path has been computed accurately through a simple Monte Carlo simulation program [25]. A value of

$$\Omega_{\mathrm{rel}} = \frac{\Omega}{4\pi} \cong 0.202 \qquad (3.4)$$

was obtained for the present geometry. In this way, the total number of VUV photons produced by the full absorption of 5.9-keV X-rays in the detector is

$$\mathrm{N_{UV,total}} = \frac{N_{UV,APD}}{\Omega_{rel} \times T} \cong 1.74 \times 10^5 \text{ photons} \qquad (3.5)$$

where T is the wire mesh optical transparency, which is around 84%.

In addition, the average number of primary electrons produced in xenon by full absorption of the 5.9-keV X-rays is

$$N_e = \frac{5895eV}{22.4eV} \cong 263 \text{ electrons} \qquad (3.6)$$

considering a *w*-value for xenon of 22.4 eV [26].

Since the average absorption depth, d_{average}, of 5.9-keV X-rays in xenon at 1.5 bar is given by

$$d_{\text{average}} = \frac{\int_0^{4.1} x e^{-\lambda x} dx}{\int_0^{4.1} e^{-\lambda x} dx} = 0.17 \text{ cm} \qquad (3.7),$$

where $\lambda = 3.90$ cm^{-1} is the linear attenuation coefficient [27], the average distance the primary electron cloud drifts inside the xenon volume is 0.93 cm.

In this way, the reduced electroluminescence yield, Y/p, determined for a reduced electric field of 4.1 kVcm^{-1}bar^{-1} is

$$\frac{Y}{p}(4.1 \text{ kVcm}^{-1}\text{bar}^{-1}) = \frac{N_{UV,total}}{N_e \times d_{\text{average}} \times p} = 466 \text{ photons} \qquad (3.8),$$

466 photons per electron per cm of path and per bar.

According to [30], the average number of primary scintillation photons produced by the interaction of a 5.9-keV X-ray is 81 ± 7. Therefore, the contribution of the primary scintillation to the detector

pulse is more than three orders of magnitude lower than that of the electroluminescence.

3.4. Scintillation production around the mesh wires

In general, the scintillation region of GPSCs is delimited by a mesh anode. Therefore, since the electrons are collected in the wires, there may be an effect of additional ionisation and scintillation present in the vicinity of the wires, due to the fact that the electric field increases with decreasing distance to the wires.

From the experience of our research group, no evidence had been found of a significant effect, because the energy resolution does not degrade with increasing mesh voltages. In opposition, the energy resolution values that have been obtained in our group with GPSCs approach the intrinsic energy resolution values. The presence of an even small amount of ionisation and additional scintillation introduces degradation in the energy resolution, due to the additional statistical fluctuations inherent to those processes [29].

In the next chapter, calculations are presented for argon, supporting the empirical thought that the amount of this additional scintillation is negligible.

3.5. Xenon Electroluminescence Yield

In the former section, the calculation of the reduced electroluminescence yield was performed for an E/p of 4.1 $kVcm^{-1}bar^{-1}$. These calculations can be made for all the data points of figure 3.3, in order to determine the electroluminescence yield for the different values of the reduced electric field.

Figure 3.4 depicts the reduced electroluminescence yield, Y/N, i.e. the electroluminescence yield divided by the number density of the gas, as a function of reduced electric field, E/N, in the scintillation region. Other results presented in the literature are also depicted for comparison. Since some of the datasets were obtained for different xenon temperatures, the graph is presented in temperature independent units.

The variation of the reduced electroluminescence yield with reduced electric field in temperature independent units can be approximately represented by

$$Y/N\ (10^{-17}\ \text{photons electron}^{-1}\ \text{cm}^2\ \text{atom}^{-1}) = 0.140\ E/N - 0.4 \qquad (3.9),$$

where E/N is given in Td (10^{-17} V cm^2 $atom^{-1}$).

The above equation can also be expressed by

$$Y/p\ (\text{photons electron}^{-1}\ \text{cm}^{-1}\ \text{bar}^{-1}) = 140\ E/p - 116 \qquad (3.10),$$

where E/p is given in kV cm^{-1} bar^{-1}.

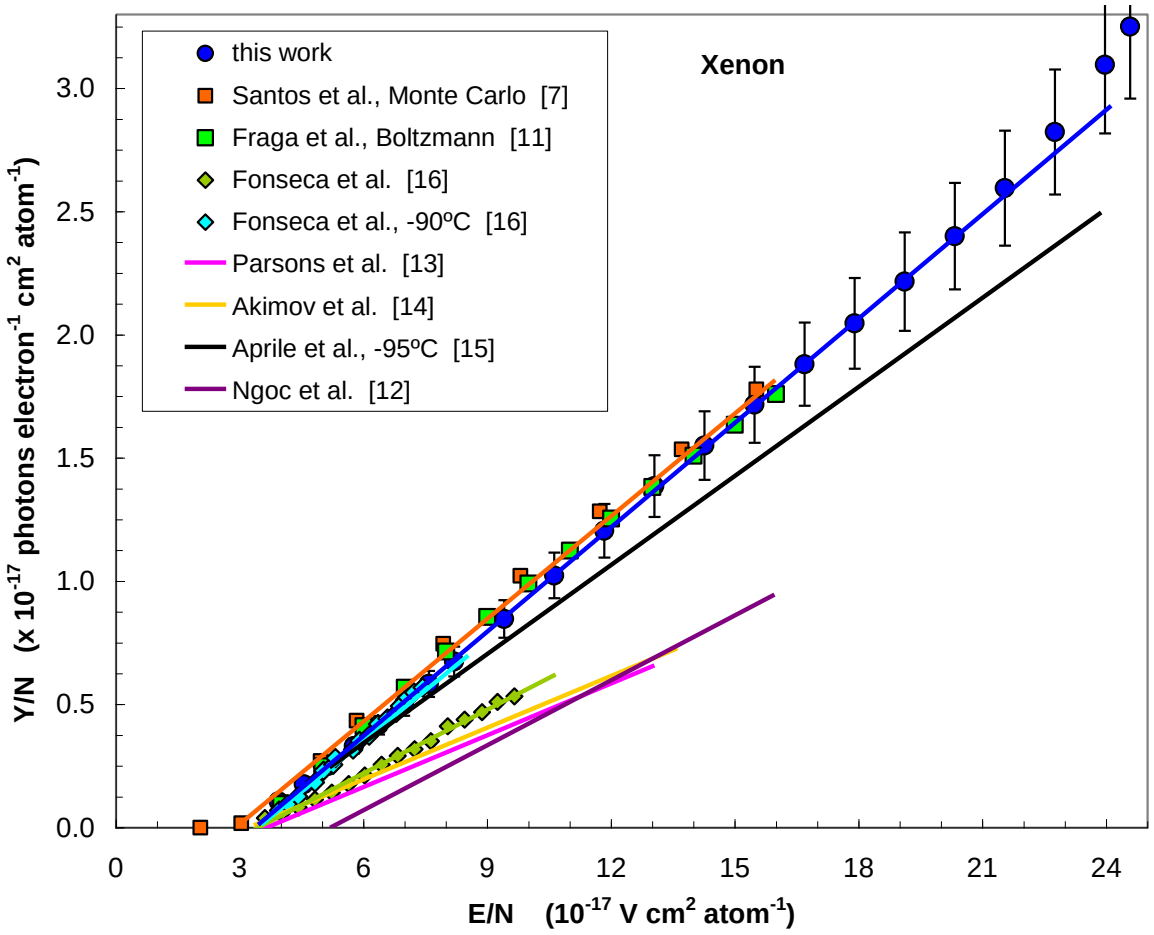

Figure 3.4 – Xenon reduced electroluminescence yield as a function of reduced electric field for these studies, as well as for the different data reported in the literature.

The results are in good agreement with those obtained with Monte Carlo simulation and Boltzmann calculation for room temperature.

Table I summarizes the different values found in the literature for the scintillation amplification parameter and their respective experimental conditions concerning pressure and temperature. The value of 70 photons kV^{-1}, obtained by Parsons et al. (1989) [13] and

confirmed by Akimov et al. (1997) [14] is a factor of two lower than that obtained by Monte Carlo simulation and Boltzmann calculation. In 2003, Aprile et al. [15] have estimated a value of 120 photons kV^{-1} from their experimental measurements in saturated xenon vapour, a value that is in much better agreement with the Monte Carlo simulation and Boltzmann calculation. The value obtained by Fonseca et al. [16] for the amplification parameter in saturated xenon vapour, at -90°C, is in very good agreement with that obtained by simulation and calculation for room temperature, but their value obtained at room temperature is about 90 photons kV^{-1}, a similar value to what had been obtained by Ngoc et al. (1980) [12].

The measurements presented in this chapter have shown, for the first time that, even for room temperature, the scintillation amplification parameter can be as high as those predicted by Monte Carlo simulation and/or Boltzmann analysis and those experimentally obtained for saturated xenon vapour at cryogenic temperatures. The differences in the experimental values obtained at room temperature can be attributed to different levels of gas purity achieved in each experimental set-up. Electron collisions with molecular impurities lead to energy losses through excitation of rotational and vibrational molecular states, which de-excite without emitting scintillation. Hence, higher impurity content will result in less efficient energy transfer from the electric field to photons, leading to lower scintillation amplification values.

Table I – Xenon scintillation amplification parameter, reduced electroluminescence yield linear trends and experimental conditions of pressure and temperature for the present studies, as well as for the different data reported in the literature.

Work	Amplification parameter (photon/kV)	Linear Trend		Pressure	Temperature
		Density units*	Pressure units**		
Present studies	140	Y/N = 0.140 E/N - 0.474	Y/p = 140 E/p - 116	1.52 bar	20ºC
Santos et al. (MC) [7]	139	Y/N = 0.139 E/N - 0.402	Y/p = 139 E/p - 100	1 atm	20ºC
Fraga et al. (Boltzmann) [11]	138	Y/N = 0.138 E/N - 0.413	Y/p = 138 E/p - 102	1 atm	20ºC
Fonseca et al. [16]	137	Y/N = 0.137 E/N - 0.470	Y/p = 137 E/p - 125	2 bar	-90ºC
Aprile et al. [15]	120	Y/N = 0.120 E/N - 0.378	Y/p = 120 E/p - 154	2 atm	-95ºC
Ngoc et al. [12]	88	Y/N = 0.088 E/N - 0.479	Y/p = 88 E/p - 113	2 - 10 atm	20ºC
Fonseca et al. [16]	86	Y/N = 0.086 E/N - 0.296	Y/p = 86 E/p - 73	2 bar	20ºC
Parsons et al. [13]	70	Y/N = 0.070 E/N - 0.255	Y/p = 70 E/p - 63	5 atm	20ºC
Akimov et al. [14]	70	Y/N = 0.070 E/N - 0.224	Y/p = 70 E/p - 56	2, 4, 8 atm	20ºC

* E/N in Td (10^{-17} V cm^2 atom^{-1});

** E/p in kV cm^{-1} bar^{-1}

3.6. Conclusions

Since the early years of study and development of gas proportional scintillation counters, it was well established that the reduced electroluminescence yield presents an approximately linear dependence on the reduced electric field in the scintillation region, presenting a scintillation threshold at a reduced electric field of about 0.8 $kVcm^{-1}bar^{-1}$ (e.g. Ref. [28] and references therein), as exhibited in figure 3.4. However, the scintillation amplification parameter - the number of photons produced per drifting electron and per volt, i.e. the slope of the linear dependence - presented many different values in the literature and was not well established yet. Above a reduced electric field of 4.5 $kVcm^{-1}bar^{-1}$, the xenon ionisation threshold, the reduced scintillation yield variation departs from the linear behaviour, reflecting the exponential growth in the number of electrons produced in the scintillation gap. This is due to the fact that secondary electrons also produce electroluminescence, while Y/N is calculated per primary electron. Favata et al. [31] reported a detailed study of the electroluminescence yield as a function of reduced electric field and compiled the different studies on electroluminescence yield published up to then (1990), concluding that the reduced electroluminescence yield is pressure-independent. Fonseca et al. [16] have shown that the scintillation yield does not depend on the xenon temperature, in the range from 20 down to -88ºC. On the other hand, for -90ºC and at constant gas pressure, the scintillation amplification factor near the

saturation point varies significantly, depending on the amount of xenon present in the liquid phase.

A scintillation amplification parameter, i.e., number of photons produced per drifting electron and per volt, of 140 photons kV^{-1}, was measured in the present studies. The results are in good agreement with those predicted by Monte Carlo simulation and Boltzmann calculation for room temperature and also with those observed for saturated xenon vapour at cryogenic temperatures. The above result is about a factor of two higher than earlier results measured at room temperature. The differences exhibited in the experimental results obtained at room temperature may be attributed to different levels of gas purity, or else, to the more complex methods used in the former calibration procedures, which may lead to higher inaccuracies and larger errors.

3.7. References

[1] J.M.F. Dos Santos, J.A.M. Lopes, J.F.C.A. Veloso, P.C.P.S. Simões, T.H.V.T. Dias, F.P. Santos, P.J.B.M. Rachinhas, L.F. Requicha Ferreira, C.A.N. Conde, *Development of portable gas proportional scintillation counters for x-ray spectrometry*, X-Ray Spectrom. **30** (2001) 373.

[2] C.A.N. Conde, *Gas Proportional Scintillation Counters for X-ray Spectrometry*, in X-Ray Spectrometry: Recent Technological Advances, Eds. K. Tsuji, J. Injuk and R. van Grieken, John Wiley & Sons (2004), ISBN: 0-471-48640-X.

[3] E.Aprile et al., *The XENON Dark Matter Experiment*, New Astronomy Reviews, 49 (2005) 289-295

[4] H.M. Araújo *et al. The ZEPLIN-III dark matter detector: performance study using an end-to-end simulation tool*, Astroparticle Physics **26** (2006) 140.

[5] H. Wang, *Xenon as a detector for dark matter search*, Phys. Reports 307 (1998) 263.

[6] T.H.V.T. Dias, F.P. Santos, A.D. Stauffer, C.A.N. Conde, *Monte Carlo simulation of x-ray absorption and electron drift in gaseous xenon*, Phys. Rev. A **48** (1993) 2887.

[7] F.P. Santos, T.H.V.T. Dias, A.D. Stauffer, C.A.N. Conde, *Three dimensional Monte Carlo calculation of the VUV electroluminescence and other electron transport parameters in xenon*, J. Phys. D: Appl. Phys. **27** (1994) 42.

[8] M. Suzuki, S. Kubota, *Mechanism of proportional scintillation in argon, krypton and xenon,* Nucl. Instrum. Meth. 164 (1979) 197.

[9] M.S.C.P. Leite, *Radioluminescence of rare gases*, Portugal. Phys. **11** (1980) 53.

[10] T. Takahashi, S. Himi, J. Ruan, S. Kubota, *Emission spectra from Ar-Xe, Ar-Kr, Ar-N2, Ar-CH4, Ar-CO2 and Xe-N2 gas scintillation proportional counters*, Nucl. Instrum. Meth. **205** (1983) 591.

[11] M.M.F.R. Fraga, C.M. Ferreira, J. Loureiro, M.S.C.P. Leite, presented at the 1990 ESCAMPIG, 28-31 Aug., Orleans, France.

[12] H.N. Ngoc, J. Jeanjean, H. Itoh, G. Charpak, *A xenon high-pressure proportional scintillation camera for x and γ-ray imaging*, Nucl. Instrum. Meth. **172** (1980) 603.

[13] A. Parsons, B. Sadoulet, S. Weiss, T. Edberg, J. Wilkerson, G. Smith, R.P. Lin, K. Hurley, *High pressure gas scintillation drift chambers with wave shifter fiber readout*, IEEE Trans. Nucl. Sci. **36** (1989) 931.

[14] D.Y. Akimov, A.A. Burenkov, D.L. Churakov, V.F. Kuzichev, V.L. Morgunov, G.N. Smirnov, V.N. Solovov, *Development of high pressure Xe scintillation proportional counter for experiments in "low-background" physics*, arXiv:hep-ex/9703011 v1 20 Mar 1997.

[15] E. Aprile, K.L. Giboni, P. Majewski, K. Ni, M. Yamashita, *Proportional Light in a Dual-Phase Xenon Chamber*, IEEE Trans. Nucl. Sci. **51** (2004) 1986; presented at the IEEE Nucl. Sci. Symp., November 2003, Seattle, USA.

[16] A.C. Fonseca, R. Meleiro, V. Chepel, A. Pereira, V. Solovov and M.I. Lopes, Study of Secondary Scintillation in Xenon Vapour, *2004 IEEE Nucl. Sci. Symp. Conference Record (2005)*.

[17] M. Moszynski, M. Szawlowski, M. Kapusta, M. Balcerzyk, *Large area avalanche photodiodes in scintillation and X-rays detection*, Nucl. Instrum. Meth. A **485** (2002) 504-521.

[18] Deep-UV series, Advanced Photonix Inc., http://www.advancedphotonix.com/

[19] L.M.P. Fernandes, J.A.M. Lopes, C.M.B. Monteiro, J.M.F. Dos Santos, C.A.N. Conde, *Non-linear behavior of large-area avalanche photodiodes*, Nucl. Instrum. Meth. A **478** (2002) 395.

[20] J.F.C.Veloso, J.A.M. Lopes, C.A.N.Conde, L.M.P. Fernandes, E.D.C. Freitas, O. Huot, P. Knowles, F: Kottmann, F. Mulhauser, J.M.F. dos Santos and D. Taqqu, *Gas proportional scintillation counters for the μp Lamb-shift experiment*, IEEE Trans. Nucl. Sci. **49** (2002) 899.

[21] M. Szawlowski, Advanced Photonix Inc., private communication (2002).

[22] B. Zhou, M. Szawlowski, *An explanation on the APD spectral quantum efficiency in the deep UV range*, Interoffice Memo, Advanced Photonix Inc., 1240 Avenida Acaso, Camarillo, CA 93012, EUA, 1999.

[23] J.A.M. Lopes, J.M.F. Dos Santos, R.E. Morgado, C.A.N. Conde, *A xenon gas proportional scintillation counter with a UV-sensitive, large-area avalanche photodiode*, IEEE Trans. Nucl. Sci., **48** (2001) 312-319.

[24] G.F. Knoll, Radiation Detection and Measurement, 3rd Edition, Wiley, New York, 2000.

[25] J.M.F. dos Santos, A.C.S.M. Bento, C.A.N. Conde, *The dependence of the energy resolution of gas proportional scintillation counters on the scintillation region to photomultiplier distance*, IEEE Trans. Nucl. Sci. **39** (1992) 541.

[26] T.H.V.T. Dias, J.M.F. dos Santos, P.J.B.M. Rachinhas, F.P. Santos, C.A.N. Conde, A.D. Stauffer, *Full-energy absorption of x-ray energies near the Xe L-and K-photoionization thresholds in xenon gas detectors: Simulation and experimental results*, J. Appl. Phys. **82** (1997) 2742.

[27] http://physics.nist.gov/PhysRefData/Xcom/html/xcom1.html

[28] M.A. Feio, A.J.P.L. Policarpo, M.A.F. Alves, Jap. J. Appl. Phys. **8** (1982) 1184.

[29] F.I.M.G. Borges, J.M.F. dos Santos, T.H.VT..Dias, F.P. Santos, P.J.B.M. Rachinhas, C.A.N. Conde, *Operation of gas proportional scintillation counters in a low charge multiplication regime*, Nucl. Instrum. Meth. A **422** (1999) 321.

[30] L.M.N. Fernandes, E.D.C. Freitas, M. Ball, J.J. Gómez-Cadenas, C.M.B. Monteiro, N. Yahlali, D. Nygren and J.M.F. dos Santos, *Primary and secondary scintillation measurements in a xenon Gas Proportional Scintillation Counter*, J. Inst. **5** (2010), in press.

[31] F. Favata, A. Smith, M. Badvaz, T. Kowalski, *Light yield as a function of gas pressure and electric field in gas scintillation proportional counters*, Nucl. Instrum. Meth. A **294** (1990) 595.

[32] R. Neilson, F. LePort, A. Pocara, K. Kumar, A. Odian et al. (EXO Collaboration), *Characterization of large area APDs for the EXO-200 detector*, Nucl. Instrum. Meth. A **608** (2009) 68.

CHAPTER 4

Argon Electroluminescence in Uniform Electric Field

4. Motivation

Experiments to search for "cold" Dark Matter predicted by the Standard Model are a high point in contemporary particle physics and cosmology. Double phase detectors with a noble gas as the active target are used, not only in several of the ongoing Dark Matter search experiments [1-4], but also in the future large-scale particle detectors proposed in Europe as the next generation underground observatories [5]. The selection of the target material is of capital importance and significantly depends on the expected detection thresholds, along with

the level of background contamination coming from radioactive isotopes.

The weakly interacting, massive sub-atomic sized Weakly Interacting Massive Particles (WIMPs) may produce nuclear recoils with energies ranging from 10 to 100 keV. The simultaneous detection of both ionisation and scintillation signals in a noble gas/liquid can lead to a unique signature for the energy deposited by the recoiling nucleus in the target volume, like the ICARUS collaboration already showed in 1993 [6]. The low event rate, which is for argon and xenon typically of the order of 0-6 event/kg/day, compels the detector to have a very large mass, which is realistically feasible for both liquid argon and xenon. Yet, a number of arguments validate the preference for argon over xenon. Besides being much more expensive and difficult to produce large quantities of ultra-pure liquid xenon than of ultra-pure liquid argon, for energy thresholds above 30 keV the sensitivity for argon is similar to that for xenon. For higher recoil energies, one can expect higher signal rates in argon because the form factor decreases faster for xenon [7], so that gold-plated high energy recoil events are less suppressed in argon. In addition, fast extraction of electrons through the liquid-gas boundary, for primary ionisation amplification, occurs much earlier for argon than for xenon. For the latter, there is practically no fast extraction for electric fields below 2 $kVcm^{-1}$, being the extraction efficiency only about 90% even at 5 $kV\ cm^{-1}$ [8,9], while for argon the fast electron extraction is almost complete at field values of 3 $kV\ cm^{-1}$ [8,10]. To obtain similar efficiencies, the extraction field in xenon must be circa a factor of 4 larger than the one needed for argon

[4]. Nevertheless, the kinematics of recoils in argon and xenon are different, providing different spectra, which presents a useful cross-check.

Argon Dark Matter (ArDM) [3] and the recently proposed GLACIER [5] programmes use large mass liquid argon detectors based on the dual-phase technique. Following an ionisation event, the detector readout collects the primary scintillation, while the produced primary ionisation is extracted from the liquid into the gas phase to be amplified by Large Electron Multipliers (LEMs). The ratio of the secondary ionisation over the primary scintillation gives the signature for the different nuclear recoil events.

Regarding the characteristically low rate and high background of these experiments, to effectively discriminate de recoiling events from the background it is crucial to have the highest possible gain in the detector.

Since long it has been known that electroluminescence provides signals several orders of magnitude larger than the corresponding charge signals [11,12], making them most suitable to apply to this kind of experiments. Therefore, especially in experiments with very low event rates and/or high background levels, as are the Dark Matter experiments, it is of great importance to use the electroluminescence signal rather than the charge signal.

The WIMP Argon Programme (WARP) [4,10] and the study of coherent neutrino nucleus scattering [13] make use of the

electroluminescence amplification method in the gas phase of their argon double-phase detectors.

While for xenon the electroluminescence yield is already well-established [14 and references therein], for argon this is not the case. In the literature, the only references found were a Monte Carlo simulation study [15] and an experimental study of WARP [10]. While [13] quotes the results of Dias et al. [15], the WARP collaboration reports a value of 32 photons/primary electron/cm in argon, at a pressure of 1 bar and at a temperature of 87 K, for an electric field of 5 kV cm^{-1}, which is almost one order of magnitude lower than the Monte Carlo values of [15]. This disagreement created a gap in this issue and, considering the convenience of the direct application e.g. in high-gain double-phase argon detectors for Dark Matter search, led to the necessity of determining the electroluminescence yield in argon more accurately.

The current chapter presents the results for the electroluminescence yield obtained for argon through the simple method already used for the determination of the xenon electroluminescence yield, in the former chapter. The obtained results were in very good agreement both with experimental results from other groups as well as with Monte Carlo simulation studies and Boltzmann calculations [14 and references therein], which brings out the reliability of the method. The results for argon are compared with those from [4,10,15] in the literature, as well as with the results obtained earlier for xenon [14] presented in the former chapter.

4.1. Experimental Setup

The experimental system used for these studies is a Gas Proportional Scintillation Counter which used a Large Area Avalanche Photodiode as the VUV photosensor, depicted schematically in figure 4.1 and was already used in [16]. For these studies, the used fill gas was argon.

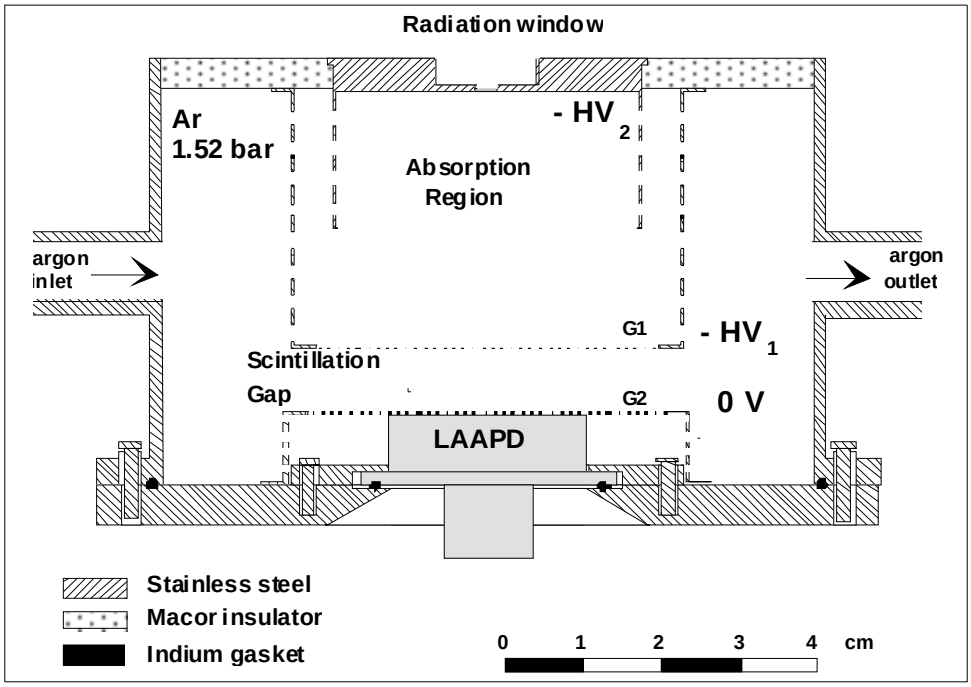

Figure 4.1 – Schematic of the GPSC equipped with an LAAPD as the VUV-photosensor, used in the studies of this chapter with a large area avalanche photodiode as the VUV photosensor.

The GPSC enclosure is a stainless steel cylinder with 10 cm in diameter and 5 cm in height. It is a standard, uniform field type GPSC

with a 2.5-cm deep drift/absorption region and a 0.8-cm deep scintillation region. This region is limited by two grids, G1 and G2, which are of highly transparent stainless steel wire, 80 μm in diameter and 900-μm spacing. The detector radiation window is made of Melinex, 6-μm thick and 2 mm in diameter. A Macor piece insulates the holders of both radiation window and grid G1. A low vapour pressure epoxy was used to vacuum-seal the Macor piece, the radiation window and holder as well as the voltage feedthrough of G1. The LAAPD was placed just below the second grid, G2, and was vacuum-sealed by compressing the photodiode enclosure against the stainless steel detector body, using an indium ring. The GPSC was vacuum pumped to pressures below 10^{-5} mbar and, then, filled with argon at a pressure of 1.52 bar. The gas was continuously purified by convection through St707 SAES getters [17], which were set at a stable temperature of about 150ºC.

The GPSC radiation window and its focusing electrode were operated at negative voltage while G2-holder, as well as the LAAPD enclosure, were maintained at ground potential. The voltage difference between the radiation window and G1 determines the reduced electric field E/p - the electric field intensity divided by the gas pressure-, in the absorption region, while the voltage of G1 determines the reduced electric field in the scintillation region. The LAAPD is a deep-UV enhanced series [18], has a 16-mm active diameter and was biased at 1725 V, corresponding to a gain of approximately 40. The LAAPD signals were fed through a low-noise, 1.5 V/pC, charge pre-amplifier to an amplifier with 2-μs shaping time, and were pulse-height analysed with a multi-channel analyser (MCA).

The pulse-height distributions were fit to Gaussian functions superimposed on a linear background, from which the pulse amplitudes, taken as the Gaussian centroid, were determined.

4.2. Experimental Results

Incident X-rays interact mostly in the absorption region, where the electric field is lower than the argon excitation threshold, and the resulting primary electron cloud drifts towards the scintillation region, where the value of the electric field is stronger than in the absorption region, yet lower than the argon ionisation threshold. Upon crossing the scintillation region, the drifting primary electrons gain from the electric field enough energy to excite but not ionise the argon atoms producing, as a result of the argon atoms de-excitation processes, a light-pulse that is, in average, proportional to the number of primary electrons, and so, to the incident X-ray energy. The statistical fluctuations associated to the light amplification processes are negligible when compared to those associated to charge avalanche amplification characteristic of the proportional counters, as well as to those associated to the primary electron cloud formation.

The secondary scintillation, or proportional scintillation, is also called electroluminescence, which reduced yield, Y/p, is defined as being the number of secondary scintillation photons produced per drifting primary electron per unit path length and per unit pressure. It

can also be given as Y/N, i.e. the number of secondary scintillation photons produced per drifting primary electron per unit path length divided by the number density of the gas, N.

For pressures above a few tens of bar the electroluminescence spectrum of argon consists of a narrow line peaking at 128 nm, with 5 nm FWHM [19], called the second continuum. It corresponds to transitions of the singlet and triplet bound molecular states, from vibrationally relaxed levels, to the repulsive ground state. At atmospheric pressure, most of the emission is centered in the second continuum, being the emissions in the visible and in the infra-red regions negligible in comparison to those in the VUV range [19,20].

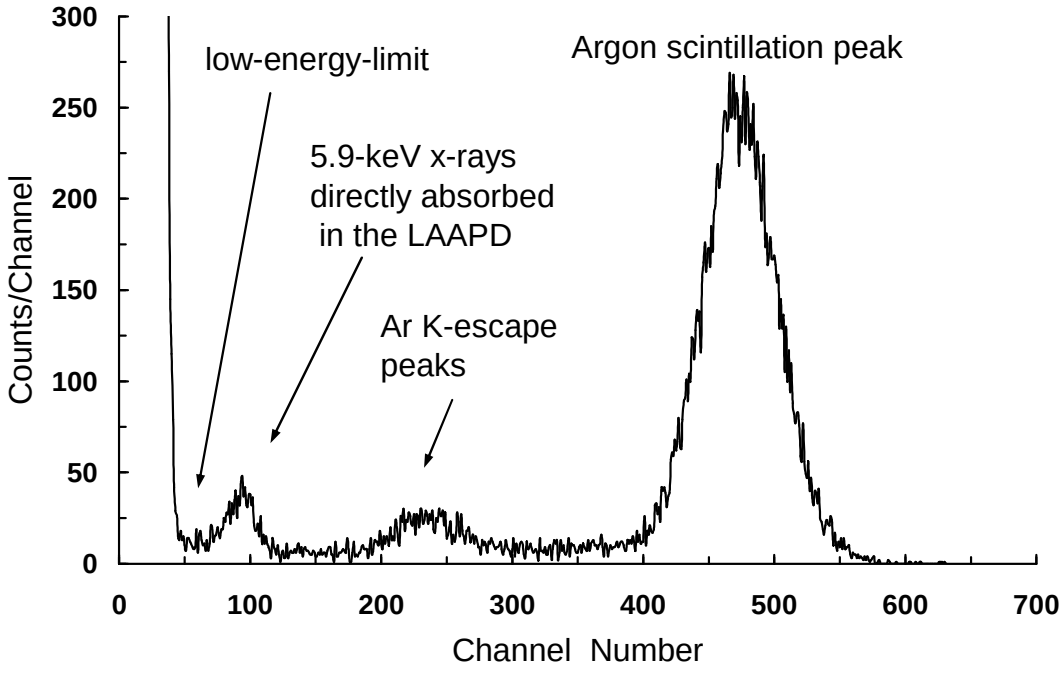

Figure 4.2 – Pulse-height distribution obtained for 5.9-keV X-rays, with the argon GPSC having a LAAPD as photosensor. E/p values of 0.15 and 3.75 kV cm^{-1} bar^{-1} were used in the absorption and scintillation region, respectively. The LAAPD was operated at a gain of approximately 40.

Figure 4.2 depicts a typical pulse-height distribution taken with this detector when irradiated with 5.9-keV X-rays from a ^{55}Fe radioactive source. The Mn K_β-line was absorbed by means of a chromium film placed in front of the radiation window. The spectral features comprise the argon scintillation peak, the argon K-fluorescence escape peaks, a peak resulting from the direct interaction of the 5.9-keV X-rays in the LAAPD, and the electronic noise tail in the low-energy limit.

The amplitude of the scintillation peaks depends on the biasing of the scintillation region of the GSPC as well as on the biasing of the LAAPD. As for the amplitude of the events resulting from direct X-ray interaction in the LAAPD, it just depends on the voltage applied to the LAAPD. The events ensuing direct interaction in the LAAPD are visible even when the electric field applied to the scintillation region is zero or reversed.

Figure 4.3 depicts the GPSC relative amplitude as a function of reduced electric field, E/p, in the scintillation region. The results follow the typical behaviour of electroluminescence in noble gases, i.e. an approximately linear dependence on the reduced electric field in the scintillation region, with the scintillation threshold at an E/p value of about 0.55 $kVcm^{-1}bar^{-1}$ for argon (e.g. Ref. [30] and references therein). Above a reduced electric field of 2.8 $kVcm^{-1}bar^{-1}$, the argon ionisation threshold, the relative amplitude variation departs from the linear behaviour, reflecting the exponential growth in the number of electrons produced in the scintillation region by the drifting electron cloud.

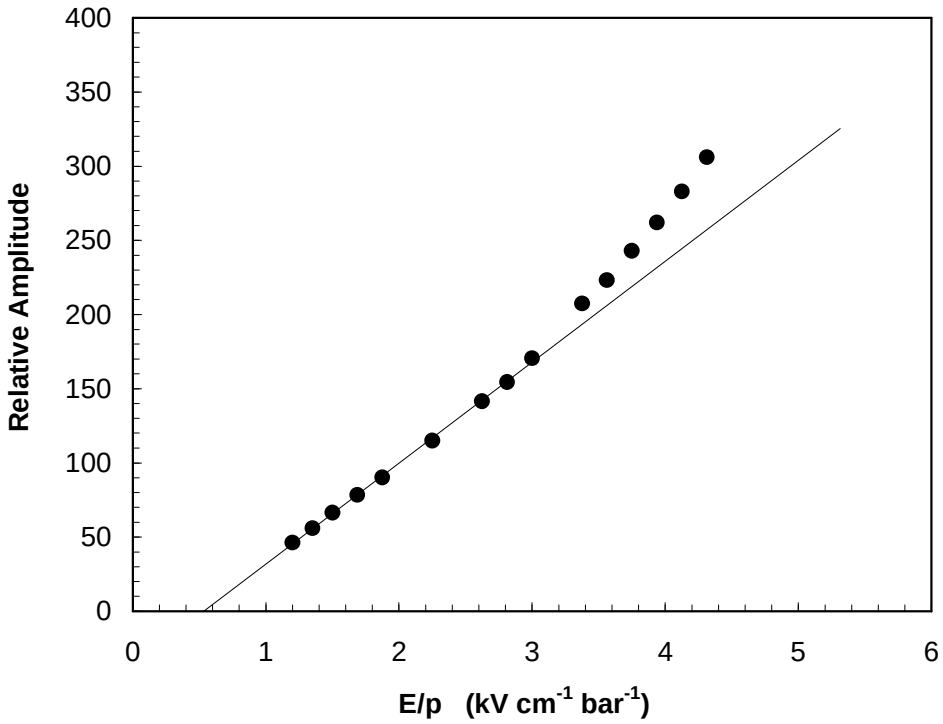

Figure 4.3 – Detector relative pulse amplitude as a function of reduced electric field in the scintillation region. The line represents the least square fit to the points below 4.0 $V^{-1}cm^{-1}Torr^{-1}$. The reduced electric field in the drift region and the LAAPD biasing were kept constant throughout the measurements.

4.3. Absolute Measurement of Electroluminescence Yield

For each pulse-height distribution, a ratio can be found between the pulse amplitudes resulting from the 5.9 keV X-ray full-absorption in the gas, i.e. from the argon electroluminescence, and direct absorption in the LAAPD. This ratio allows a direct quantification of the number of VUV-photons impinging the LAAPD, given its quantum efficiency. For

the LAAPDs acquired by our group, the manufacturer [22] provided for the quantum efficiency, QE, a value of approximately 0.55 for the number of charge carriers produced in the LAAPD per incident 128-nm VUV photon, figure 2.4 of chapter 2. An uncertainty of about ± 0.10 was considered for the LAAPD quantum efficiency [21,23,24], being this the major source of uncertainty in the presented measurements.

The average number of primary electrons produced by the full absorption of the 5.9-keV X-rays in argon is

$$N_e = \frac{5895\ eV}{26.4\ eV} \cong 223 \text{ electrons} \qquad (4.1)$$

considering a w-value for argon of 26.4 eV [25].

For a reduced electric field of 3.75 $kVcm^{-1}bar^{-1}$, and for low LAAPD gains, around 40, where gain non-linearity in the photodiode is less than 1% [26], the ratio between the pulse amplitudes resulting from 5.9-keV X-ray full-absorption in argon and those absorbed in the LAAPD is A_{UV}/A_{XR} = 4.8. Considering a w-value in silicon of 3.62 eV [27], the average number of free electrons produced by full absorption of the 5.9-keV X-rays in the photodiode is

$$N_{XR} = \frac{5895\ eV}{3.62\ eV} \cong 1.63 \times 10^3 \text{ electrons.} \qquad (4.2)$$

For the scintillation pulses due to the 5.9-keV X-ray full-absorption in the gas, the average number of VUV photons that reach the photodiode is

$$N_{UV,APD} = \frac{A_{UV}}{A_{XR}} \times \frac{N_{XR}}{QE} \cong 1.42 \times 10^4 \text{ photons.} \qquad (4.3)$$

The average solid angle, Ω, subtended by the active area of the photosensor for the primary electron path has been computed accurately by Monte Carlo simulation [28]. A value of

$$\Omega_{rel} = \frac{\Omega}{4\pi} \cong 0.215 \qquad (4.4)$$

was obtained for the geometry used. Hence, the total number of VUV photons produced by full absorption of the 5.9-keV X-rays in the detector is

$$N_{UV,total} = \frac{N_{UV,APD}}{\Omega_{rel} \times T} \cong 7.8 \times 10^4 \text{ photons} \qquad (4.5)$$

where T is the grid optical transparency, which was calculated to be 84%.

In this way, the reduced electroluminescence yield, Y/p, determined for 3.75 kVcm^{-1}bar^{-1} is

$$\frac{Y}{p}\ (3.75 \text{ kVcm}^{-1}\text{bar}^{-1}) = \frac{N_{UV,APD}}{N_e \times d \times p} \cong 290 \qquad (4.6)$$

photons, per primary electron, per cm of drift path and per bar.

Taking into account the distortion of the electric field around the wires of the anode mesh, G2, the above obtained electroluminescence yield is somewhat overestimated due to the additional scintillation

produced in the more intense field around the wires. This scintillation can be estimated and the calculations are presented in the next section.

4.4. Scintillation production around the grid wires

To calculate the amount of the additional scintillation produced around the grid wires, a 3D electric field simulator was used to obtain the field values in the scintillation gap and around the wires. Figure 4.4 depicts a 3D simulation of the electric field intensity in the mesh plane, x-y. The electric field intensity increases only around the wires while in the region between the wires the intensity is low.

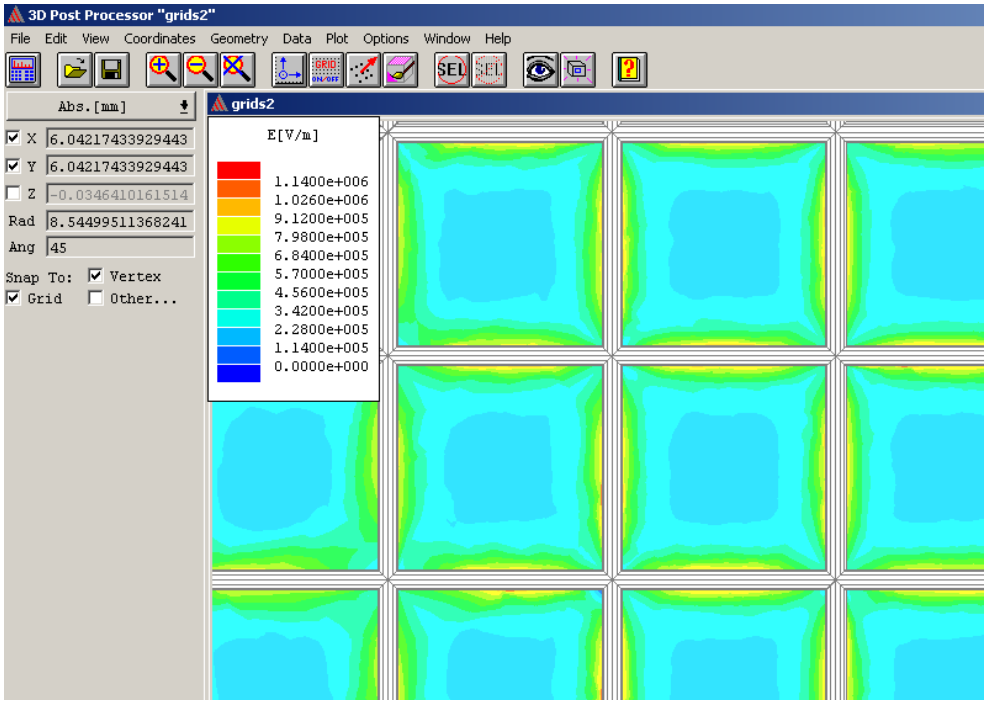

Figure 4.4 – 3D simulation of the electric field in the mesh plane (x-y plane).

Figure 4.5 shows the electric field intensities around the wires in a plane perpendicular to the mesh, y-z, which contains one wire. This

situation represents the worst of all cases for the increase of the electric field near the wires, in comparison to other planes with angles less than 90º in respect to the mesh plane. The most favourable case will be the 0º, i.e. the mesh plane itself, figure 4.4. As seen in figure 4.5, the electric field departs from a constant value in the scintillation gap, increasing towards the wires for distances lower than 500 μm. A reduced electric field value of 4 V $cm^{-1}torr^{-1}$ in the scintillation region was used for the simulation presented in figure 4.5.

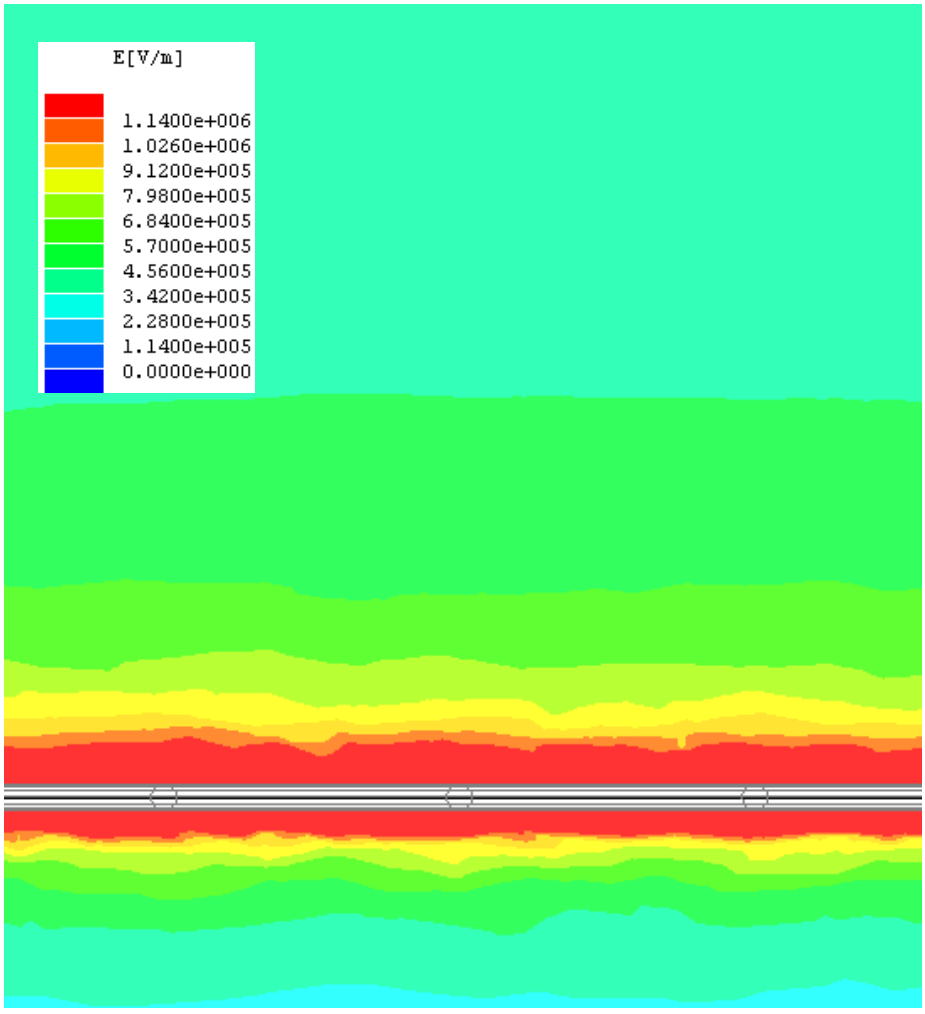

Figure 4.5 – Detail of the electric field 3D simulation around the wires of the mesh in a plane perpendicular to the mesh (y-z plane), containing one wire. A reduced electric field value of 4 V $cm^{-1}torr^{-1}$ in the scintillation region was used for the simulation presented in figure 4.5.

For each value of the reduced electric field in the scintillation region, the values of the reduced electric field as a function of distance to the wire centre can be obtained from the simulator. From these values, the first Townsend coefficient and the excitation coefficient can be obtained as a function of distance to the wire centre.

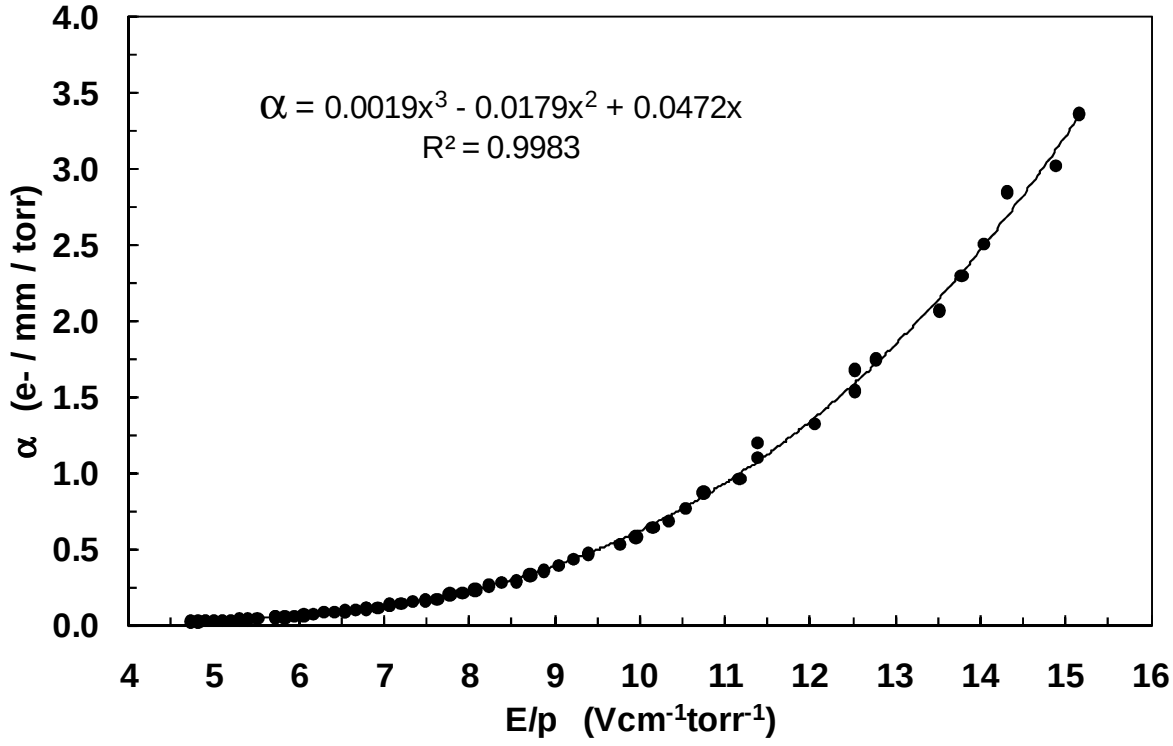

Figure 4.6 – The first Townsend coefficient as a function of reduced electric field, as extracted from the data of [29].

The first Townsend coefficient, for argon, as a function of reduced electric field was obtained from [29], figure 4.6, and the excitation coefficient, also as a function of reduced electric field, was obtained

from a 3D Monte Carlo Simulation of electron transport in noble gases [30,31], figure 4.7.

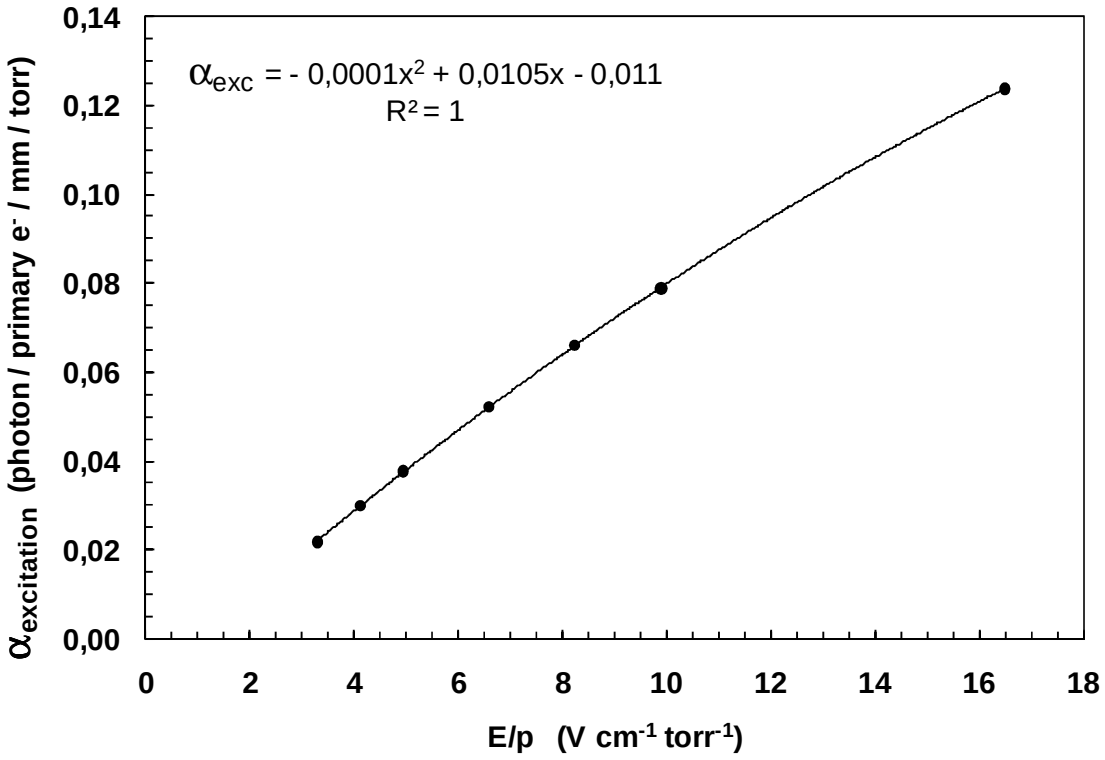

Figure 4.7 – Excitation coefficient as a function of reduced electric field, according to [15,31].

In figure 4.8, the average values of the reduced electric field are shown as a function of distance to the wire centre, in a plane perpendicular to the mesh, containing one wire, figure 4.5, and for two cases, namely in the nodes and at half-distance between two nodes. A reduced electric field value of 4 V $cm^{-1}torr^{-1}$ in the scintillation region was used in this case.

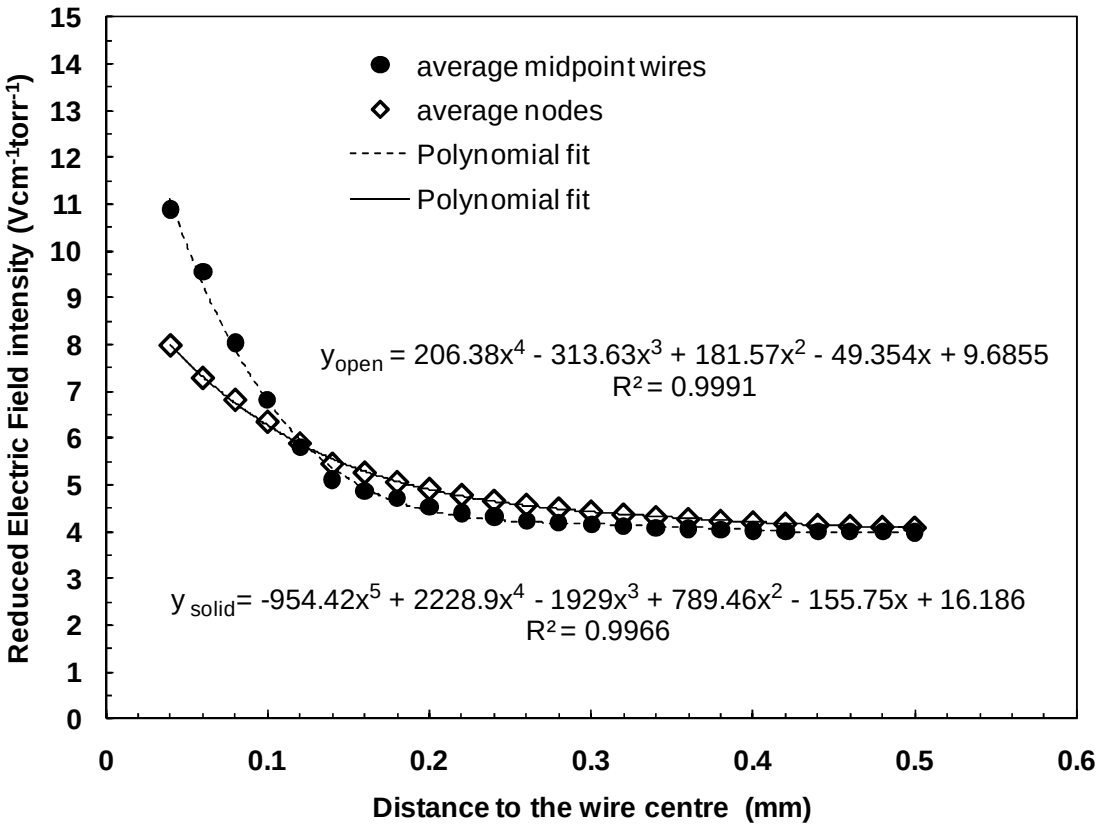

Figure 4.8 – Average values of the reduced electric field as a function of distance to the wire centre in a plane perpendicular to the mesh (y-z plane), containing one wire, and for two cases: in the nodes (open symbols) and at half-distance between two nodes (solid symbols), as given by the 3D electric field simulator.

In figure 4.9 the first Townsend coefficient is depicted as a function of distance covered by the electrons on their path towards the wire, for the worst case of figure 4.8, that is, considering the electric field for the path ending at a point located half-way between two nodes and a reduced electric field of 4 Vcm^{-1}torr^{-1} in the scintillation region. In this figure, a different axis, z', has been chosen, namely z' = 0 mm at z = 0.5 mm and z' = 0.5 mm at z = 0 mm, i.e. at the centre of the wire, to match

the direction of the electron drift. From figure 4.9 it is clear that the first Townsend coefficient only begins to increase significantly in the last 0.1 mm from the wire centre.

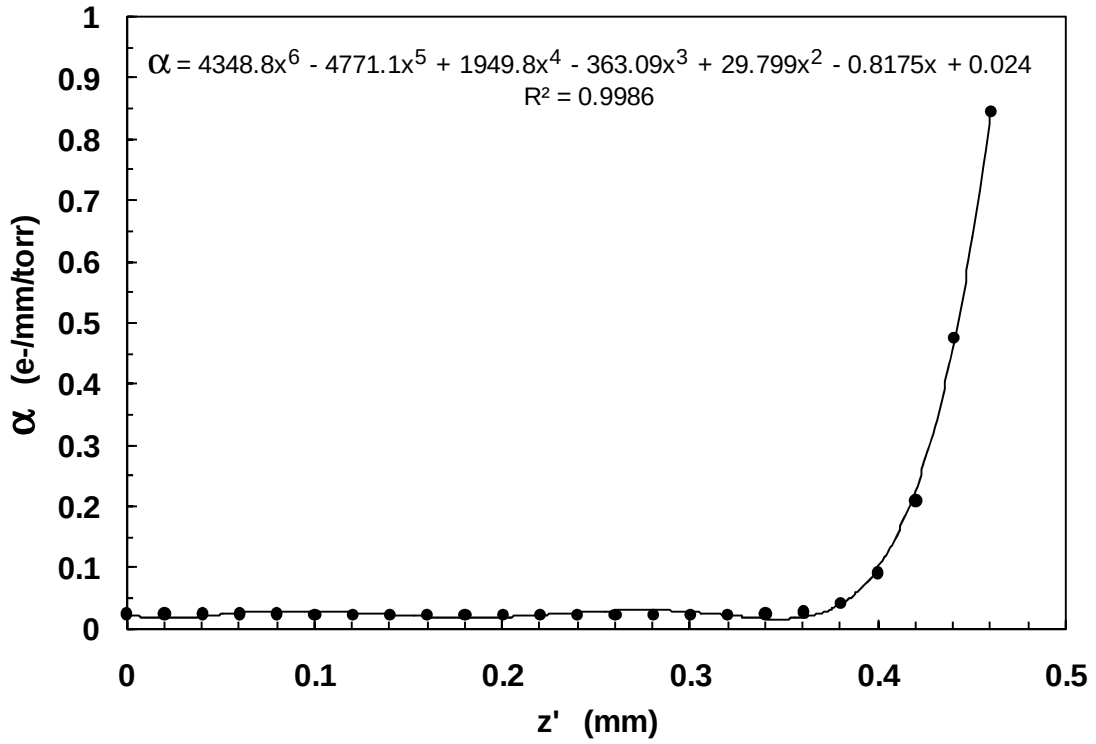

Figure 4.9 - First Townsend coefficient as a function of distance covered by the electrons starting at 0.5 mm distance from the wire centre, z' = 0 mm, and for the path ending in the wires, at a point located half-way between two nodes and for a reduced field of 4 $Vcm^{-1}torr^{-1}$ in the scintillation region.

From the polynomial fit, it is possible to calculate the charge multiplication gain, G, in the vicinity of the wires. G is given by [27],

$$\text{Ln G} = \int_0^{0.46} \alpha\,(z')\,dz' \qquad (4.7)$$

being α the expression for the polynomial fit of figure 4.9. A value of G = 1.033 electron per primary electron was obtained for this gain.

In figure 4.10 the excitation coefficient is depicted as a function of distance z', for the worst case of figure 4.8, using a similar procedure as for the first Townsend coefficient in figure 4.9. The excitation coefficient only begins to increase significantly in the last 0.2 mm from the wire centre.

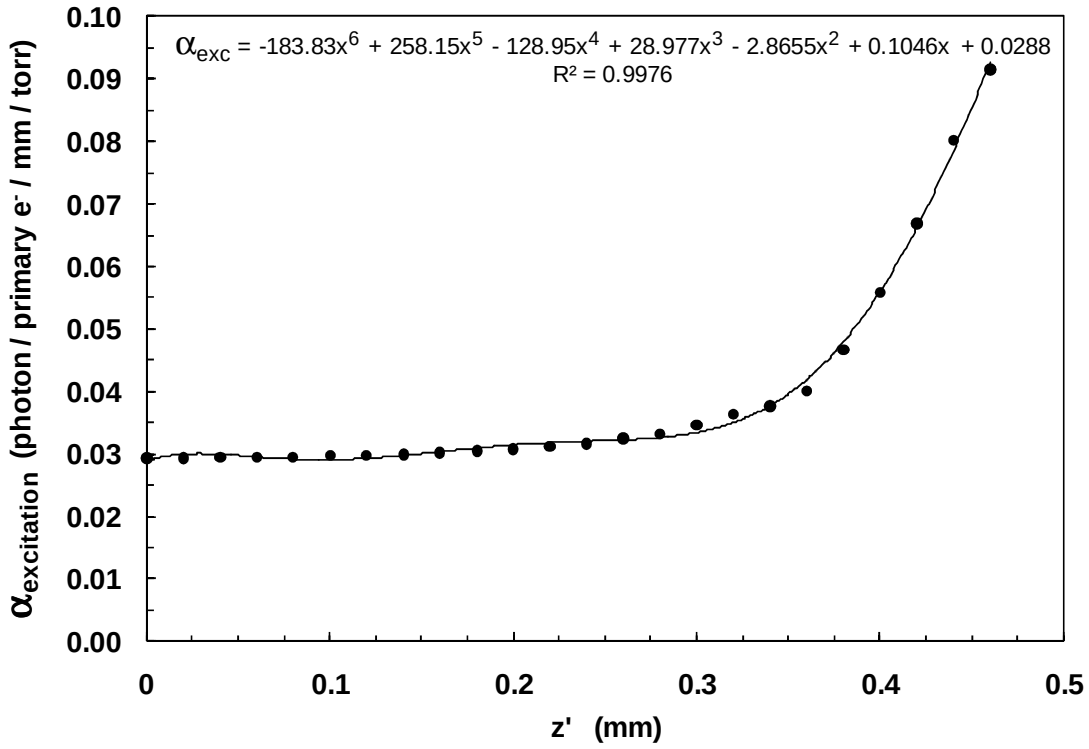

Figure 4.10 - Excitation coefficient as function of distance z' for the same conditions of figure 4.9.

Similarly to the ionisation, the scintillation produced along the path can be calculated from the polynomial fit. The number of photons produced per primary electron and per unit of pressure is given by

$$N_{uv} = \int_0^{0.46} G\,(z') \times \alpha_{exc}\, dz' \qquad (4.8)$$

being G(z') given by equation 4.7 with integration limits of 0 and z', and α_{excit} given by the expression for the polynomial fit of figure 4.10. Equation 4.8 can be simplified assuming for G(z') a constant value, equal to its maximum

$$N_{uv} = 1.033 \times \int_0^{0.46} \alpha_{exc}\, dz' \qquad (4.9),$$

i.e. assuming that all the electrons produced around the wires start at z' = 0 mm and transverse the whole path. Even though, once again, the calculation of the additional scintillation produced around the wires is overestimated, it will be shown to be small, not justifying more complex calculations.

From equation 4.9 a value of 0.0183 photons per primary electron and per unit of pressure is obtained. This should be compared with the value of 0.0147 photons per primary electron and per unit of pressure that would be obtained in the last 0.5 mm, if the reduced electric field around the wires was constant and equal to 4 $Vcm^{-1}torr^{-1}$, assuming the excitation coefficient from figure 4.7. Therefore, the number of additional photons produced around the wires is much less than 0.0036 photons per primary electron and per unit of pressure. Assuming once more an excitation coefficient from figure 4.7, for a reduced electric field of 4 $Vcm^{-1}torr^{-1}$ in the scintillation region, a total number of 15 × 0.0147 + 0.0183 = 0.2388 photons per primary electron and per unit of pressure, in a 8-mm thick scintillation region. This means that the total additional number of photons produced around

the wires is much less than 1.5%, what can be considered negligible, compared to the uncertainties in the experimental determination of the electroluminescence yield.

The same calculations were performed for several values of the reduced electric field in the scintillation region, down to 1.6 $Vcm^{-1}torr^{-1}$. The additional amount of scintillation around the wires increases with decreasing E/p in the scintillation gap and reaches an upper limit of 6% of the total amount of scintillation for an E/p value of 1.6 $Vcm^{-1}torr^{-1}$.

4.5. Argon Electroluminescence Yield

Figure 4.11 depicts Y/N, the electroluminescence yield divided by the number density of the gas, as a function of reduced electric field, E/N, in the scintillation region. Simulation results from one-dimensional Monte Carlo and experimental results from WARP are also presented for comparison [10,15]. The results obtained earlier for xenon [14] have also been included so that the behaviour for both gases, argon and xenon, can be observed simultaneously.

As expected [32], the behaviour of Y/N with E/N is approximately linear and can be given by

$$Y/N \ (10^{-17} \text{ photons electron}^{-1} \text{ cm}^2 \text{ atom}^{-1}) = 0.081 \ E/N - 0.190 \quad (4.10),$$

where E/N is given in Td (10^{-17} V cm^2 $atom^{-1}$). Equation (4.10) is universally valid, e.g. for room temperature as in the case of the present

measurements, and also at liquid argon temperature, as is the case of the WARP experiment.

The electroluminescence yield can also be represented as a function of pressure,

$$Y/p \text{ (photons electron}^{-1} \text{ cm}^{-1} \text{ bar}^{-1}) = 81\ E/p - 47 \qquad (4.11),$$

where E/p is given in kV cm^{-1} bar^{-1}. Equation (4.11) is valid at a given temperature, T, being T used to convert the density into pressure.

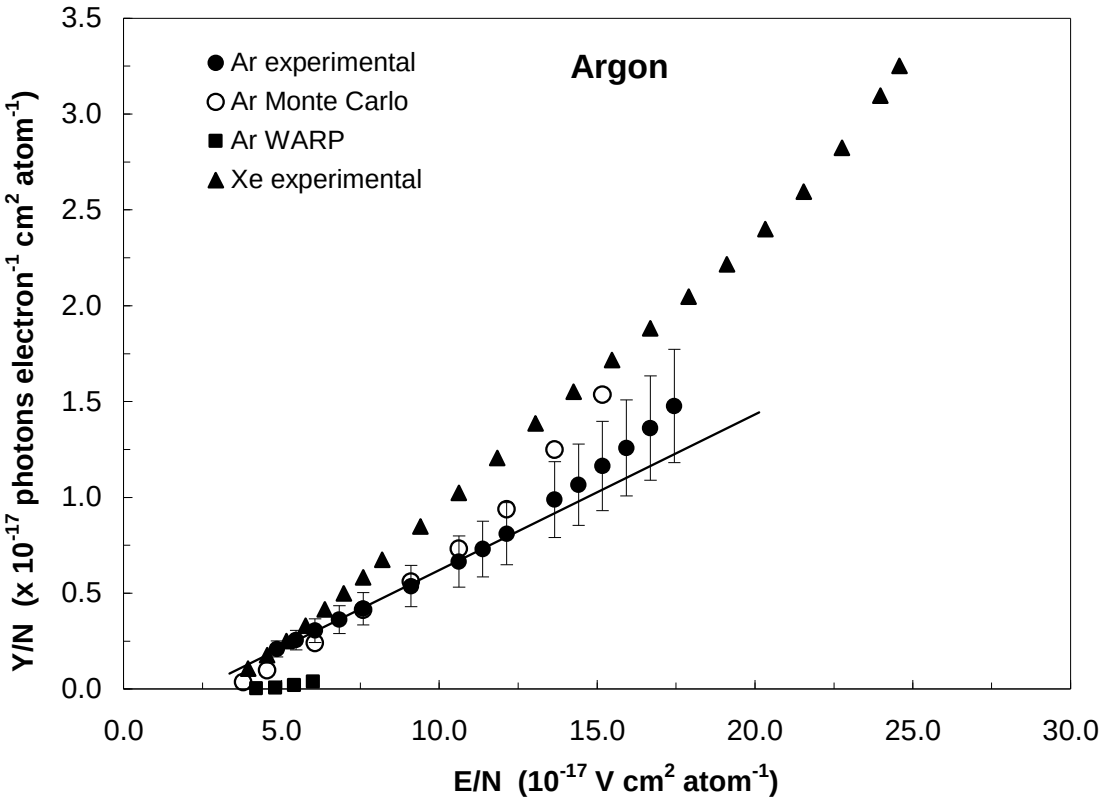

Figure 4.11 –Argon reduced electroluminescence yield as a function of reduced electric field obtained in these studies, as well as for data from Monte Carlo simulation [15] and experimental data from WARP [10] reported in the literature. For comparison, the experimental results obtained for xenon in the former chapter have also been included.

The slope of the linear dependence denotes the scintillation amplification parameter, i.e. the number of photons produced per drifting electron and per volt. Above the argon ionisation threshold, about 3 kV cm^{-1} bar^{-1} (corresponding to E/N of about 12 Td at 293° K), the reduced scintillation yield exhibits the typical exponential growth in the number of ionisation electrons in the scintillation gap. This is due to the fact that these electrons produce additional scintillation, while Y/N is calculated per primary electron.

By extrapolating to zero scintillation, the excitation threshold for argon was found to be about 0.7 ± 0.1 kV cm^{-1} bar^{-1} (corresponding to E/N ~ 2.7 ± 0.3 Td at 293° K).

Comparing these experimental results for argon with the Monte Carlo simulation results from [15] for a one-dimensional model, one can see that the present results agree well with the former, within errors. The main difference is the excitation threshold which, however, is in good agreement with [32-34]. According to the simulation studies, for an E/p value of 0.7 kV cm^{-1} bar^{-1}, the scintillation produced around the wires is more than 90% of the total scintillation produced in the gap. Preliminary results from a detailed 3D Monte Carlo program do not present significant differences from those obtained with one-dimensional Monte Carlo simulation [31].

Also, one can see that the experimental results from WARP are about one order of magnitude lower, which could be due to incorrect calibration/normalization procedures, or else to the presence of impurities in their active target, since the scintillation production is

very sensitive to this parameter [35], unlike charge production. Electron collisions with molecular impurities lead to energy losses through excitation of rotational and vibrational molecular states, which de-excite without emitting scintillation. Thus, higher impurity content will result in less efficient energy transfer from the electric field to photons, leading to lower scintillation amplification values.

The difference in temperature of both experimental setups, namely room temperature and 87 K, do not justify the difference in the results, as demonstrated, for xenon, in [36,14 and references therein].

The scintillation amplification parameter in argon is about 60% of that in xenon.

4.6. Conclusions

Experimental studies on the reduced electroluminescence yield of pure argon at room temperature have been performed and compared with both Monte Carlo simulation and experimental results from WARP, reported in the literature. The experimental measurements were taken with a gas proportional scintillation counter instrumented with a large area avalanche photodiode for the VUV secondary scintillation readout. X-rays with energy of 5.9 keV were used to induce the electroluminescence production in the GPSC or to interact in the photodiode. The X-ray direct interactions in the LAAPD were used as a

reference for the determination of the number of charge carriers produced by the scintillation pulse and, thus, the number of VUV photons impinging the photodiode, given its quantum efficiency.

These measurements have shown, for the first time that, even for room temperature, the scintillation amplification parameter can be as high as that predicted by Monte Carlo simulation. A scintillation amplification parameter, i.e. the number of photons produced per drifting electron and per volt, of 81 photons/kV was measured for reduced electric fields between 1.2 and 3.0 kV cm^{-1} bar^{-1}. The results are in good agreement with those predicted by Monte Carlo simulation for room temperature and about one order of magnitude higher than what was experimentally obtained by WARP. Differences in gas purity during the experimental measurements of the latter, or else, incorrect calibration/normalization procedures may be the factors responsible for the difference in their experimental results.

4.7. References

[1] J. Angle, E. Aprile, F. Arneodo, L. Baudis, A. Bernstein et al., *First Results from the XENON10 Dark Matter Experiment at the Gran Sasso National Laboratory*, Phys. Rev. Lett. 100, 021303 (2008),

[2] D.Yu. Akimov, G.J. Alner, H.M. Araújo, A. Bewick, C. Bungau et al., *The ZEPLIN-III dark matter detector: Instrument design, manufacture and commissioning,* Astroparticle Phys. 27 (2007) 46-60.

[3] A. Rubbia, *ArDM: a ton-scale liquid Argon experiment for direct detection of Dark Matter in the Universe,* arXiv:hep-ph/0510320 v1 24 Oct 2005

[4] *P. Benetti, R. Acciarri, F. Adamo, B. Baibussinov, M. Baldo-Ceolin et al., First results from a Dark Matter search with liquid Argon at 87 K in the Gran Sasso Underground Laboratory*, Astroparticle Phys. 28 (2008) 495–507.

[5] D. Autiero et al., *Large underground, liquid based detectors for astro-particle physics in Europe: scientific case and prospects*, arXiv:0705.0116v1

[6] P. Benetti, E. Calligarich, R. Dolfini, A. Gigli Berzolari, F. Mauriet al., *Detection of energy deposition down to the keV region using liquid xenon scintillation*, Nucl. Instr. Meth. A 327 (1993) 203-206.

[7] Bueno, M. C. Carmona, J. Lozano, and S. Navas, *Observation of coherent neutrino-nucleus elastic scattering at a beta beam*, Phys. Rev. D 74, 033010 (2006) DOI: 10.1103/PhysRevD.74.033010

[8] E.M. Gushchin, A.A. Krulov, I.M. Obodovskii, *Electron dynamics in condensed argon and xenon*, Sov. Phys. JETP 55 (5) (1982) 650-655.

[9] A. F. Borghesani, G. Carugno, M. Cavenago, and E. Conti, *Electron transmission through the Ar liquid-vapor interface*, Phys. Lett. A149 (1990) 481–484.

[10] WARP: Wimp ARgon Programme – Experiment Proposal. http://warp.lngs.infn.it/papers/proposal.pdf.

[11] C. A. N. Conde and A. J. P. L. Policarpo, *A gas proportional scintillation counter*, Nucl. Instr. Meth. Vol. 53 (1967) 7-12.

[12] A. S. Conceição, L. F. Requicha Ferreira, L. M. P. Fernandes, C. M. B. Monteiro, L. C. C. Coelho, C. D. R. Azevedo, J. F. C. A. Veloso, J. A. M. Lopes and J. M. F. dos Santos, *GEM scintillation readout with avalanche photodiodes,* JINST 2 P09010 (2007).

[13] C. Hagmann and A. Bernstein, *Two-Phase Emission Detector for Measuring Coherent Neutrino-Nucleus Scattering*, IEEE Trans. Nucl. Sci., Vol. 51 (2004) 2151-2155.

[14] C.M.B. Monteiro, L.M.P. Fernandes, J.A.M. Lopes, L.C.C. Coelho, J.F.C.A. Veloso, J.M.F. dos Santos, K. Giboni and E. Aprile, *Secondary scintillation yield in pure xenon*, JINST 2 P05001 (2007)

[15] THVT Dias, A D Stauffer and CAN Conde, *A unidimensional Monte Carlo simulation of electron drift velocities and electroluminescence in argon, krypton and xenon*, J. Phys. D: Appl. Phys.19 (1986) 527-545.

[16] C. M. B. Monteiro, J. A. M. Lopes, P. C. P. S. Simões, J. M. F. dos Santos, C. A. N. Conde, *An Argon Gas Proportional Scintillation Counter With UV Avalanche Photodiode Scintillation Readout*, IEEE Trans. Nucl. Sci., Vol. 48 (2001) 1081-1086.

[17] SAES Advanced Technologies S.p.A., Nucleo Industriale CP 9367 051-Avezzano (AQ), Italy.

[18] Advanced Photonix, Inc., 1240 Avenida Acaso, Camarillo, CA 93012, USA.

[17] M. Suzuki and S. Kubota, *Mechanism of proportional scintillation in argon, krypton and xenon*, Nucl.Instrum.Meth. 164 (1979) 197-199

[20] M.M.Fraga, F.A.F. Fraga, and A.J.P.L. Policarpo, *Modelling of an IR scintillation counter*, Nucl. Instrum. Meth. A 442 (2000) 423-427.

[21] M. Szawlowski, Advanced Photonix Inc., private communication (2002).

[22] B.-L. Zhou and M. Szawlowski, *An explanation on the APD spectral quantum efficiency in the deep UV range*, Advanced Photonix Inc., Interoffice Memo, Apr. 1999.

[23] R. Chandrasekharan, M. Messina, A. Rubbia, *Detection of noble gas scintillation light with large area avalanche photodiodes (LAAPDs)*, Nucl. Instrum. Meth. A 546 (2005) 426–437.

[24] R. Chandrasekharan, A. Knecht, M. Messina, C. Regenfus, and A. Rubbia, *High Efficiency Detection of Argon Scintillation Light of 128nm Using LAAPDs*, arXiv:physics/0511093 v1 10 Nov 2005.

[25] I. K. Bronic, *W values and Fano factors for electrons in rare gases and rare gas mixtures*, Hoshasen : Ionizing Radiation, vol. 24 (1998) 101-125.

[26] L.M.P. Fernandes, J.A.M. Lopes, C.M.B. Monteiro, J.M.F. Dos Santos and C.A.N. Conde, *Nonlinear behaviour of large-area avalanche photodiodes*, Nucl. Instrum. Meth. A 478 (2002) 395-399.

[27] G.F. Knoll, *Radiation detection and measurement*, 3rd Edition, Wiley, New York (2000).

[28] J.M.F. dos Santos, A.C.S.M. Bento and C.A.N. Conde, *The dependence of the energy resolution of gas proportional scintillation counters on the scintillation region to photomultiplier distance*, IEEE Trans. Nucl. Sci. 39 (1992) 541-545.

[29] A.E.D. Heylen, *Ionization Coefficients and Sparking Voltages in Argon and Argon-Ethane Mixtures*, Brit. J. Appl. Phys. (J. Phys. D), Vol.1, Ser.2 (1968) 179;

[30] F.P. Santos, T.H.V.T. Dias, A.D. Stauffer, C.A.N. Conde, *Three-dimensional Monte Carlo calculation of the VUV electroluminescence and other electron transport parameters in xenon*, J. Phys. D: Appl. Phys. 27 (1994) 42.

[31] T.H.V.T. Dias, Private communication.

[32] M.A. Feio, A.J.P.L. Policarpo and M.A.F. Alves, *Thresholds for secondary light emission by noble gases*, Jap. J. Appl. Phys., Vol. 21 (1982) 1184-1190.

[33] C.A.N. Conde, M.C.M. Santos, M.F.A. Ferreira and C.A. Sousa, *An Argon Gas Scintillation Counter with Uniform Electric Field*, IEEE Trans. Nucl. Sci. Vol.22 (1975) 104-108.

[34] M.S.S.C.P. Leite, A.J.P.L. Policarpo, M.A. Feio and M.A.F. Alves, *Detector of VUV Photons With A Photoionization Proportional Scintillation Chamber*, Nucl. Instrum. Meth. 179 (1981) 295-300.

[35] T. Takahashi, S. Himi, M. Susuki, J. Ruan(Gen) and S. Kubota, *Emission Spectra from Ar-Xe, Ar-Kr, Ar-N2, Ar-CH4, Ar-CO2 and Xe-N2 Gas Scintillation Proportional Counters*, Nucl. Instr. and Meth. A 205 (1983) 591-596.

[36] A.C. Fonseca, R. Meleiro, V. Chepel, A. Pereira, V. Solovov and M.I. Lopes, *Study of Secondary Scintillation in Xenon Vapour*, 2004 IEEE Nucl. Sci. Symp. Conference Record (2005).

CHAPTER 5

Electroluminescence Yield from GEM and THGEM Gaseous Electron Multipliers

5. Motivation

The simultaneous detection of both ionisation and scintillation signals in a noble-liquid leads to a unique signature for the energy deposited by a recoiling nucleus in the target volume [1]. Cryogenic, dual-phase optical TPCs have been recently developed for dark matter search, in experiments such as XENON, ZEPLIN, LUX and WARP, e.g. [2-4]. The primary ionisation resulting from radiation interaction in the liquid is extracted to the gas phase and amplified through

electroluminescence production in a uniform-field scintillation gap, being the scintillation recorded by photomultiplier tubes (PMTs).

Alternatives to electroluminescence production and readout, as amplification process for primary ionisation, are under investigation and/or implementation for large scale detectors, making use of the secondary avalanche ionisation produced in micropattern electron multipliers, such as Gas Electron Multipliers (GEMs), Thick-GEMs (THGEMs), MICROMEGAS and Large Electron Multipliers (LEMs) [5,12]. LEMs [12], which are not different from THGEMs, are to be used in ArDM [13] and in the recently proposed GLACIER [14] programmes. GEMs and THGEMs are under investigation for ZEPLIN and LUX, respectively [8,11]. The simplicity, low cost and much less mass burden of the charge readout system would be an important advantage over the scintillation readout with PMTs.

However, the limited signal amplification achieved in charge readout mode presents a serious drawback to these attempts. Given the characteristic low rate and high radiation background of these experiments, to effectively discriminate nucleus recoiling events from the background it is crucial to have the highest possible gain in the detector. Therefore, it is of great importance to use the electroluminescence signal rather than the secondary charge signal. In addition, in opposition to the conventional electronic readout of secondary avalanche charge, the optical recording of the electroluminescence results in fast propagating pulses that are insensitive to electronic noise, RF pick-up and high-voltage issues,

since the readout is physically and electrically decoupled from the gas-multiplication elements.

Hence, it is important to investigate not only the charge but, also, the scintillation capabilities of modern micropattern electron multipliers, to demonstrate their capacity of rendering much higher amplification gains with much less statistical fluctuations, when compared to the charge avalanche [15,16]. In addition, for large scale detectors, the electroluminescence produced in those micropattern electron multipliers presents an alternative to the electroluminescence produced in uniform field scintillation gaps, commonly used in this type of instrumentation. It is possible to reach larger scintillation outputs for much lower applied voltages at the cost of a small degradation in the statistical fluctuations of electroluminescence. The increase in the electroluminescence output is important if other type of readout, such as large area avalanche photodiodes (LAAPD) or Avalanche photodiodes working in Geiger mode (G-APDs) are used substituting for PMTs [17-19].

Initial studies on the scintillation produced in GEMs operating in xenon have been performed in [20]. However, the xenon purity was not up to its best because the gas purity was maintained only by diffusion as there was no gas circulation through the getters. Under the present work, the system was improved to allow gas circulation through the getters and, for the THGEM studies, the detector was modified to include an induction electrode (anode) between the THGEM and the LAAPD.

In the present Chapter, the electroluminescence yield of GEMs and THGEMs has been studied in pure xenon and pure argon, in the pressure range of 1-2.5 bar. The GEM and the THGEM electroluminescence yield as well as the amplitude and energy resolution of the scintillation pulse-height distributions were determined as a function of applied voltage and compared to those of charge pulses. The studies have been performed in pulse-mode, using 22.1-keV X-rays from a ^{109}Cd radioactive source. The results here obtained for the electroluminescence yield of GEMs operating in xenon have been published in [21].

5.1. Experimental Setup

A stainless-steel chamber was used to accommodate both GEM and LAAPD and was filled with pure xenon or argon at different pressures, being sealed off during the measurements. Figure 5.1 schematically depicts the GEM and the scintillation-readout LAAPD elements. This detector has already been used in [22]. The drift and induction gaps were 8- and 3-mm thick, respectively. For the THGEM studies the same setup was used, substituting the THGEM for the GEM. In this case, the drift and induction gaps were 6- and 2-mm thick, respectively. While for the GEM the LAAPD was used to define the induction plane, for the THGEM a stainless steel mesh was used as the induction plane, placed 2 mm above the LAAPD enclosure, figure 5.1.

The GEMs used in this work were manufactured at CERN and had standard dimensions, i.e. a 50-μm Kapton foil with a 5-μm copper clad on both sides and bi-conical holes of 50- and 70-μm diameter in the Kapton and copper, respectively, arranged in an hexagonal layout of 140-μm edges, as shown in figure 5.2. The THGEMs were fabricated in an Israeli company (Print Electronics, http://www.print-e.co.il/) and were made of standard printed circuit boards, G-10 insulator copper clad on both sides. The THGEM had a thickness of 0.4 mm, 0.4-mm hole diameter with a copperless rim of 0.1 mm and a pitch of 0.8 mm, as shown in figure 5.3. The GEM's and THGEM's active areas were 2.8 × 2.8 cm^2.

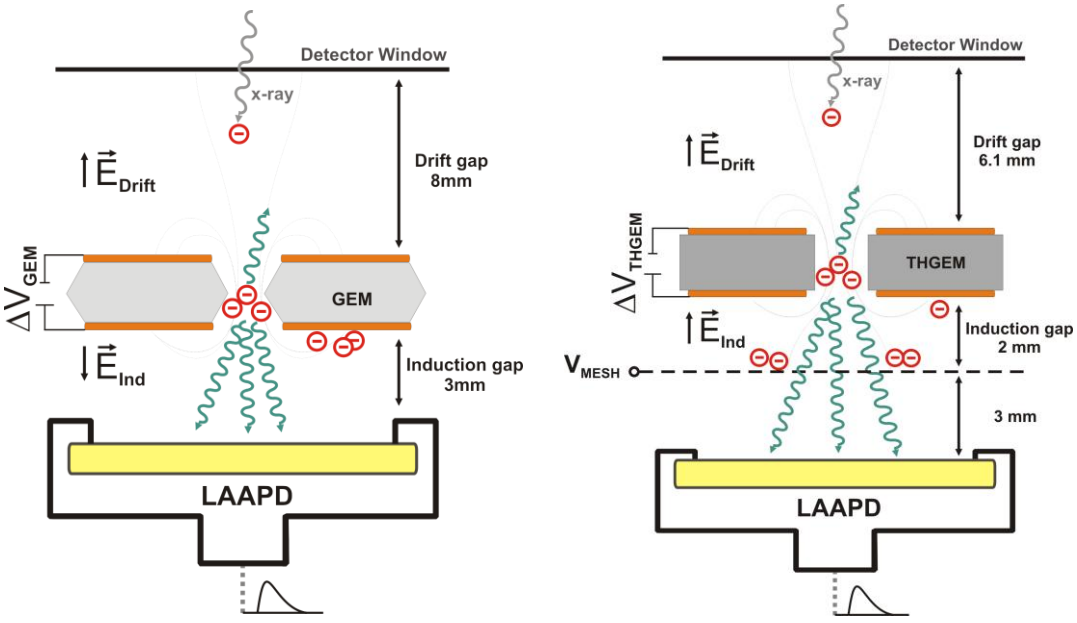

Figure 5.1 - Schematic of the GPSC instrumented with a GEM, or a THGEM, and an LAAPD as the photosensor. While for the GEM the LAAPD was used to define the induction plane, being the charge collected in the GEM bottom electrode, for the THGEM a stainless steel mesh was used as the induction plane, where the charge was collected.

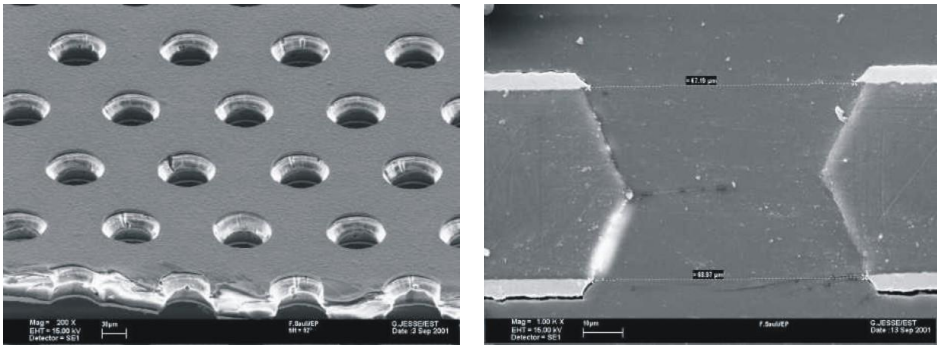

Figure 5.2 – GEM detailed photograph. [23]

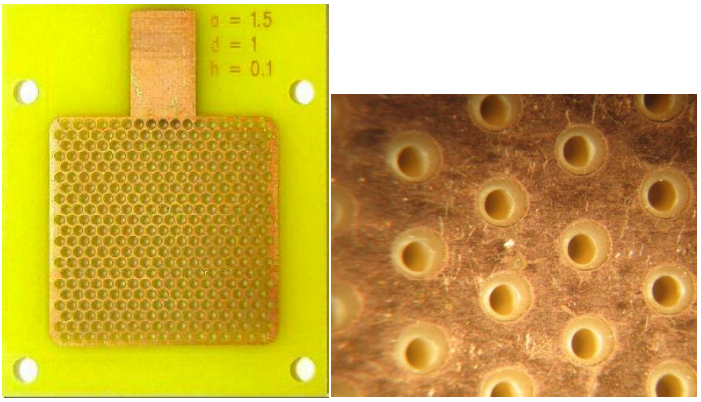

Figure 5.3 – THGEM detailed photograph. [24]

A 1-mm diameter collimated 22.1 keV X-ray beam interacting in the drift region induces the production of primary electron clouds that are focused into the GEM or THGEM holes, where they undergo charge avalanche multiplication. For the GEM, a reversed electric field is applied across the induction region to allow full collection of the avalanche electrons on the bottom electrode (anode) of the GEM, as shown in figure 5.1. For the THGEM, the avalanche electrons were chosen to be collected in the induction plane, i.e. a stainless steel mesh (80-μm wire diameter, 900 μm spacing) placed just above the LAAPD,

figure 5.1. This latter configuration is the standard one and has the advantage of allowing the decoupling of the multiplication stage from the readout that, for instance, could have 2D-readout capability.

A large number of VUV scintillation photons are produced in the charge avalanche as a result of the gas de-excitation processes. A fraction of these photons reaches the LAAPD active-area and the corresponding electric signal is amplified in the photodiode.

The maximum pressure at which the LAAPD can operate safely is 2.5 bar. Therefore, the present studies were performed for gas filling pressures of 1, 1.5, 2.0, and 2.5 bar. The gas purity was maintained, circulating by convection through non-evaporable getters (SAES St707), heated up to about 140ºC.

The LAAPD enclosure and the chamber were grounded, while the radiation window and the GEM's (THGEM's) top and bottom electrodes were biased independently. For the GEM, constant drift- and induction-fields of 0.5- and -0.1 kV cm^{-1}, respectively, were used throughout the measurements. For the THGEM, a constant drift field of 0.5 kV cm^{-1} was used, while for the induction region electric fields between 3 and 4 kV cm^{-1} were used throughout the measurements. An LAAPD bias-voltage of 1840 V was used throughout all the measurements, corresponding to an LAAPD gain around 130 [25-27]. The electroluminescence gain was set by varying the voltage across the GEM's or THGEM's holes.

The pulses from the LAAPD were fed through a low-noise, 1.5 V/pC, charge pre-amplifier to an amplifier, and were pulse-height

analysed with a multi-channel analyser (MCA). The pulse-height distributions were fit to Gaussian functions superimposed on a linear background, from which the pulse amplitudes, taken as the Gaussian centroid, and the respective full width at half maximum (FWHM) were determined. For absolute gain determination, the electronic chain was calibrated using a pulse generator to feed a calibrated capacitor directly connected to the preamplifier input and determining the respective pulse-height channels.

5.2. Methodology

The electroluminescence yield produced in the GEM or THGEM gaseous electron multiplier is defined as the number of secondary scintillation photons produced in the electron avalanches, per primary electron created in the drift region. As in the case of the scintillation produced in uniform electric fields, at atmospheric pressures, the emission is centred in the second continuum, being the emission in the visible and in the IR regions negligible in comparison with those in the VUV range [28,29].

As in the case of the experimental setups of chapters 3 and 4, concurrent with the electroluminescence due to the absorption of X-rays in the gas, a large fraction of the X-rays is detected directly by the LAAPD. For a given X-ray energy, the amplitude of the signals due to X-ray interaction in the photodiode depends only on the LAAPD bias

voltage, regardless of the GEM voltage and, therefore, the corresponding position of the peak in the pulse-height distributions is easy to identify. The number of electron-hole pairs, $N_{e,XR}$, produced by direct absorption of the X-ray in the LAAPD is determined from the energy of the X-ray and the w-value in silicon (w = 3.62 eV [30]) and is approximately 6.1×10^3 electron-hole pairs for the X-ray energy of E_X = 22.104 keV.

Similarly to the method described before, in chapters 3 and 4, a direct comparison between the amplitudes of the GEM electroluminescence, A_{Sc}, and of the X-rays directly absorbed in the LAAPD, A_X, provides a quantification of the number of VUV-photons, N_{UV}, impinging the LAAPD per x-ray absorbed in the drift gap,

$$N_{UV} = \frac{A_{Sc}}{A_X} \times \frac{N_{e,XR}}{QE} \qquad (5.1),$$

where QE is the quantum efficiency of the LAAPD, defined as the number of charge carriers produced per incident VUV photon, being 1.1 for 172-nm photons and 0.55 for 128-nm photons [31,32]. The non-linear response of the LAAPD to X-rays was taken into account and A_X, was corrected for this effect [26,52] with a factor of 1.1 for xenon and 1.12 for argon.

The electroluminescence yield can be directly obtained from

$$Y = N_{UV} \times \frac{4\pi}{T \times \Omega_{Sc}} \times \left(\frac{E_x}{w_{E_x}} \right)^{-1} \qquad (5.2),$$

where Ω_{SC} is the solid angle subtended by the LAAPD, E_X is the energy of the incident X-ray, T is the mesh optical transparency and w_{Ex} the respective w-value for the fill gas. In the present conditions, the w-value for xenon is 21.77 eV and for argon 26.4 eV, for 22.1-keV X-rays [33, 34]. The relative solid angle subtended by the LAAPD is determined from the geometry of the setup, assuming the scintillation to be produced in the detector axis, $\Omega_{SC}/4\pi = 0.28$ for the GEM geometry and $\Omega_{SC}/4\pi = 0.24$ for the THGEM geometry. The mesh optical transparency is 100% for the GEM setup and 84% for the THGEM setup. The dominating sources of uncertainty in the calculated yield are QE and Ω_{SC}, which values are estimated in ± 10% each.

5.3. Experimental results

5.3.1. GEM Electroluminescence Yield Studies

5.3.1.1. Xenon

In order to obtain the effective charge amplification gain achieved using the scintillation readout, i.e. the charge delivered per primary electron at the LAAPD anode, the total charge delivered at the LAAPD output was measured. The effective gain is obtained from the pulse-height distributions collected in the LAAPD anode electrode, corrected

by the electronic chain calibration factor. Figure 5.4 presents the gain obtained for the electroluminescence readout as a function of GEM voltage, for different xenon pressures. The GEM voltage, ΔV_{GEM}, was gradually increased up to the onset of micro-discharges. For comparison, the gain obtained for the charge readout in the bottom electrode of the GEM [20] is included. The decrease in gain with increasing pressure is less pronounced for the electroluminescence mode. The gains achieved in electroluminescence mode were two orders of magnitude higher than in charge mode. Maximum gains of about 2×10^5 and 4×10^4 were reached for the electroluminescence readout mode and for xenon at 1.0 and 2.5 bar, respectively.

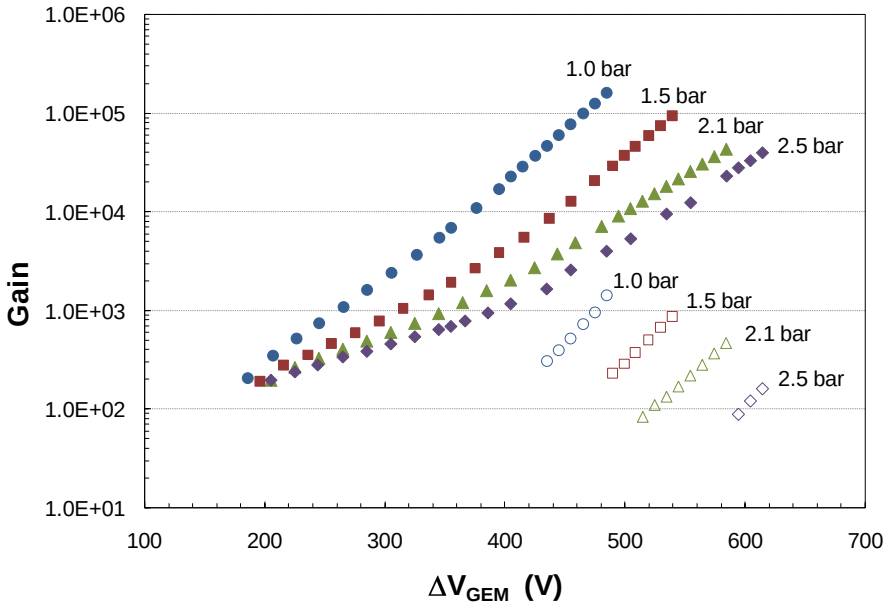

Figure 5.4 – Total gain as a function of voltage applied to the GEM operating in xenon, for electroluminescence readout (solid symbols) [this work] and for the charge readout (open symbols) [20]. The photosensor gain is about 130 [25-27].

The electron avalanche development in the GEM holes is determined by the electron-impact mechanism [35], which explains the maximum gain-drop for higher pressures. The maximum applied voltage does not increase as fast as pressure, thus, the reduced electric field, *E/p*, decreases with increasing pressure. For the applied electric fields, the excitation coefficient is less strongly dependent on *E/p* than the Townsend coefficient (e.g. see Fig.2 of Ref.[36]). Therefore, the maximum electroluminescence gain is less affected by the increase in pressure than the charge gain.

The GEM electroluminescence yield, *Y*, i.e. the number of photons produced in the GEM holes per primary electron deposited in the drift region, is depicted in figure 5.5 as a function of GEM voltage. The maximum achieved electroluminescence yield decreases about four-fold, from about 5×10^3 photons per primary electron, at 1 bar, to about 1.3×10^3 photons per primary electron, at 2.5 bar. Taking into account the values for pressure, temperature, voltage difference applied to the scintillation gap and its thickness in XENON10 [37] and ZEPLIN-III [3] setups, values of 210 and 340 photons per primary electron have been obtained for the respective electroluminescence yields [38]. These values are about one order of magnitude lower than what can be achieved using a GEM instead of a uniform electric field scintillation gap. Moreover, the voltage difference applied to the GEM is at least a factor of 4 lower than what is being applied to the scintillation gaps in [3,37]. Although in the present setups the amount of electroluminescence obtained is sufficient in view of the use of PMTs, if a different readout is considered, such as LAAPDs, it will be important to increase the

amount of electroluminescence. LAAPD gains as low as few hundred and the prospect of covering an area less than 100% are strong reasons advocating such increase.

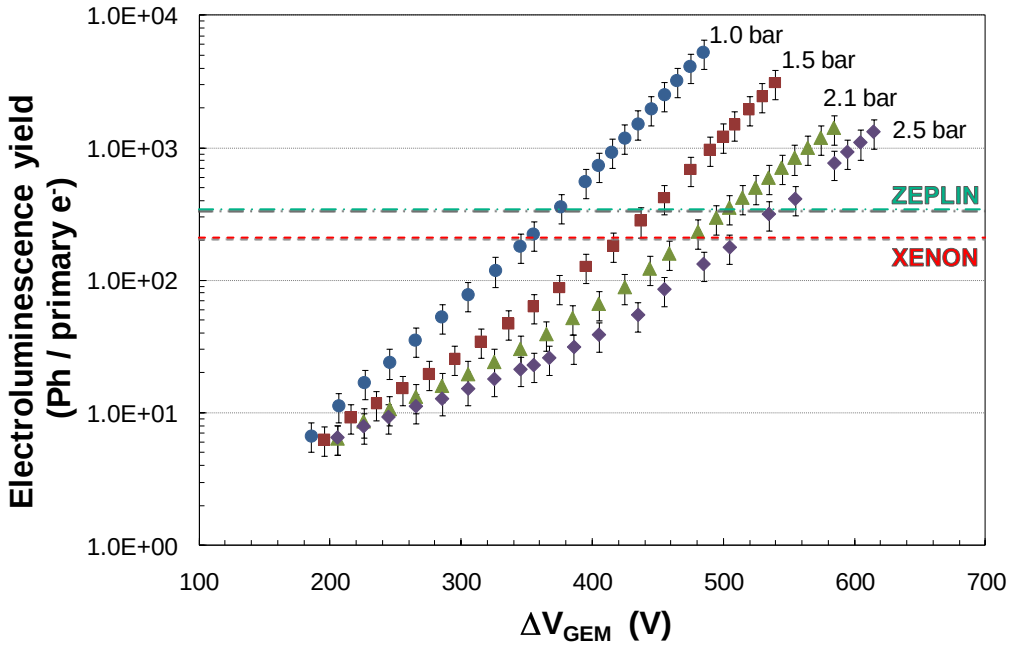

Figure 5.5 – Electroluminescence yield, Y, i.e. number of photons produced per primary electron produced in the drift region as a function of voltage applied to the GEM operating in xenon. The horizontal lines correspond to the electroluminescence yields of XENON10 and ZEPLIN-III setups.

The calibration of the electronic chain of the scintillation readout channel allows an independent determination of the GEM electroluminescence yield. This calibration allows the calculation of the number of electrons collected in the LAAPD anode per primary electron produced in the scintillation region, G_{tot}, i.e. the data presented in figure 5.4. Assuming the LAAPD gain for the 1840 V bias to be about G_{APD} = 130 [25-27], the number of charge carriers produced in the

LAAPD by the scintillation pulse can be determined by the ratio of these two gains. Therefore, the number of photons impinging the LAAPD per primary electron, $N_{uv,e}$, can be given by

$$N_{UV,e} = QE^{-1} \times \frac{G_{tot}}{G_{APD}} \qquad (5.3),$$

and the GEM electroluminescence yield is obtained from

$$Y_{eff} = N_{UV,e} \times \frac{4\pi}{T \times \Omega_{Sc}} \qquad (5.4).$$

The values obtained from equation 5.4 are similar to those obtained with the former method, within less than 20%. However, the uncertainty in the yield obtained by this last method is higher, because of the uncertainty in G_{APD} and in G_{tot}, which are larger than that of QE.

The energy resolution obtained for 22.1-keV X-rays using the electroluminescence readout is depicted in figure 5.6 as a function of ΔV_{GEM} for the different xenon pressures. For comparison, the energy resolution obtained for 22.1-keV X-rays using charge readout [20] is also depicted in figure 5.6. As shown, the scintillation readout presents significant advantages. The energy resolution is superior to that obtained for charge readout and the degradation in energy resolution with increasing pressure is less pronounced when compared to the charge readout. For the scintillation readout, best energy resolutions were achieved for GEM voltages well below the onset of discharges, while for charge readout the best energy resolutions were achieved at maximum GEM voltages, close to the discharge onset, degrading rapidly as ΔV_{GEM} decreases. At 2.5 bar, the best energy resolutions achieved for

22.1-keV X-rays were about 10% and 27% (FWHM) in electroluminescence and charge readout mode, respectively. The energy resolution obtained in uniform field scintillation gaps with PMT or LAAPD readout is between 4.5 and 6.0% (FWHM) for 22.1-keV X-rays [e.g. 31,39,40 and references therein], about a factor of two lower than what is obtained with the GEM+LAAPD combination. Nevertheless, the values obtained in this work are similar to those attained in a double-phase Xe TPC used in Dark Matter detection, being the latter 13.5% (FWHM) at 60 keV [3]. The energy resolution in double-phase TPCs is limited by the loss of primary electrons during the drift inside the liquid xenon and in the extraction of the electrons to the gas phase. Therefore, the increase in statistical fluctuations of the electroluminescence output will have a small impact on the achieved energy resolution.

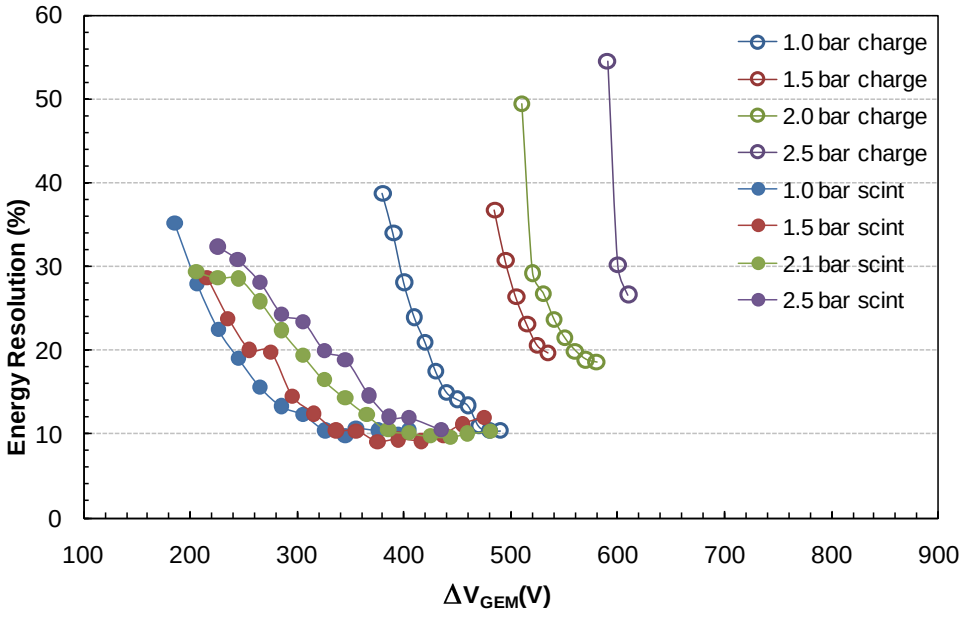

Figure 5.6 – Energy resolution as a function of voltage applied to the GEM operating in xenon, for 22.1-keV X-rays. Solid symbols: electroluminescence readout [this work]; open symbols: charge readout [20].

Yet, the energy resolution for the electroluminescence readout mode is determined by the statistical fluctuations in the charge production process, since the scintillation produced in the charge avalanche results mostly from the impact of the secondary electrons, produced in the avalanche, with the xenon atoms. The better energy resolution obtained for electroluminescence readout when compared to charge readout is due to the fact that, for the same voltages, the gain and signal-to-noise ratio achieved in electroluminescence readout mode are much higher than in charge readout mode. Figure 5.7, which depicts the energy resolution as a function of gain for both readout modes shows that, for high gains, the energy resolution for charge and scintillation readout modes tends to similar values. The lowest values for the energy resolution are obtained for gains above 10^3.

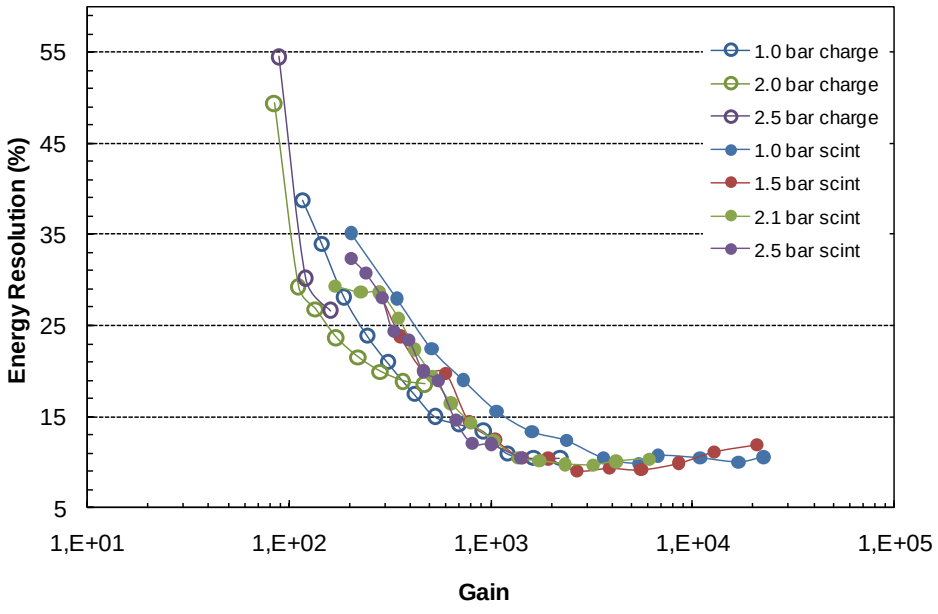

Figure 5.7 – Energy resolution as a function of gain for the GEM operating in xenon, for 22.1-keV X-rays. Solid symbols: electroluminescence readout [this work]; open symbols: charge readout [20].

5.3.1.2. Argon

The studies presented in the former section for the GEM operating in pure xenon were also performed for the GEM operating in pure argon. The geometry, electric fields and LAAPD biasing conditions were the same as for xenon.

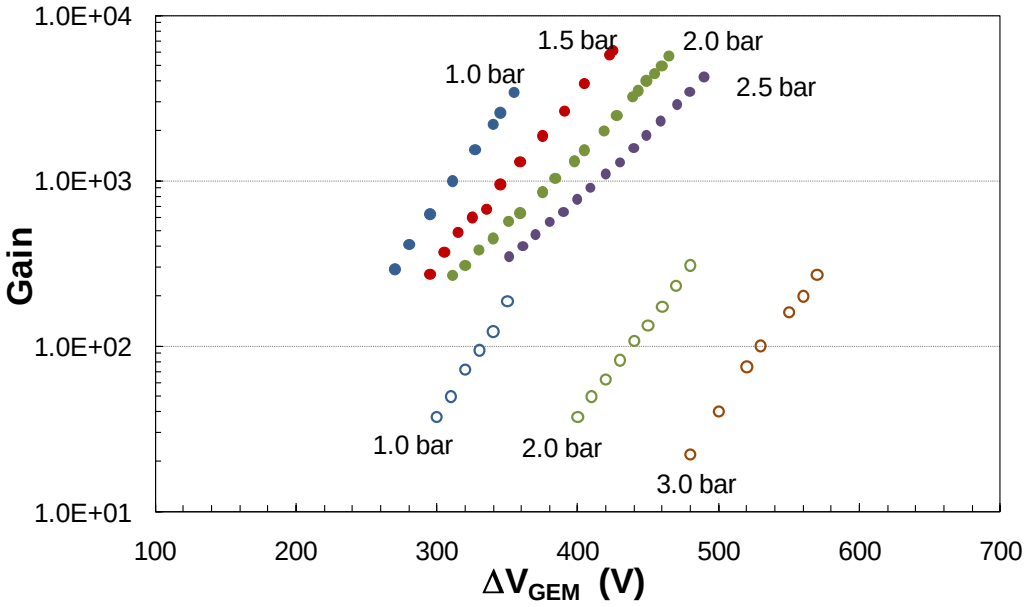

Figure 5.8 – Total gain as a function of voltage applied to the GEM operating in argon, for electroluminescence readout (solid symbols) [this work] and for charge readout (open symbols) [41]. The photosensor gain is about 130 [25-27].

In figure 5.8 the total gain obtained for the electroluminescence readout as a function of GEM voltage is presented for different argon pressures. The GEM voltage, ΔV_{GEM}, was gradually increased, up to the onset of micro-discharges. For comparison, the gain obtained for the

charge readout in the bottom electrode of the GEM [41] is included. As in the charge readout mode, the maximum achievable gain with the electroluminescence readout mode does not depend significantly on the pressure, presenting values around 5×10^3. Nevertheless, the latter gain is more than one order of magnitude higher than for the charge readout. Compared to xenon, the gains in argon are more than one order of magnitude lower.

The GEM electroluminescence yield for argon is depicted in figure 5.9 as a function of GEM voltage. The maximum achieved electroluminescence yield does not depend significantly on the pressure, being around 3×10^2 photons per primary electron. Since there are no data in the literature for the amount of electroluminescence produced in the WARP detector, no comparison can be made with this experiment. Nevertheless, the electroluminescence produced in a 1-cm uniform field scintillation gap for 3.75 $kVcm^{-1}bar^{-1}$, from equation 4.6, was included in figure 5.9 for comparison, and is represented by the horizontal broken lines. One can see that, for argon, the electroluminescence yield produced in GEMs is similar or even lower than in a uniform field scintillation gap. Therefore, in argon, there is no advantage in using GEMs for scintillation amplification, in opposition to xenon. The best achieved energy resolution for 22.1-keV X-rays was around 10% (FWHM) for all the studied argon pressures. This value is not much different from the 7% achieved for uniform field argon GPSCs.

Using the data of figure 5.8 and the value of 130 for the LAAPD gain, equations 5.3 and 5.4 render values for the electroluminescence yield that agree with those of figure 5.9, within 30%.

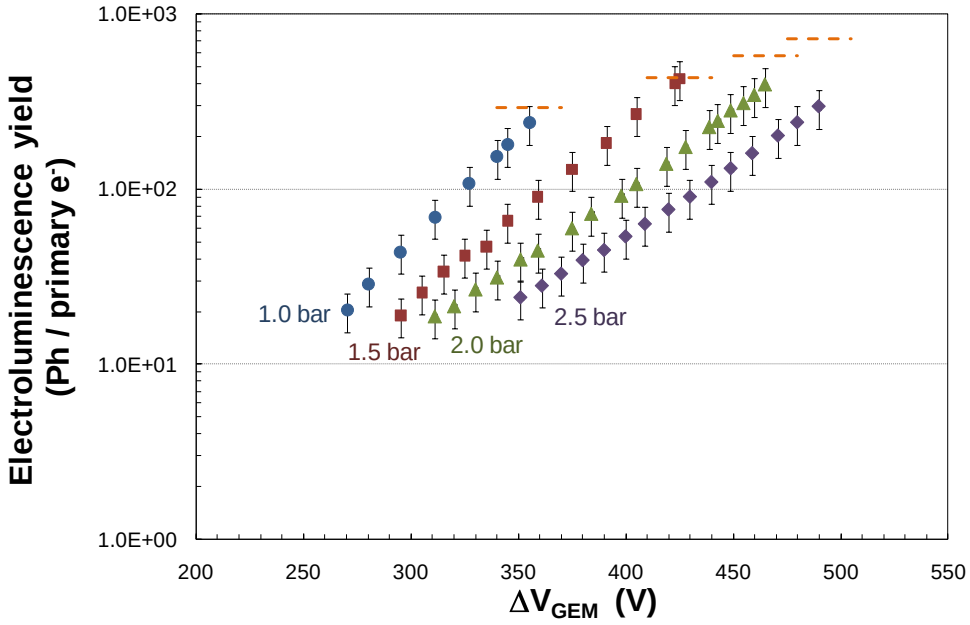

Figure 5.9 – Electroluminescence yield, Y, i.e. number of photons per primary electron produced in the drift region as a function of voltage applied to the GEM operating in argon. The horizontal lines correspond to the electroluminescence yields for a 1-cm uniform-field scintillation gap and for 3.75 kVcm^{-1}bar^{-1}.

5.3.2. THGEM Electroluminescence Yield

The detector used in [20] and in this work for the GEM studies, was modified in order to accommodate an induction plane, between the THGEM and the LAAPD, as can be seen in figure 5.1. This design is the

most used in the literature, for it decouples the amplification stage from the readout, with the advantage of using the most suitable readout pad for each application. On the other hand, the amount of charge collected on the induction (readout) plane is less than the total charge produced in the avalanches, because some of the electrons are collected in the THGEM (or GEM) bottom electrode, e.g. as is shown in [41]. This induction plane was a stainless steel mesh, of 80-μm wire diameter and 900-μm spacing, having an optical transparency of 84%. With this geometry, one can find values in the literature for the charge gain obtained in a THGEM, e.g in [7].

5.3.2.1. Xenon

The studies presented in the section for the GEM were also performed for the THGEM, with the geometry, electric fields and LAAPD biasing conditions as described in section 5.1.

In figure 5.10 the total gain obtained for the electroluminescence readout as a function of THGEM voltage is presented for different xenon pressures. The THGEM voltage, ΔV_{THGEM}, was gradually increased, until a microdischarge in about every 2 to 3 minutes occurred. For comparison, the THGEM charge gain, i.e. the gain obtained for the charge readout [7], is also included in figure 5.10. The difference from 100 to 130 V in the maximum voltage that can be applied to the THGEM in both cases, noticeable at 1 and 2 bar, may be due to

differences in the quality of the THGEM, an effect inherent to the THGEM fabrication process.

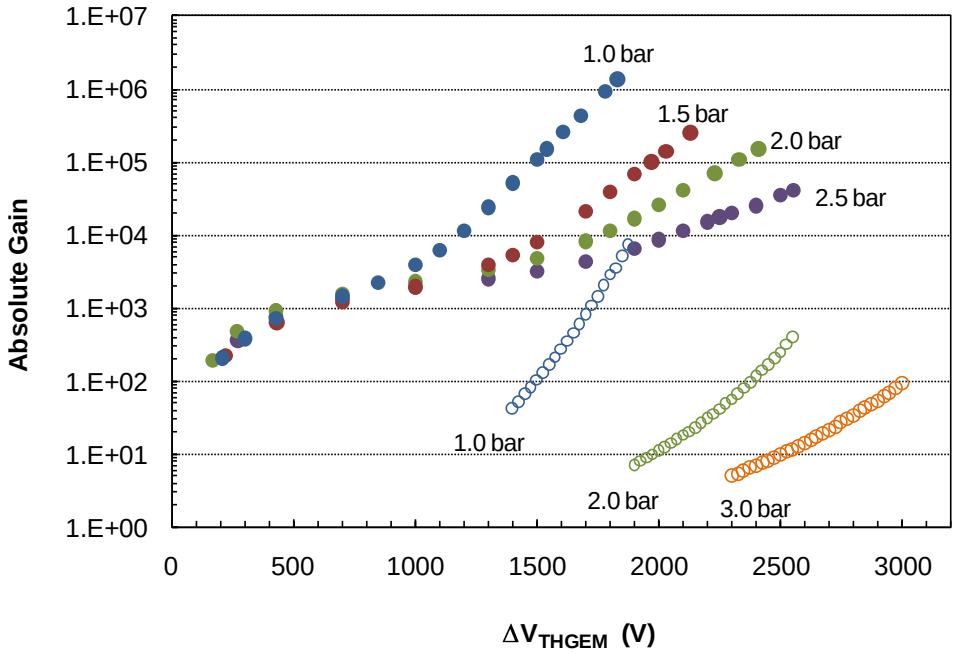

Figure 5.10 – Total gain as a function of voltage applied to the THGEM operating in xenon, for electroluminescence readout (solid symbols) [this work] and for charge readout (open symbols) [7]. The photosensor gain is about 130 [25-27].

Similarly to GEMs, the values for the gain obtained in the scintillation readout mode are more than two orders of magnitude higher than those obtained using charge readout. However, at 1 bar, the gains achieved with THGEMs, either in charge or scintillation readout modes, are almost one order of magnitude higher than those achieved with GEMs. This difference is reduced with increasing pressure, presenting the THGEM and the GEM similar gains at 2.5 bar. This is due to the lower values of the reduced electric field in THGEMs,

resulting in a faster dependence of the Townsend coefficient on the reduced electric field.

THGEM gains above 10^6 are achieved for the scintillation readout mode and for 1 bar, decreasing to about 5×10^4 for 2.5 bar. Gains well above 10^5 make single electron detection with high efficiency possible, being these gains similar to the gains achieved with PMTs. Therefore, the present setup can be considered an alternative to PMTs, as a gas photomultiplier (GPM), being more compact and less power consuming.

The THGEM electroluminescence yield, *Y*, is depicted in figure 5.11 as a function of THGEM voltage for the different xenon pressures.

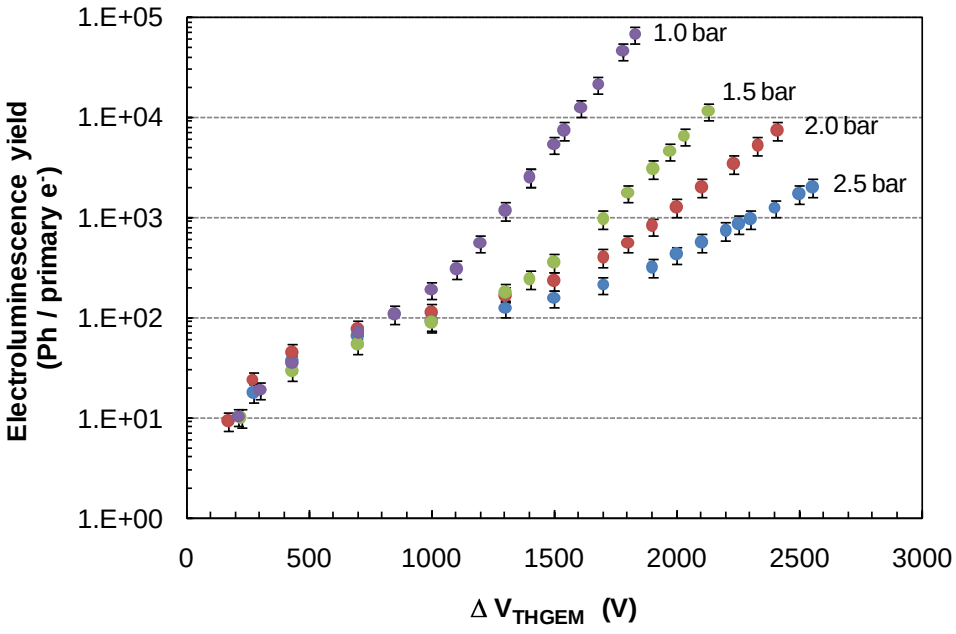

Figure 5.11 – Electroluminescence yield, Y, i.e. number of photons produced per primary electron produced in the drift region as a function of voltage applied to the THGEM operating in xenon.

The maximum achieved electroluminescence yield reaches very high values, but presents a fast decrease with increasing pressure, from about 7 $\times 10^4$ photons per primary electron, at 1 bar, to about 2 $\times$ 10^3 photons per primary electron, at 2.5 bar. Compared to the GEM, the THGEM electroluminescence yield follows the same trend as the gain for the scintillation readout, i.e. the electroluminescence yield achieved with THGEMs is one order of magnitude higher than those achieved in GEMs, at 1 bar, but presents already similar yields at 2.5 bar.

Using the data of figure 5.10 and the value of 130 for the LAAPD gain, equations 5.3 and 5.4 render values for the electroluminescence yield in THGEMs that agree with those of figure 5.11, within 20%.

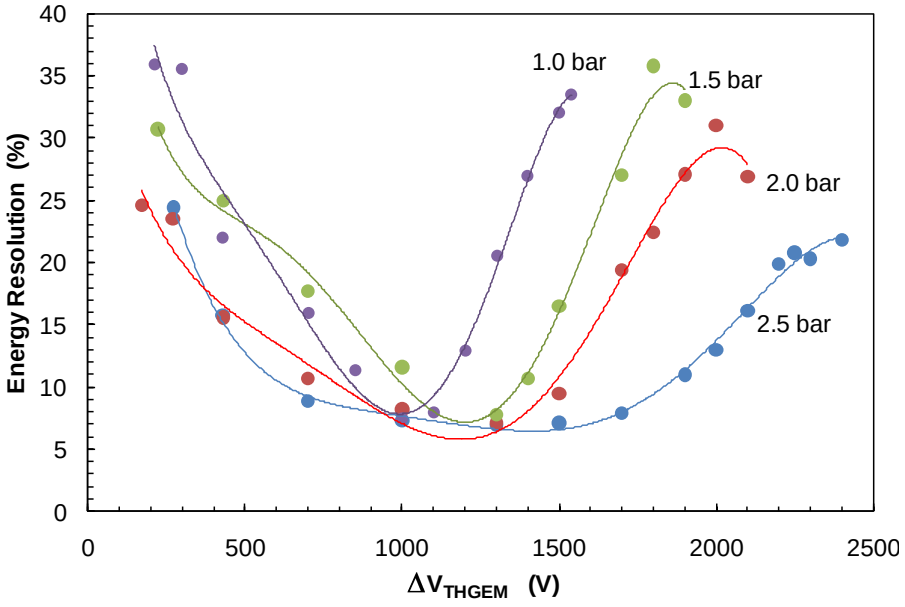

Figure 5.12 – Energy resolution as a function of voltage applied to the THGEM operating in xenon, for 22.1-keV X-rays and for electroluminescence readout.

The energy resolution obtained for 22.1-keV X-rays using the electroluminescence readout is depicted in figure 5.12 as a function of

ΔV_{THGEM}, for the different xenon pressures studied. The energy resolution presents an initial fast drop with increasing voltage, and reaches a minimum, although increasing again as the THGEM voltage continues to rise. The same trend is observed for all the pressures.

As in the case of the GEM, the energy resolution depends mostly on the THGEM gain, which is shown in figure 5.13.

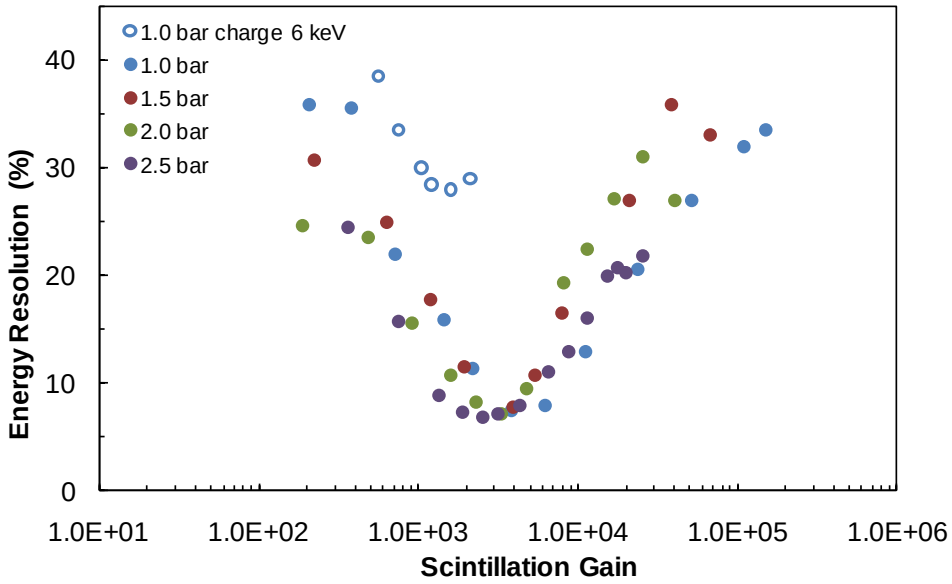

Figure 5.13 – Energy resolution as a function of gain for the THGEM operating in xenon, for 22.1-keV x-rays and for electroluminescence readout (solid symbols) [this work]. The data from [7] (open symbols) for energy resolution obtained with charge readout, for 6-keV X-rays and for 1 bar of Ar:Xe (95:5) gas mixture, are also presented in the graph.

This figure shows that optimum values for the energy resolution are achieved for gains within a small plateau, between about 2×10^3 and 5×10^3. In the literature, only one data set was found for the energy resolution versus THGEM gain [7] and that was for 5.9-keV X-rays in an

Ar:Xe (95:5) mixture at 1 bar. These data are included in figure 5.13 and present a similar trend as obtained for 22-keV X-rays. However, while for 5.9-keV X-rays the energy resolution obtained with the THGEM is worse than that obtained with a GEM, 28% and 18%, respectively, the THGEM presents energy resolutions for 22.1-keV X-rays that are better than those obtained in GEMs, 7% versus 10%. The value of 7% is close to that obtained in a uniform field GPSC, which is about 5% [42]. For 60-keV photons, the best values for the energy resolution obtained with the present setup was about 5%, even closer to the 4% that is attained in a GPSC [42]. This can be an advantage favouring the THGEM option.

5.3.2.2. Argon

In figure 5.14 the total gain obtained for the electroluminescence readout as a function of THGEM voltage is presented for different argon pressures. The THGEM voltage, ΔV_{THGEM}, was gradually increased, until a microdischarge occurred in about every 2 to 3 minutes. To the best of our knowledge, the only data available in the literature for the gain of a THGEM operating in pure argon in a sealed system with gas circulation through getters (conditions similar to those of the present study) is from [7]. These data are included in figure 5.14 for comparison. The maximum achieved gain for the scintillation readout mode was about 10^5 at 1 bar, reducing smoothly to about 3×10^4 at 2.5 bar, in opposition to the constant trend presented in the results with the GEM. This

different behaviour is due to the lower values of the reduced electric field achieved in THGEMs, resulting in a faster dependence of the Townsend coefficient on the reduced electric field.

Comparing with the GEM, the values for the gains achieved in THGEMs are more than one order of magnitude higher, for 1 and 1.5 bar, while for higher pressures it is only a factor of around 7. Comparing to the THGEM operation in xenon, the THGEM operating in argon presents gains that are one order of magnitude lower at 1 bar, but presents already similar gains at 2.5 bar, a similar trend to what is observed in GEMs. This effect is due to the fact that the charge avalanche gain reduction with increasing pressure is much more pronounced for GEM/THGEM operation in xenon than it is for their operation in argon.

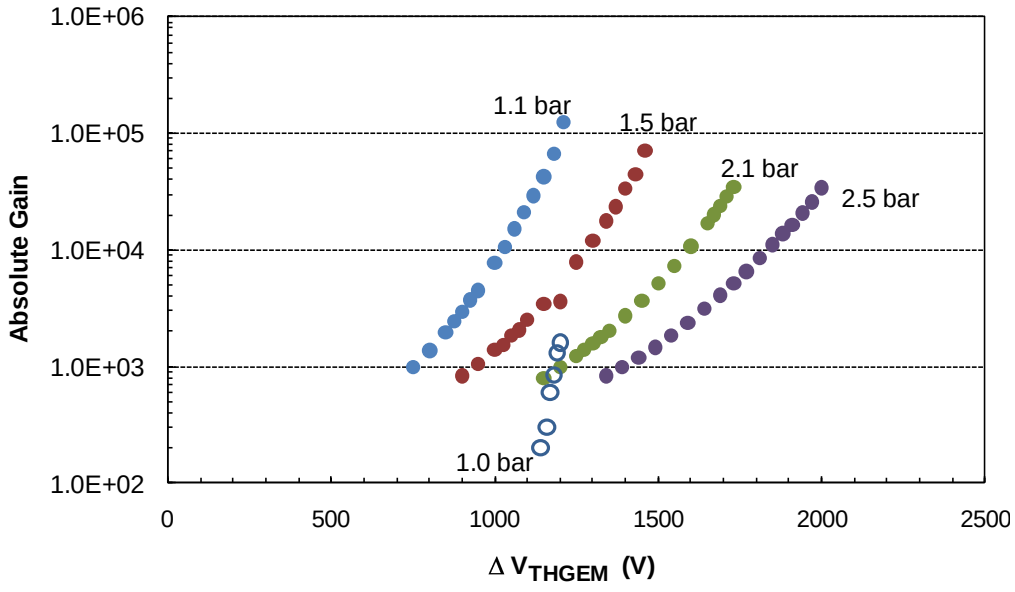

Figure 5.14 – Total gain as a function of voltage applied to the THGEM operating in argon, for electroluminescence readout (solid symbols) [this work] and for charge readout (open symbols) [7]. The photosensor gain is about 130 [25-27].

The THGEM electroluminescence yield, *Y*, in argon is depicted in figure 5.15 as a function of THGEM voltage. The maximum achieved gain for the scintillation readout mode was about 1.5×10^5 at 1 bar, reducing slowly to about 3.8×10^4 at 2.5 bar, in opposition to the constant trend presented in the results for the GEM. Comparing to the GEM, the values for the electroluminescence yield achieved in THGEMs in argon are much more than one order of magnitude higher at 1 bar, reducing to about one order of magnitude at 2.5 bar. Comparing to the THGEM operation in xenon, the THGEM operating in argon presents electroluminescence yields that are only 5-fold lower at 1 bar, but only 2-fold lower at 1.5 bar and at 2.5 bar the yield in argon is already higher.

The electroluminescence produced in a 1-cm uniform field scintillation gap, for 3.75 $kVcm^{-1}bar^{-1}$, from equation 4.6, was included in figure 5.15 for comparison, and is denoted by the horizontal solid lines. One can see that, in opposition to the GEM operating in argon, the scintillation produced in THGEMs operating in argon for 1bar and 1.5 bar is more than one order of magnitude higher than that produced in 1-cm thick, uniform-field scintillation gap with a reduced electric field of 3.75 $kVcm^{-1}bar^{-1}$, being eight-fold and five-fold higher for 2.1 and 2.5 bar. Therefore, the use of a THGEM as a mean to produce electroluminescence in argon-filled detectors has advantages over the use of uniform electric field scintillation gaps.

Using the data of figure 5.14 and the value of 130 for the LAAPD gain, equations 5.3 and 5.4 render values for the electroluminescence yield that agree with those of figure 5.15, within 30%.

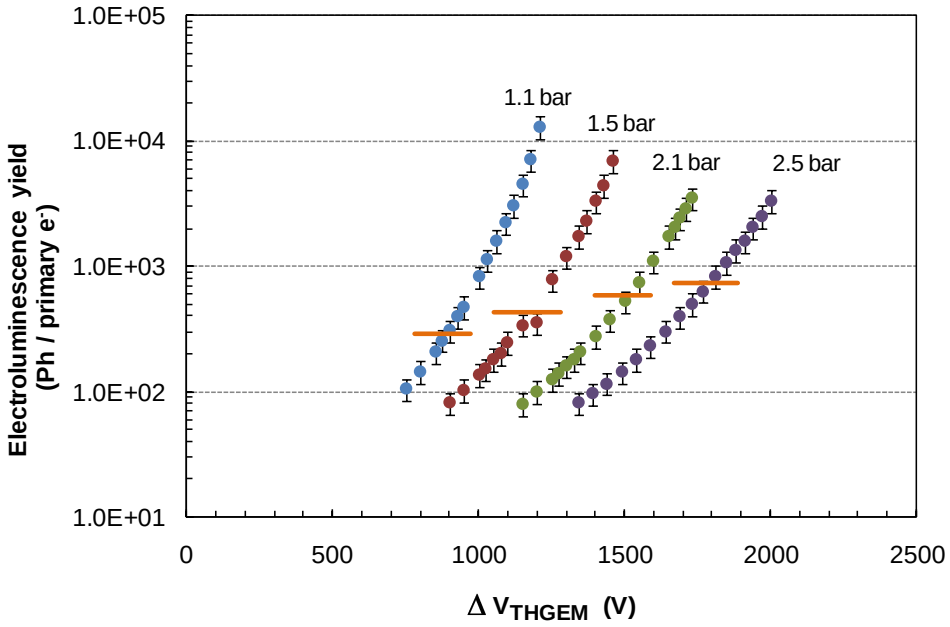

Figure 5.15 – Electroluminescence yield, Y, i.e. number of photons produced per primary electron produced in the drift region as a function of voltage applied to the THGEM operating in argon. The horizontal lines correspond to the electroluminescence yields for a 1-cm uniform-field scintillation gap and for 3.75 kVcm^{-1}bar^{-1}.

As in the cases of the GEM and THGEM operating in xenon, the energy resolution for argon depends mostly on the gain. Figure 5.16 depicts the energy resolution as a function of gain for the THGEM operating in argon, for 22.1-keV X-rays and for the electroluminescence readout. This figure shows that optimum values for the energy resolution are achieved for gains within a small plateau, between about 2×10^3 and 5×10^3. The best energy resolution was about 11%, similar to that obtained in GEMs operating in argon for the scintillation readout mode and somewhat above the 7% energy resolution obtained in an argon uniform field GPSC.

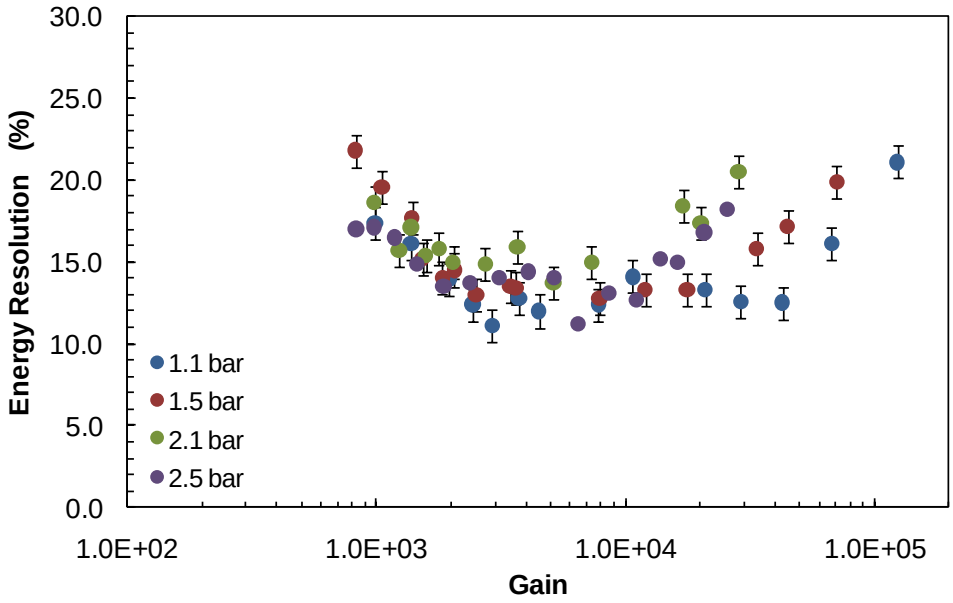

Figure 5.16 – Energy resolution as a function of gain for the THGEM operating in xenon, for 22.1-keV X-rays and for electroluminescence readout.

5.3.3. Simultaneous readout of charge and scintillation pulses

Equipment with multiple sampling channels, i.e. with multiple ADCs working in parallel, has been developed for some time, mainly for the readout of pixelized detectors and imaging. With the increase of computing capacities and performance, signal digitalization with high resolution, fast sampling rate and fast data storage allows to implement simple but effective pulse-time correlation.

Therefore, the simultaneous readout of the charge and scintillation produced in charge avalanches of micropattern detectors, as in GEMs

or THGEMs, is a possibility to be explored, aiming the improvement of the detector response to ionising radiation. These studies have been performed with the present setup and are presented in this section.

A CAEN™ 1728b NIM module [43], equipped with 4 ADCs having a resolution of 14 bits and a 100-MHz sampling rate was available from the Detector Radiation and Medical Imaging (DRIM) group of the University of Aveiro. The module performs real-time digital signal sampling and shaping, as well as data storage for offline analysis. It has a Xilinx Virtex II FPGA for pulse processing and hardware control and a Spartan II FPGA for system configuration [44]. For the purpose of this study, it was used in energy mode, wherein every event was stored up in a matrix with the pulse amplitude, the time stamp (i.e. the time of the event occurrence), the input channel and the trigger number. In this mode, the information on pulse-shape is not stored up, which saves processing time and memory. All the parameters concerning data acquisition and processing can be adjusted by the user according to the needs.

Each pulse triggered in the module was recorded in a binary file, which was processed with a program developed in the DRIM group of the University of Aveiro, the RADIX, which is based on the MATLAB™ platform. Each photon interacting in the gas provides two pulses, one from the scintillation and another from the charge readout channel, which are fed to two different channels of the module. This routine organizes the pulses in groups of two, which enter the module input channels in coincidence, within a time window defined by the user. The

pulses of both channels that do not appear as a pair within the set time window may not be considered. RADIX allows displaying merely the selected pulses that are within a certain parameter region, e.g. time window, amplitude ratio or any other relation of amplitudes. Figure 5.17 presents an example of typical parameters that can be displayed and selected to be used for pulse discrimination. These include the time difference between two consecutive pulses from the scintillation channel and the charge channel, within a 1-μs time window, the scintillation-to-charge pulse amplitude ratio, A_{sc}/A_{ch}, and the plot of the amplitudes, of each pair of pulses, (A_{sc},A_{ch}).

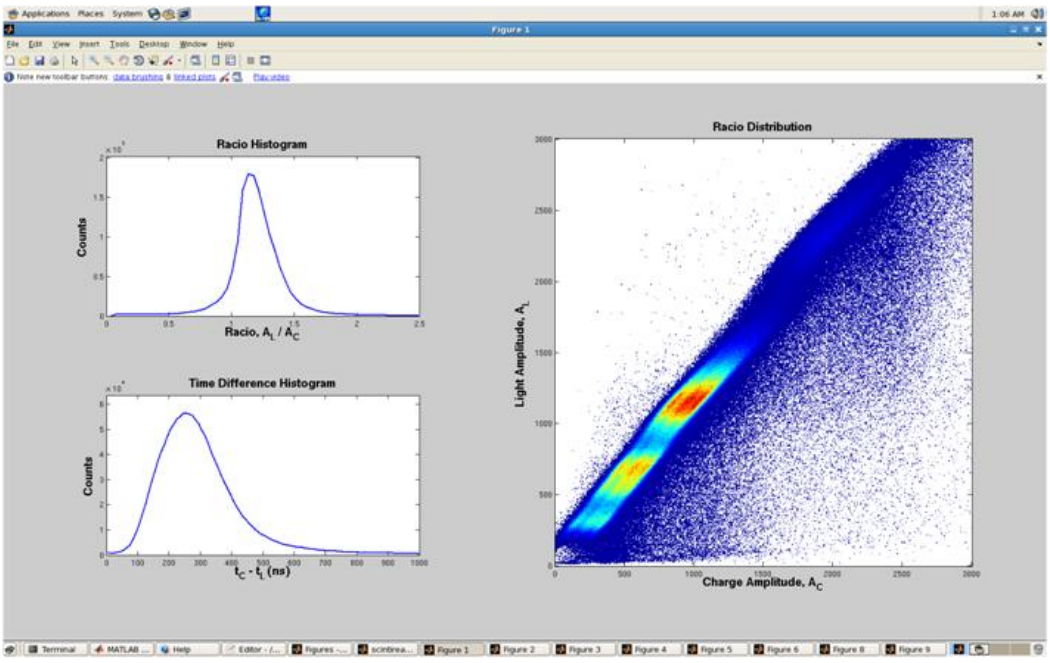

Figure 5.17 - Scintillation and charge pulses correlation from a ^{241}Am radioactive source in a GEM operating in xenon a 1.0 bar, taken with the CAEN 1728b board: amplitude ratio, time difference between two consecutive scintillation–charge pulses and amplitude-space parameter, i.e. pulse amplitude correlation plot.

This allows obtaining pulse-height distributions for both scintillation and charge channels, with or without any discrimination constrains.

Figure 5.18 depicts the pulse height distributions for ^{241}Am photons obtained with a GEM operating in xenon, for both channels and for two different cases: no discrimination implemented (raw pulse-height distributions) and selecting only the pairs of pulses, one in each channel, that appear within a microsecond (correlated pulse-height distributions). The raw pulse-height distributions exhibit the 59.6-keV peak (1), the xenon K-fluorescence escape peak (2), the Np L_α- and L_β-fluorescence emitted by the source (3,4) and the electronic noise tail, in the low energy limit region (6). The scintillation channel has also an additional peak due to direct X-ray interactions in the LAAPD (5). Figure 5.18 shows that pulse correlation results in pulse-height distributions free of electronic noise and free of pulses that are only present in one of the channels, as are those resulting from direct X-ray interactions in the LAAPD. The small peak still present in the position of the LAAPD direct interactions is the peak corresponding to the Np L_l-fluorescence and/or events resulting from the xenon L-fluorescence escapes resulting from Np L_α- and L_β-fluorescence interactions in the xenon. This peak is not resolved (but noticeable) in the pulse-height distribution of the charge channel due to the poor energy resolution and it was superimposed on the peak resulting from direct X-ray absorptions in the LAAPD in the scintillation channel.

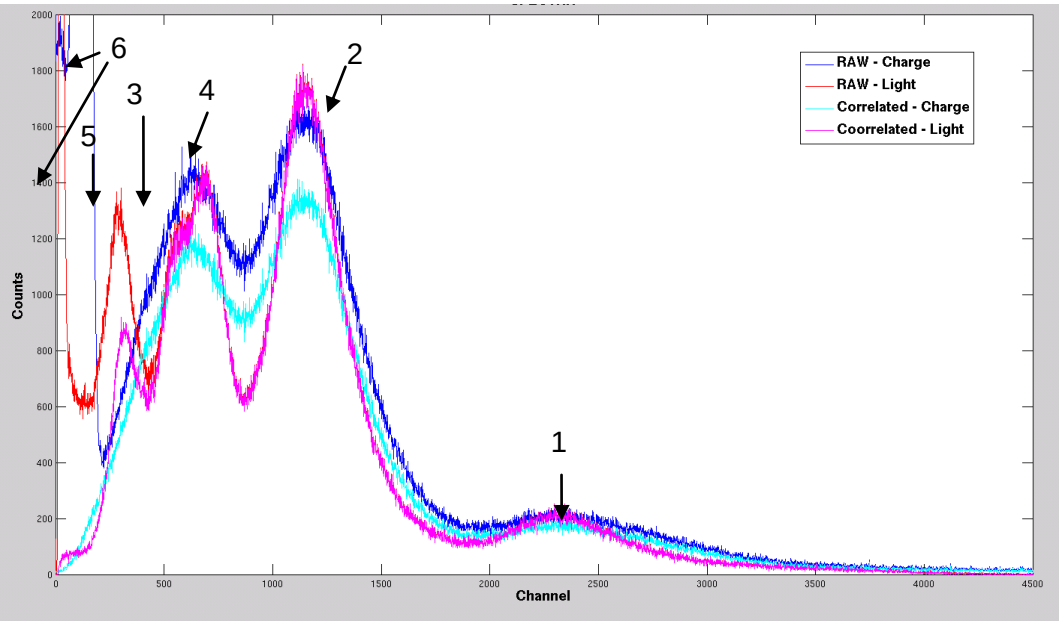

Figure 5.18 - Scintillation and charge pulse height distributions for ^{241}Am photons obtained with a GEM operating in xenon, for the scintillation and charge channels and for two different cases: for no discrimination implemented (raw pulse-height distributions) and selecting only the pairs of pulses, one in each channel, that are within a microsecond (correlated pulse-height distributions). See text for details.

A more detailed discrimination can be performed, by making use of the scintillation and charge amplitude correlation plot, (A_{sc},A_{ch}). As shown in figure 5.17, most of the pulse amplitudes are in a specific region. This is a consequence of the strong correlation that bonds both type of pulses, i.e. the scintillation pulse in the avalanche is produced by the secondary electrons meanwhile produced in the avalanche. Nevertheless, a small fraction of the pulses fall outside this area. In an offline analysis, one can define a small slab of the amplitude correlation

plot and select only the events that fall in that slab. However, the smaller the selected area for pulse discrimination, the lower the count-rate and pulse-height distribution statistics.

Figure 5.19 presents different pulse-height distributions from ^{241}Am photon interactions obtained with a GEM operating in xenon at 1.0 bar and using increasing areas of the pulse amplitude correlation plot for pulse discrimination, as indicated in each graph. For comparison, the total correlated pulse height distributions, i.e. taking into account the whole area of the amplitude correlation plot, is depicted in all the different graphs.

Figure 5.19 is intended to show that, if a narrow slab is chosen, the effective count-rate is low but the correlated charge and scintillation pulse-height distributions are similar, presenting the charge pulse distribution the same energy resolutions as those of the scintillation pulses. However, as the chosen slab widens and the effective count-rate increases, the good energy resolution of the charge pulse-height distribution is lost, as the fluctuations in the charge collected in the anode increase. For instance, after exiting the GEM holes, the avalanche charge is shared between the GEM bottom electrode and the induction plane, while the scintillation collected in the LAAPD is the same, independent of the particular charge sharing occurred in each pulse.

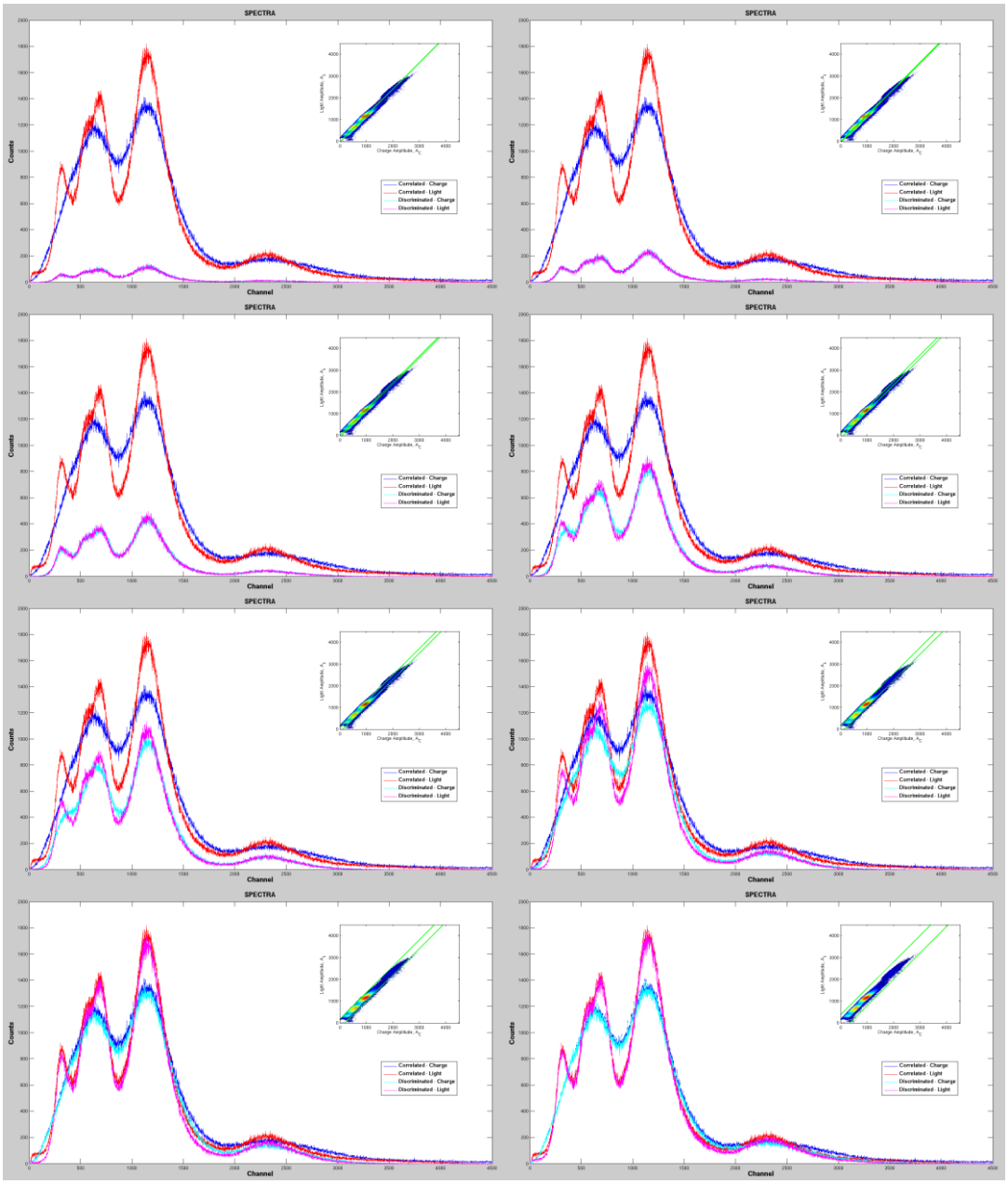

Figure 5.19 - Scintillation and charge pulse-height distributions from ^{241}Am photon interactions obtained with a GEM operating in xenon at 1.0 bar, using increasing areas of the pulse amplitude correlation plot for pulse discriminations, as indicated in each plot. For comparison, the total correlated pulse-height distributions, i.e. taking into account the whole area of the plot, is depicted in all the different graphs

With RADIX it is possible to do further pulse discrimination and perform pulse amplitude corrections. If the amplitude of the scintillation pulses are taken as a reference, given a certain pair of correlated amplitudes (A_{sc},A_{ch}), it is possible to correct the charge amplitude, so that the pair (A_{sc},A_{ch}) falls inside a narrow slab of the plot, e.g. the one chosen for the first graph of figure 5.19. This correction can be done for all the "points" of the plot avoiding, in this way, the reduction of the count rate. Figure 5.20 shows such a corrected pulse height distribution, where the corrected charge distribution becomes similar to the scintillation pulse-height distribution and good performance of the charge readout channel is restored.

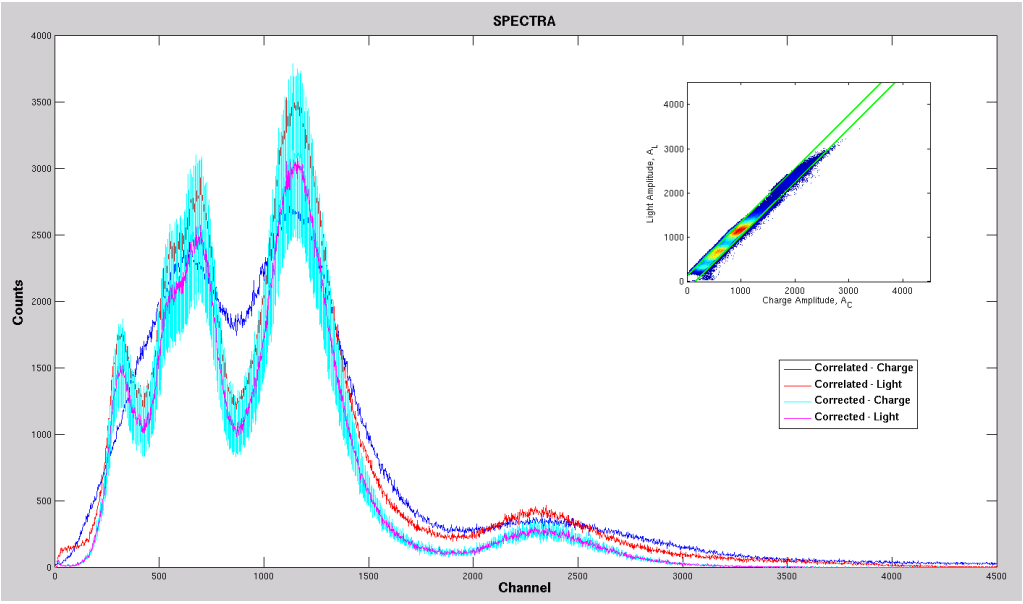

Figure 5.20 - Scintillation and charge pulse-height distributions from ^{241}Am photons, obtained with a GEM operating in xenon at 1.0 bar, after charge amplitude correction has been implemented. The correlated charge and scintillation pulse-height distributions are also presented for comparison.

The implementation of this correction may be useful for improving the performance achieved in micropattern based detectors based on charge readout. Charge readout is a simple, straightforward method to readout the energy released in the detector, avoiding the complexity of a photosensor, and is by far the most used readout method. Yet, its performance is also, most of the times, worse than the scintillation amplification and readout method, and means to improve that performance are always an interesting path to follow. Ideally, a single small area photosensor could be enough to implement such correction. However, in the real world, the area of coverage of the photosensor(s) is ruled by the need to read an enough amount of scintillation as to assure that the statistical fluctuations associated with the scintillation detection are close to optimum. These studies lead to a new collaboration between our group and Ioannis Giomataris group [45], the inventor of the Micromegas micropattern electron multiplier [46,47], to perform studies on scintillation produced in Micromegas.

The effectiveness of other possible pulse discrimination criteria, such as the time delay between the scintillation and the charge pulse, was also studied. The scintillation pulse takes place as the avalanche is developing, while the charge pulse takes place after the drifting of the avalanche electrons towards the induction plane (anode electrode). Figure 5.21 presents correlated pulse-height distributions using a given charge-to-scintillation pulse-time difference range for pulse discrimination. As shown, this discrimination criterion is not as effective as the former one in improving the energy resolution of the charge pulse-height distributions, and was not further followed.

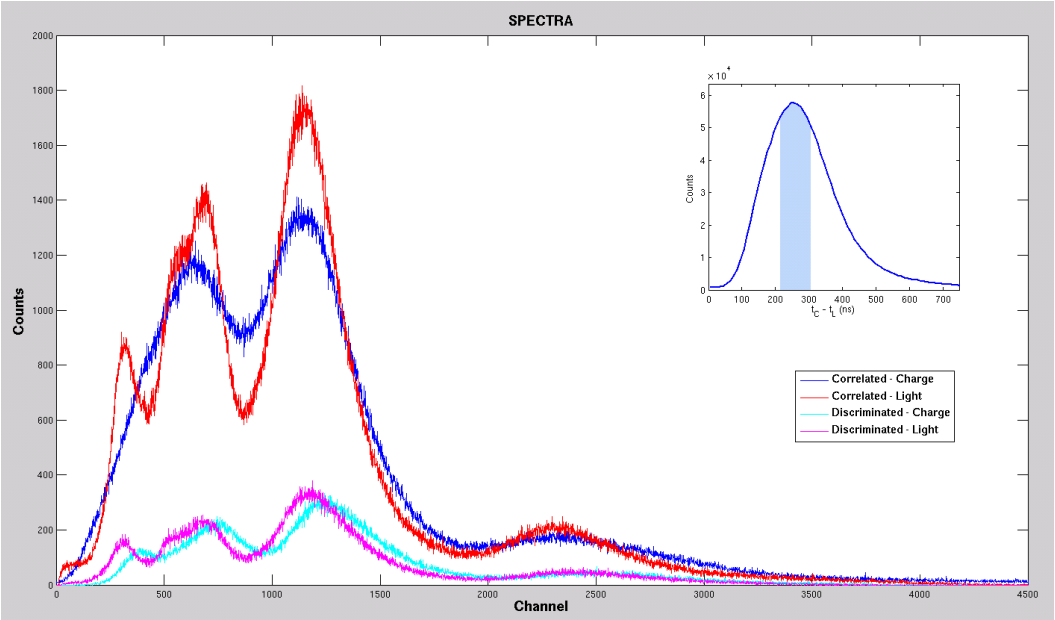

Figure 5.21 – Correlated scintillation and charge pulse-height distributions from ^{241}Am photons obtained with a GEM operating in xenon at 1.0 bar, using a given window, as indicated in the graph, for the time difference between the scintillation and the charge pulses for pulse discriminations. For comparison, the total correlated pulse height distributions, i.e. taking into account the whole time window, is shown.

5.4. Conclusions

The electroluminescence yields produced in GEM and THGEM electron multipliers have been determined and it was demonstrated that the electroluminescence produced in charge avalanches of hole-multipliers permits to achieve yields that can be up to few order of magnitude higher with fairly good energy resolutions, when compared

to what is obtained in uniform field scintillation gaps, commonly used in experiments for Dark Matter search. In view of the large amount of electroluminescence produced in the avalanches of hole-multipliers, photosensors with gains as low as 100, such as LAAPDs, can be effectively used to readout the xenon and argon electroluminescence.

Furthermore, in face of the recent efforts made in Dark Matter search experiments to implement the readout of the secondary avalanche ionisation produced in micropattern electron multipliers for amplification of the primary ionisation signal, the clear advantages of using, instead, the readout of their electroluminescence have been demonstrated. This is true for all the studied cases except for GEMs operating in argon where there is no advantage in using the GEM scintillation when compared to that produced in a uniform electric field gap.

Compared to the traditional charge-readout mode, more stable operation in xenon is reached in GEM in scintillation mode, at lower operating voltages, far below the onset of microdischarges, having gains that are more than two orders of magnitude higher. Scintillation recorded in gaseous hole-multipliers presents significant advantages over and is a valid alternative to large-volume rare-event detectors. It is noted that, since our publication on this issue [21], several papers on optical readout from micropattern electron multipliers, aiming rare event detection, have appeared in the literature [18,48,49]. We have also presented the idea for performing the simultaneous readout of charge

and scintillation pulses in micropattern electron multipliers [50]. This was already used in [18].

Table I summarizes the values for the maximum gain and electroluminescence yield, in terms of number of photons produced in the hole avalanches per primary electron produced in the drift region. We note that the LAAPD gain of 130, used in the current measurements, can increase by two- to 5-fold by increasing the LAAPD voltage biasing and/or reducing its temperature of operation [51]. Naturally, this will increase the overall gain of the scintillation channel, but has no impact on the measured yield. From Table I it is clear that THGEMs, when compared to GEMs, deliver gains and yields that are one order of magnitude higher in xenon at 1 bar, and even more than one order of magnitude higher for argon at 1 bar. However, the THGEM gain and yield have a faster decrease with pressure than those for GEMs presenting, at 2.5 bar, similar gain and yield for xenon, and a seven-fold higher gain and yield for argon. Comparing to argon, the gain and yield of GEMs and THGEMs in xenon are one order of magnitude higher at 1 bar, but present a faster decrease with pressure for xenon having gains and yields that are similar at 2.5 bar for the THGEM and less than one order of magnitude higher for GEMs.

Comparing to the gains achieved in charge readout, the gains achieved with scintillation readout can be more than two orders of magnitude higher, except for the case of the GEM operating in argon, which cannot provide such a large difference.

Table I – Maximum gain and scintillation yield for GEMs and THGEMs operating in argon and xenon at 1 bar and 2.5 bar.

		Xenon		Argon	
		1 bar	**2.5 bar**	**1 bar**	**2.5 bar**
GEM	**Gain**	1.5×10^5	4×10^4	5×10^3	5×10^3
	Yield	6×10^3	1.5×10^3	3×10^2	3×10^2
THGEM	**Gain**	1.2×10^6	4×10^4	1.2×10^5	3×10^4
	Yield	7×10^4	2×10^3	1.5×10^4	4×10^3

As far as scintillation readout is concerned, LAAPDs are good candidates for the scintillation readout, as an alternative to PMTs. They are compact and present low power consumption and high quantum efficiency. In particular, their negligible natural radioactivity is attractive for low-background experiments, such as direct Dark Matter search. On the other hand, the cost of VUV-sensitive LAAPDs can be a drawback but, in recent years, efforts have been made to develop low-cost, LAAPDs with spectral sensitivity below 200 nm and high quantum efficiencies [Hamamatsu].

5.5. References

[1] P. Benetti, E. Calligarich, R. Dolfini, A.G. Berzolari, F. Mauri et al., *Detection of energy deposition down to the keV region using liquid xenon scintillation,* Nucl. Instr. Meth. A 327 (1993) 203.

[2] J. Angle, et al. (XENON10 Collaboration), *Limits on spin-dependent WIMP-nucleon cross sections from the XENON10 experiment*, Phys. Rev. Lett. 101, 091301 (2008).

[3] D.Yu. Akimov, GJ Alner, HM Araujo, A Bewick, C Bungau et al., *The ZEPLIN-III dark matter detector: Instrument design, manufacture and commissioning*, Astropart. Phys. 27 (2007) 46.

[4] P. Benetti, et al. (WARP Collaboration), *First results from a dark matter search with liquid argon at 87 K in the Gran Sasso underground laboratory*, Astropart. Phys. 28 (2008) 495.

[5] P.K. Lightfoot, R. Hollingworth, N.J.C. Spooner, D. Tovey, *Development of a double-phase Xenon cell using micromegas charge readout for applications in dark matter physics*, Nucl. Instrum. Meth. A 554 (2005) 266.

[6] A. Bondar, A. Buzulutskov, A. Grebenuk, D. Pavlyuchenko, R. Snopkov, Y. Tikhonov, *Two-phase argon and xenon avalanche detectors based on Gas Electron Multiplier*s, Nucl. Instrum. Meth. A 556 (2006) 273.

[7] A. Bondar, A. Buzulutskov, A. Grebenuk, D. Pavlyuchenko, R. Snopkov, Y. Tikhonov, *First results of the two-phase argon avalanche detector performance with CsI photocathode*, Nucl. Instrum. Meth. A 581 (2007) 241.

[8] M. Gai, R. Alon, A. Breskin, M. Cortesi, D.N. McKinsey, J. Miyamoto, K. Ni, D.A.R. Rubin, and T. Wongjirad, *Toward Application of a Thick Gas Electron Multiplier (THGEM) Readout for a Dark Matter Detector*, Xiv:0706.1106v1 [physics.ins-det] 8 Jun 2007, presented at the "23rd Winter Workshop on Nuclear Dynamics Big Sky, Montana, USA, February 11–18, 2007.

[9] A. Bondar, A. Buzulutskov, A. Grebenuk, D. Pavlyuchenko, Y. Tikhonov, A. Breskin, *Thick GEM versus thin GEM in two-phase argon avalanche detectors*, 2008 J. Inst. 3 P07001

[10] R. Alon, J. Miyamoto, M. Cortesi, A. Breskin, R. Chechik, I. Carne, J.M. Maia, J.M.F. dos Santos, M. Gai, D. McKinsey and V. Dangendorf, *Operation of a Thick Gas Electron Multiplier (THGEM) in Ar, Xe and Ar-Xe*, 2008 J. Inst. 3 P01005.

[11] F. Balau, V.Solovov, V.Chepel, A.Pereira, M.I.Lopes, *GEM operation in double-phase xenon*, Nucl. Instrum. Meth. A 598 (2009) 126.

[12] Badertscher, L. Knecht, M. Laffranchi, A. Marchionni, G. Natterer, P. Otiougova, F. Resnati, A. Rubbia, *Construction and operation of a Double Phase LAr Large Electron Multiplier Time Projection Chamber*, 2008 IEEE Nucl. Sci. Symp. – Conf. Rec., Vol.1 (2009) 603-609

[13] L. Kaufmann, A. Rubbia, The ArDM project: a direct detection experiment, based on liquid argon, for the search of dark matter, Nuc. Phys. B-Procc. Supp. 173 (2007) 141-143.

[14] D. Autiero, J. Aysto, A. Badertscher, L. Bezrukov, J. Bouchez et al., *Large underground, liquid based detectors for astro-particle physics in Europe: scientific case and prospects*, J. Cosmol. Astrop. Phys. 11 (2007) 011.

[15] C.A.N. Conde, A.J.P.L. Policarpo, *A gas proportional scintillation counter*, Nucl. Instr. Meth. Vol. 53 (1967) 7-12.

[16] A.J.P.L. Policarpo, C.A.N. Conde, M.A.F. Alves, *Large light output gas proportional scintillation counters*, Nucl. Instrum. Meth. 55 (1968) 105.

[17] R. Neilson, F. LePorta, A. Pocara, K. Kumarb, A. Odian, *Characterization of large area APDs for the EXO-200 detector*, Nucl. Instrum. Meth. A 608 (2009) 68.

[18] A. Bondar, A. Buzulutskov, A. Grebenuk, A. Sokolov, D. Akimov et al., *Direct observation of avalanche scintillations in a THGEM-based two-phase Ar avalanche detector using Geiger-mode APD*, J. Instr. 5 (2010) P08002.

[19] P.K. Lightfoot, G.J. Barker, K. Mavrokoridis, Y.A. Ramachers, N.J.C. Spooner, *Characterisation of a silicon photomultiplier device for applications in liquid argon based neutrino physics and dark matter searches*, J. Instr. 3 (2008) P10001.

[20] Ana Sofia dos Santos Conceição, *Estudo da Cintilação em GEM's a operar em Xénon*, Dissertação de Mestrado em Instrumentação e Microelectrónica, GIAN, Departamento de Física, FCTUC, Dezembro de 2007.

[21] C. M. B. Monteiro, A. S. Conceição, F. D. Amaro, J. M. Maia, A. C. S. S. M. Bento et al., *Secondary scintillation yield from gaseous micropattern electron multipliers in direct Dark Matter detection*, Physics Letters B 677 (2009) 133.

[22] A.S. Conceição, L.F. Requicha Ferreira, L.M.P. Fernandes, C.M.B Monteiro, L.C.C. Coelho et al., *GEM scintillation readout with avalanche photodiodes*, JINST 2 (2007) P09010.

[23] F. Sauli, *GEM: a new concept for electron amplification in gas detectors*, Nucl. Instr. Meth. A 386 (1997) 531.

[24] R. Chechik, A. Breskin, C. Shalem, D. Mormann, *Thick GEM-like hole multipliers: properties and possible applications*, Nucl. Instr. Meth. A 535 (2004) 303.

[25] J.A.M. Lopes, Contadores gasosos de Cintilação proporcional: Novas aplicações e tecnologias de fotosensores integrados, Tese de Doutoramento, Departamento de Física, FCTUC, 2002. (pag.123)

[26] L.M.P. Fernandes, Caracterização dos fotodíodos de avalanche de grande área para a detecção de raios X, luz ultravioleta de vazio e luz visível, Tese de Doutoramento, Departamento de Física, FCTUC, 2005. (pag. 49).

[27] C. M. B. Monteiro, J. A. M. Lopes, P. C. P. S. Simões, J. M. F. dos Santos, C. A. N. Conde, *An Argon Gas Proportional Scintillation Counter With UV Avalanche Photodiode Scintillation Readout*, IEEE Trans. Nucl. Sci. 48 (2001) 1081.

[28] M. Suzuki and S. Kubota, *Mechanism of proportional scintillation in argon, krypton and xenon*, Nucl.Instrum.Meth. 164 (1979) 197-199.

[29] M.M.Fraga, F.A.F. Fraga, and A.J.P.L. Policarpo, *Modelling of an IR scintillation counter*, Nucl. Instrum. Meth. A 442 (2000) 423-427.

[30] G.F. Knoll, *Radiation detection and measurement*, 3rd Edition, Wiley, New York (2000).

[31] J.A.M. Lopes, J.M.F. Dos Santos, R.E. Morgado, C.A.N. Conde, *A xenon gas proportional scintillation counter with a UV-sensitive, large-area avalanche photodiode*, IEEE Trans. Nucl. Sci., **48** (2001) 312-319.

[32] B. Zhou, M. Szawlowski, *An explanation on the APD spectral quantum efficiency in the deep UV range*, Interoffice Memo, Advanced Photonix Inc., 1240 Avenida Acaso, Camarillo, CA 93012, EUA, 1999.

[33] T.H.V.T. Dias, J.M.F. dos Santos, P.J.B.M. Rachinhas, F.P. Santos, C.A.N. Conde, A.D. Stauffer, *Full-energy absorption of x-ray energies near the Xe L-and K-photoionization thresholds in xenon gas detectors: Simulation and experimental results*, J. Appl. Phys. **82** (1997) 2742.

[34] I. K. Bronic, *W values and Fano factors for electrons in rare gases and rare gas mixtures*, Hoshasen: ionizing radiation, vol. 24 (1998) 101-125.

[35] A. Buzulutskov, *Physics of multi-GEM structures*, Nucl. Instrum. Meth. A 494 (2002) 148, and references therein.

[36]] T.H.V.T. Dias, FP Santos, PJBM Rachinhas, FIGM Borges, JMF dos Santos et al., *Xenon-neon gas proportional scintillation counters: Experimental and simulation results*, J. Appl. Phys. 85 (1999) 6303.

[37] J. Angle et al. (XENON10 Collaboration), *Design and Performance of the XENON10 Dark Matter Experiment*, first revision submitted for publication to Astropart. Phys., Aug. 2010.

[38] C.M.B. Monteiro, J.F.C.A. Veloso, J.A.M. Lopes and J.M.F. dos Santos, *Secondary scintillation yield in pure argon*, Phys. Lett. B 668 (2008) 167.

[39] J.M.F. dos Santos, J.F.C.A. Veloso, R.E. Morgado, C.A.N. Conde, *The performance of a compact gas proportional scintillation counter for hard x-ray spectrometry*, Nucl. Instr. and Meth A 353 (1994) 195.

[40] A. Bolozdynya, V. Egorov, A. Koutchenkov, G. Safronov, G. Smirnov et al., *A high pressure xenon self-triggered scintillation drift chamber with 3D sensitivity in the range of 20-140 keV deposited energy*, Nucl. Instr. and Meth A 385 (1997) 225.

[41] F.D. Amaro, A.S. Conceição, J.F.C.A. Veloso, L.C.C. Coelho, L.M.P. Fernandes, L.F. Requicha Ferreira, J.A.M. Lopes, J.M.F. dos Santos, *Operation of a single-GEM in noble gases at high pressures*, Nucl. Instr. Meth. A 579 (2007) 62

[42] J.M.F. Dos Santos, J.A.M. Lopes, J.F.C.A. Veloso, P.C.P.S. Simões, T.H.V.T. Dias et al., *Development of portable gas proportional scintillation counters for x-ray spectrometry*, X-Ray Spectrometry 30 (2001) 373.

[43] CAEN, Via Vetraia, 11, 55049 – Viareggio (LU), Italy. *Model N1728A/N1728B, 4 channel flash ADC*, Revision Nº 5, October 2007.

[44] M. Ritcher, C. Santos, *TNT2 digital pulse processor functionalities & TUC control software*, Centre National de la Recherche Scientifique, Institute Pluridisciplinaire Hubert Curien – Institute National de Physique Nucléaire et de Physique des Particules, Strasbourg, July 2007.

[45] I. Giomataris, IRFU, Centre d' Études Nucléaires de Saclay (CEA-Saclay), Gif-sur-Yvette, France.

[46] Y. Giomataris, P. Rebourgeard, J.P. Robert, G. Charpak, *MICROMEGAS: A high-granularity position-sensitive gaseous detector for high particle-flux environments*, Nucl. Instr. Meth. A 376 (1996) 29.

[47] I. Giomataris, R. De Oliveira, S. Andriamonje, S. Aune, G. Charpak et al., *Micromegas in a bulk*, Nucl. Instr. Meth. A 560 (2006) 405 [arXiv:physics/0501003].

[48] PK Lightfoot, GJ Barker, K Mavrokoridis, YA Ramachers, NJC Spooner, *Optical readout tracking detector concept using secondary scintillation from liquid argon generated by a thick gas electron multiplier*, J. Inst. 4 (2009) P04002.

[49] GJ Barker, PK Lightfoot, YA Ramachers, NJC Spooner, *Optical readout tracking detector concept for future large volume liquid argon detectors*, Nucl. Instrum. Meth. A 619 (2009) 140.

[50] JMF dos Santos, *Scintillation readout from THGEMs operating in xenon*, talk presented at the "2nd RD51 collaboration meeting", 13-15 Oct. 2008, Paris.
http://indico.cern.ch/conferenceOtherViews.py?view=standard&confId=35172

[51] JAM Lopes, LMP Fernandes, JMF dos Santos, RE Morgado, CAN Conde, *VUV detection in large-area avalanche photodiodes as a function of temperature*, Nucl. Instrum. Meth. A 504 (2003) 331.

[52] LMP Fernandes, JAM Lopes, CMB Monteiro, JMF dos Santos, CAN Conde, *Non-linear behavior of large area avalanche photodiodes*, Nucl. Instrum. Meth. A 478 (2002) 395.

CHAPTER 6

Characterization of Large Area Avalanche Photodiodes for the Detection of Xenon and Argon Electroluminescence

6. Motivation

Different studies have proven the LAAPD response characteristics for VUV to be different from those for visible light, used to determine most of the characteristics of the photodiodes [1-3]. The X-ray-to-photon detection non-linearity, the sensitivity to magnetic fields and the relative variation of gain with temperature have been measured for VUV, presenting higher values when compared to visible light detection. This is due to the difference in the average interaction depth of the photons,

which is approximately 1 μm for 520-nm photons and approximately 5 nm for 172-nm photons [4]. VUV-photons interact mainly within the first atomic layers of the wafer, where the electric field is weaker. This results in higher diffusion of the charge carriers, which can be lost to the surface boundary and to impurities.

For the work to be performed under the scope of the present thesis, it was found to be important to study the photosensors to be used along the electroluminescence studies. Having results which allow to further study the performance of the LAAPD for detection of the 2nd continuum of xenon and argon scintillation, complementing the work of L.M.P. Fernandes, this chapter presents the results for the study of the response characteristics of a "Deep UV 500 windowless series" LAAPD from API to the argon and xenon electroluminescence. The LAAPD minimum detectable number of photons and the overall statistical fluctuations associated to photon detection was studied as a function of LAAPD gain. It should be noted that the wavelength of the argon electroluminescence is in the lower limit of the LAAPD spectral response.

6.1. Experimental Setup

The LAAPD was used as a photosensor substituting for the PMT and, for that purpose, it was placed inside a Gas Proportional Scintillation Counter as shown in figure 6.1.

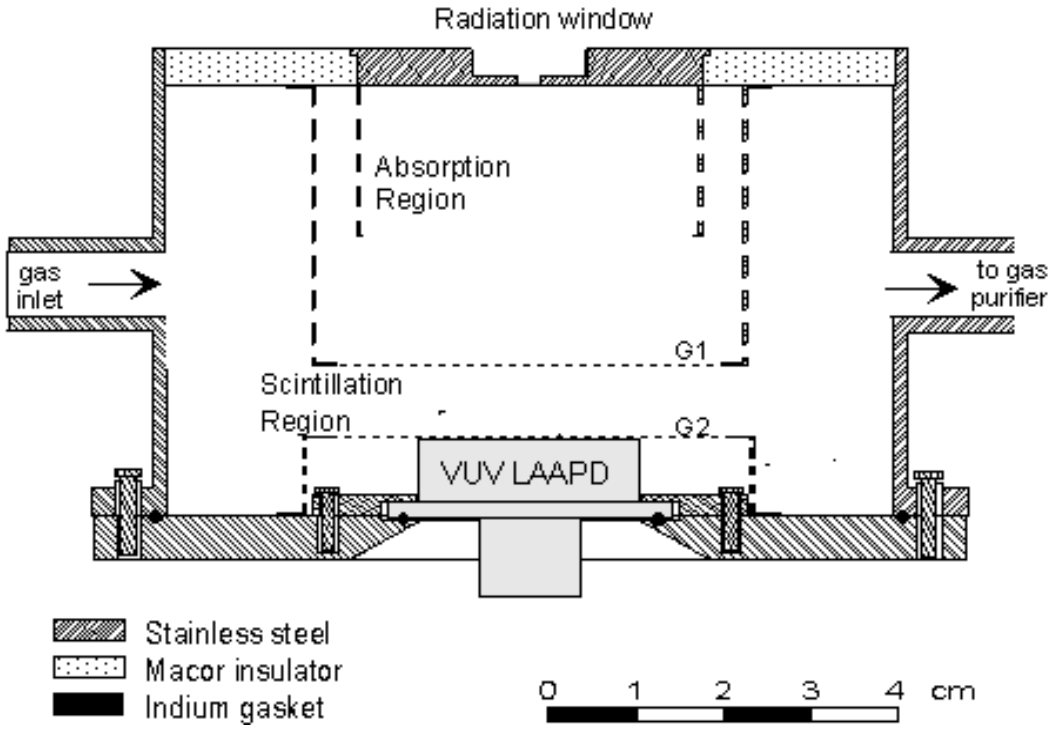

Figure 6.1 - Schematic of the GPSC instrumented with a Large Area Avalanche Photodiode as the photosensor.

This GPSC and its operation have already been described in chapter 4. The detector was filled with gas, either pure argon at 1.52 bar or pure xenon at 1.1 bar, which were continuously purified through non-evaporable getters.

Throughout the present experimental work, the reduced electric field, E/p - the electric field divided by the gas pressure - in the scintillation regions was kept constant at 3.7 kV cm^{-1} bar^{-1} for argon and 4.9 kV cm^{-1} bar^{-1} for xenon, values for which the detector energy resolution was optimum. The X-ray interaction rate in the gas was maintained at approximately a few hundred counts per second.

The LAAPD was biased with different voltage values for operation at different gains. The LAAPD signals were fed through a low-noise 1.5-V/pC charge preamplifier to an amplifier with 2-μs shaping time and were pulse-analysed with a multichannel analyser. For pulse amplitude and energy resolution measurements the pulse-height distributions were fit to Gaussian functions superimposed on a linear background, from which the centroid and the full-width-at-half-maximum, FWHM, were determined.

6.2. Experimental Results

6.2.1. Xenon

Figure 6.2 depicts a typical pulse-height distribution obtained with the xenon-GPSC when irradiated with 5.9-keV X-rays from a ^{55}Fe radiation source. The 5.9-keV X-rays are fully absorbed in the xenon gas filling and do not reach the LAAPD. The salient features of the pulse-height distributions include the xenon scintillation peaks resulting from the full absorption of the 5.9-keV X-rays in the gas and from the subsequent escape of the xenon fluorescence and the electronic noise-tail in the low-energy limit.

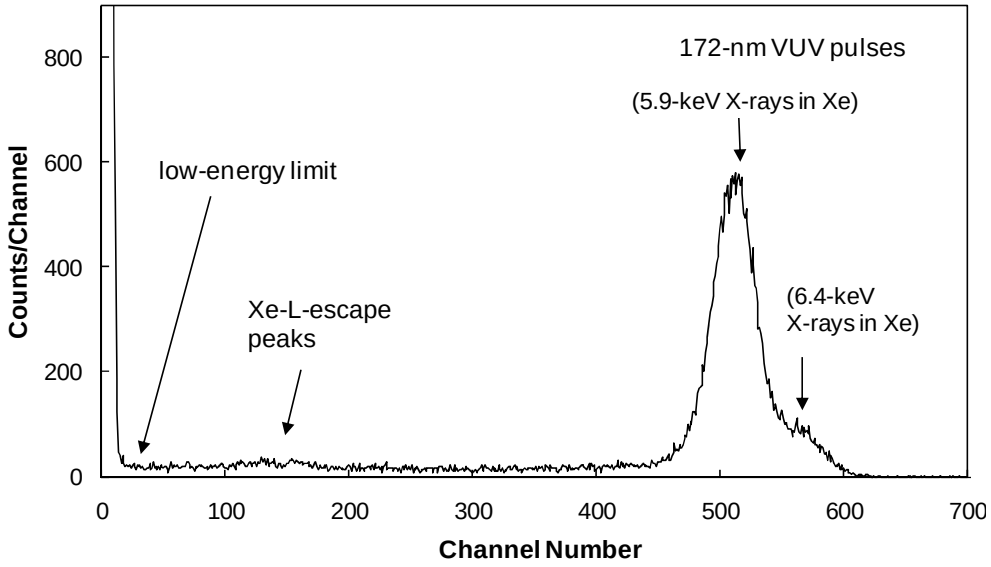

Figure 6.2 - Pulse-height distribution resulting from VUV-scintillation pulses of xenon in the LAAPD.

Under the present conditions, for each 5.9-keV X-ray interaction in the drift region of the GPSC, the average number of VUV photons for xenon can be calculated from the electroluminescence yield studies of chapter 3. From equation (3.10) one can obtain the electroluminescence yield for a reduced electric field of 4.9 kV cm^{-1} bar^{-1} in the scintillation region,

$$Y/p = 140 \times 4.9 - 116 = 570 \quad \text{photons } e^{-1}\ cm^{-1}\ bar^{-1}.$$

Knowing the gas pressure, the scintillation region thickness, 0.8 cm, the number of primary electrons produced in the drift region by the incident 5.9-keV X-rays, N_e = 263 from equation 3.6, grid G2 transmission, 0.84, and the average relative solid angle subtended by the LAAPD relative to the electron path in the scintillation region, 0.215, the calculation of the average number of photons hitting the LAAPD is

N_{uv} = 570 ×1.1 × 0.8 × 263 × 0.84 × 0.215 ≈ 2.4 × 10^4 photons.

From this value, the pulse-height distribution can be calibrated in terms of number of photons, instead of number of channels.

6.2.1.1. Detection Limit

Figure 6.3 presents the Minimum number of Detectable Photons (MDP) for the xenon electroluminescence, defined as the number of photons that would deposit, in the LAAPD, an amount of energy equivalent to the onset of the electronic noise tail. The MDP is approximately constant being, for the present conditions, about 600 photons for 172-nm VUV-light pulses, for gain values above 40, increasing significantly as the gain drops below these values and the signal approaches the noise level.

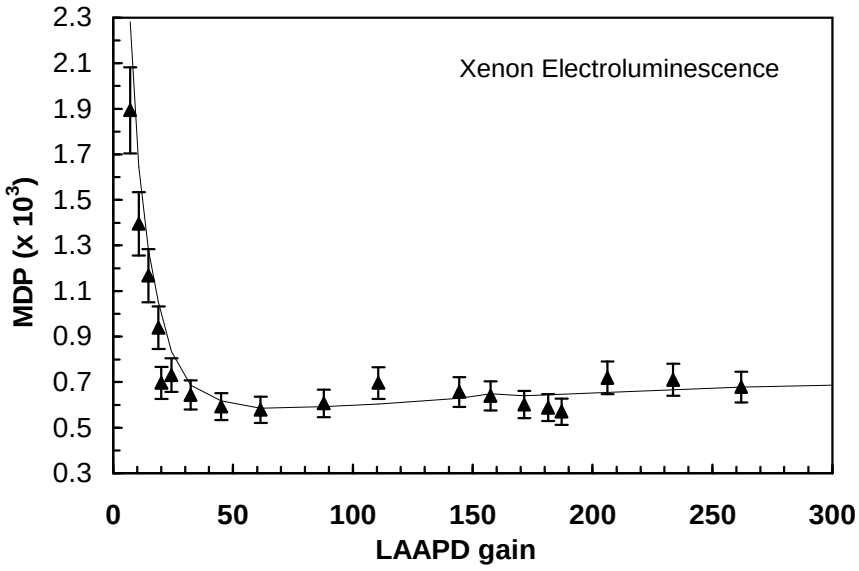

Figure 6.3 - Minimum number of detectable 172-nm VUV-photons as a function of LAAPD gain. The line serves only to guide the eyes.

The obtained MDP can decrease if further efforts are made towards the reduction of the noise level achieved in the present setup. Nevertheless, the MDP can be reduced up to a factor of two by cooling the temperature of the photodiode to temperatures below 0 ºC [3].

The results obtained with this LAAPD for MDP at 172 nm are lower than those obtained with the peltier-cooled LAAPD in [3] (~10^3 photons). The difference may be attributed to the differences in the LAAPDs dark currents, which limit the electronic noise and, thus, the MDP. It can also be attributed to the noise level present in both setups. Since the peltier-cooled LAAPD has a different enclosure, with more wiring, it is more prone to electronic noise.

6.2.1.2. Statistical Fluctuations

The statistical fluctuations associated to the detection of VUV light in the LAAPD may be estimated from the measured energy resolution of the pulse-height distributions of 5.9-keV full absorption in the gas. The energy resolution of a conventional GPSC is determined by the statistical fluctuations occurring in the primary ionisation processes in the gas, in the production of the VUV scintillation photons and in the photosensor. Since the statistical fluctuations associated to the scintillation processes are negligible when compared to those associated to the primary electron cloud formation in the gas, and those associated

to the scintillation detection in the photosensor, the energy resolution, R, of the GPSC, for an X-ray energy E_x, is given by [6]

$$R = 2.355\sqrt{\frac{F}{N_e} + \left(\frac{\Delta E}{E}\right)^2} = 2.355\sqrt{\frac{Fw}{E_x} + \left(\frac{\Delta E}{E}\right)^2} \qquad (6.1)$$

where N_e is the average number of primary electrons produced in the gas by the X-rays, F is the Fano factor, w is the average energy to create a primary electron in the gas and E is the energy deposited by the VUV-radiation in the photosensor.

The statistical fluctuations associated to the VUV-photon detection can be, thus, obtained by

$$\frac{\Delta N_{UV}}{N_{UV}} = \frac{\Delta E}{E} = \sqrt{\left(\frac{R}{2.355}\right)^2 - \frac{Fw}{E_x}} \qquad (6.2).$$

In the present case, E_x is 5.9-keV, w = 22.4 eV and F = 0.17 for xenon. The relative statistical fluctuations associated to VUV detection of 2.4×10^4 photons for ~172 nm VUV-light pulses, as a function of gain, are depicted in figure 8.4. The LAAPD relative uncertainty decreases rapidly with the onset of gain, stabilizing for gains above approximately 30 and reaching values of 2.2%. This value can be reduced by cooling the photodiode operating temperature to values around 0 °C [5].

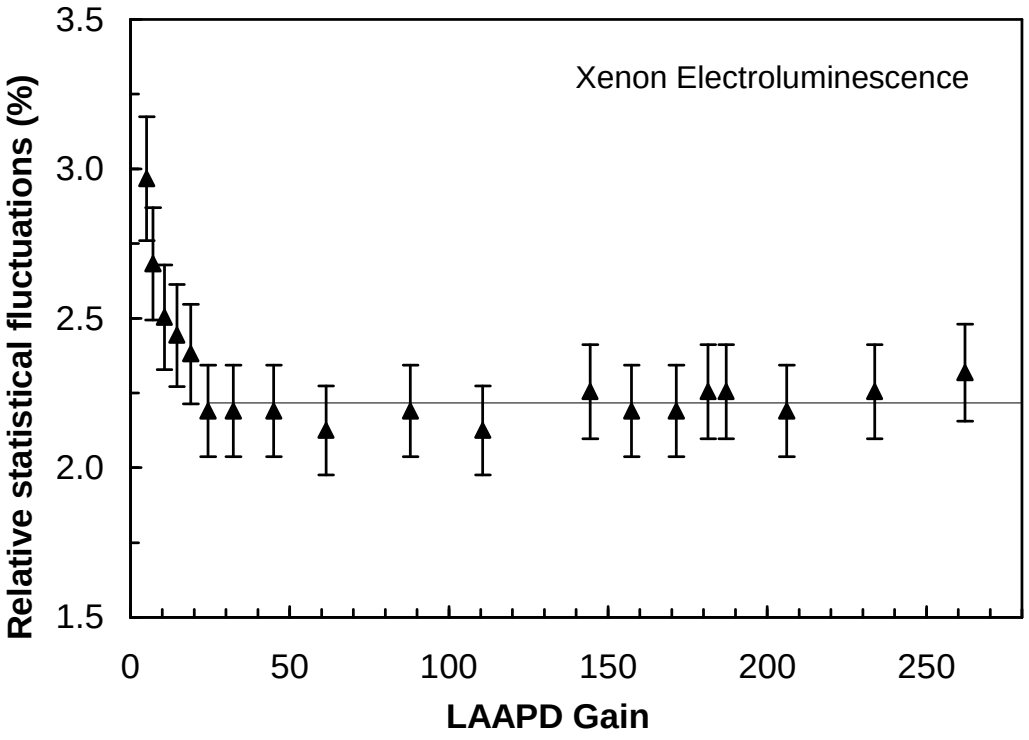

Figure 6.4 - Relative statistical fluctuations associated to the VUV detection of 2.4×10^4 photons of ~172 nm VUV-light pulses as a function of LAAPD gain. The line serves only to guide the eyes.

Figures 6.3 and 6.4 show that, for the detection of the light-levels of 172-nm photons presented in this study, best performance characteristics are achieved for gains around 40. However, gains as low as 20 are sufficient to achieve a nearly optimum performance, i.e. without presenting significant degradation of MDP and resolution. For lower light levels, higher gains may be needed to pull the signal of the light-pulse out of the noise and achieve the best possible performance.

6.2.2. Argon

Figure 6.5 depicts a typical pulse-height distribution obtained with the argon GPSC when irradiated with 5.9-keV X-rays from ^{55}Fe, with the K_β line filtered through a chromium film. Approximately 10% of the 5.9-keV X-rays are transmitted through the 3.3-cm argon depth and 40% of these are absorbed in the depletion region of the APD. The salient features of the pulse-height distributions include the argon scintillation peaks resulting from the full absorption of the 5.9-keV X-rays in the gas and from the subsequent escape of the argon fluorescence, the 5.9-keV X-ray peak from direct absorption in the LAAPD and the electronic noise-tail in the low-energy limit.

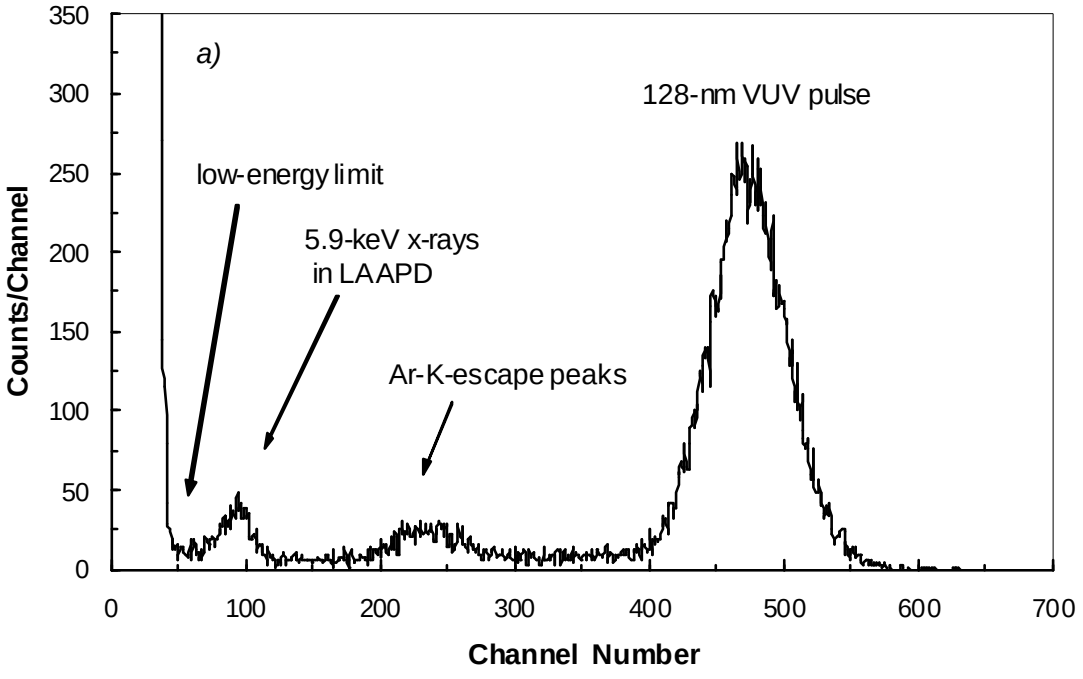

Figure 6.5 - Pulse-height distribution resulting from both argon VUV-scintillation pulses and 5.9-keV X-ray interactions in the LAAPD.

The spectra obtained with the argon GPSC allow a direct comparison of the relative amplitudes from the argon scintillation and from the X-ray interaction in the LAAPD. As can be seen in figure 6.5, the argon scintillation pulse deposits in the LAAPD an amount of energy similar to what would be deposited by the interaction of ~30-keV X-rays in the photodiode.

Similarly to what has been done for xenon, under the present conditions, for each 5.9-keV X-ray interaction in the drift region of the GPSC, the average number of VUV photons for argon can be determined from the electroluminescence yield studies of chapter 4. From figure 4.11 one can determine the electroluminescence yield for a reduced electric field of 3.7 kV cm^{-1} bar^{-1} in the scintillation region to be 290 photons e^{-1} cm^{-1} bar^{-1}.

From the gas pressure, the scintillation region thickness, the number of primary electrons produced in the drift region by the incident 5.9-keV X-rays, N_e = 223 from equation 4.1, grid G2 transmission, and the average relative solid angle subtended by the LAAPD relative to the electron path in the scintillation region, the calculation of the average number of photons hitting the LAAPD is

$$N_{uv} = 290 \times 1.52 \times 0.8 \times 223 \times 0.84 \times 0.215 \sim 1.4 \times 10^4 \text{ photons.}$$

From this value, the pulse-height distribution can be calibrated in terms of number of photons, instead of number of channels.

6.2.2.1. Detection Limit

Figure 6.6 presents the minimum number of detectable photons (MDP) for argon electroluminescence, as defined for the xenon case. The MDP shows a similar trend as for xenon; it is approximately constant, being about 1300 photons for 128-nm VUV-light pulses, for gains above 60, increasing significantly as the gain drops below this value.

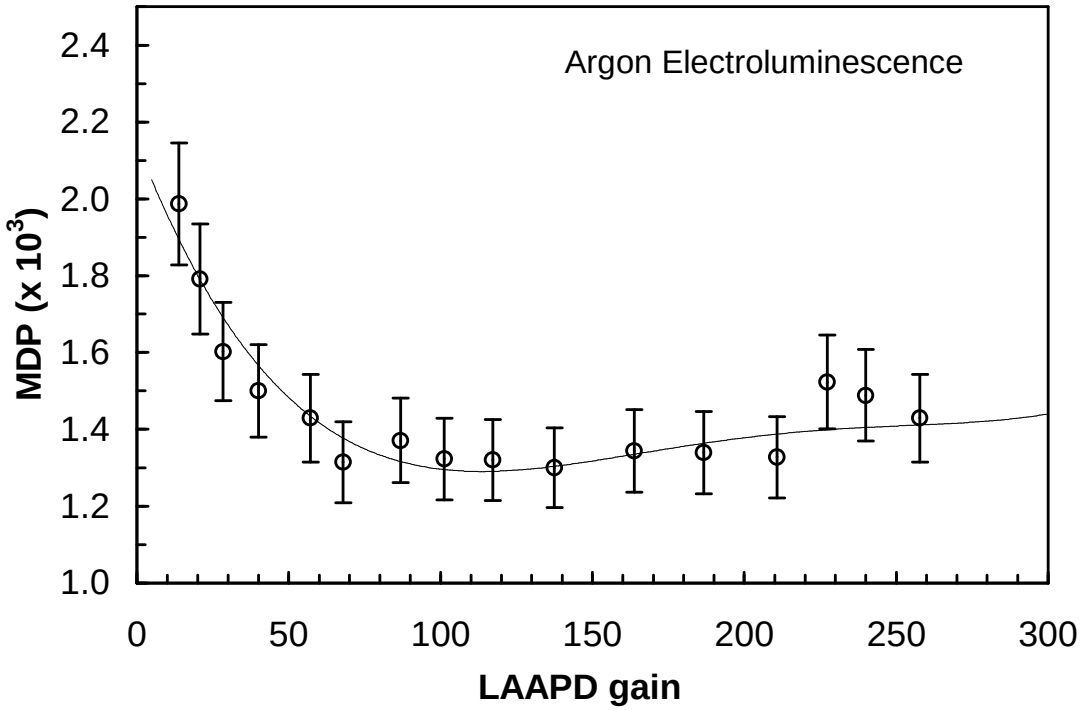

Figure 6.6 - Minimum number of detectable 128-nm VUV-photons as a function of LAAPD gain. The line serves only to guide the eyes.

As for the xenon case, the obtained MDP can decrease if further efforts are made to reduce the noise level of the present setup and can be reduced up to a factor of two by cooling the photodiode to temperatures below 0 ºC [3].

6.2.2.2. Statistical Fluctuations

As for xenon, the statistical fluctuations associated to the detection of VUV light in the LAAPD may be estimated from the measured energy resolution of the pulse-height distributions of 5.9 keV full absorption in the gas. The statistical fluctuations associated to the VUV-photon detection can, thus, be obtained from equation 6.2 where, for argon, w = 26.4 eV and F = 0.30. The relative statistical fluctuations associated to VUV detection of 1.4×10^4 photons of ~128 nm photons VUV-light pulses, as a function of gain, are depicted in figure 6.7. The LAAPD relative uncertainty decreases rapidly with the onset of gain, stabilizing for gains above ~30 and reaching values of 3.9%.

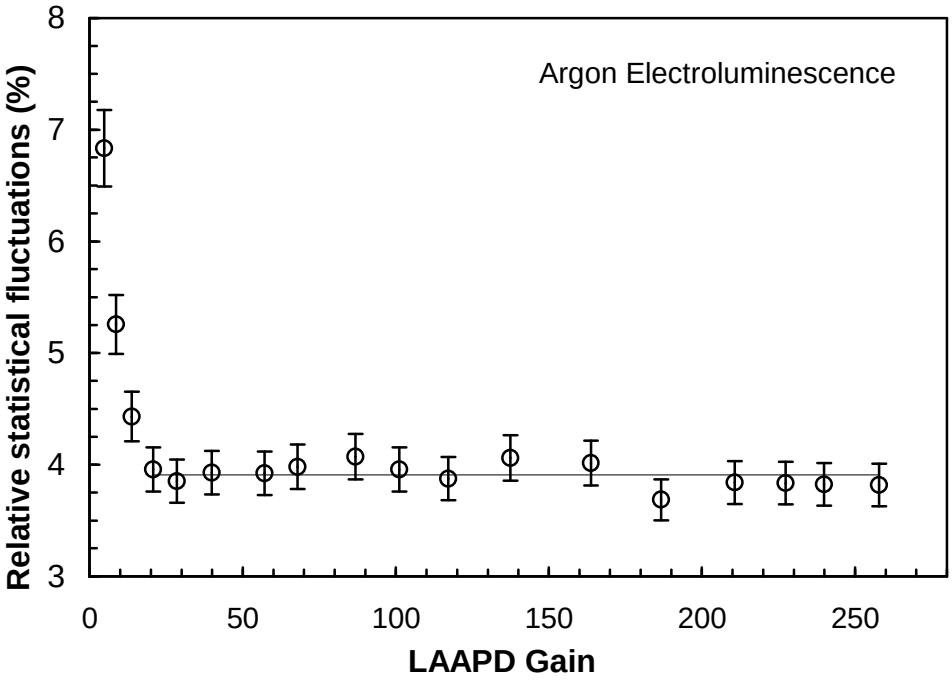

Figure 6.7 - Relative statistical fluctuations associated to VUV detection of 1.4×10^4 photons of ~128-nm VUV-light pulses as a function of LAAPD gain. The line serves only to guide the eyes.

Figures 6.6 and 6.7 show that, for the detection of the light-levels of 128-nm photons presented in this study, best performance characteristics are achieved for gains above 60. For gains lower than 60, the MDP increases significantly, while the statistical fluctuations remain constant down to gains of 20.

6.3. Conclusions

The LAAPD is a suitable device for the detection of VUV light pulses of photons down to about 120 nm. PMTs present a sensitivity range down to 115 nm (with MgF2 windows), gains above 10^7, dark currents below few nA, instead of a few hundred nA for the LAAPDs, and are suitable for single photon detection. However, the photodiode compactness, reduced power consumption, simple operation and straightforward photon calibration are significant advantages over PMTs.

Figure 6.8 presents the results of MDP for xenon and argon. The minimum numbers of photons that can be detected with the LAAPD, for this experimental setup, are about 1300 and 600 for 128- and 172 nm, respectively, almost three orders of magnitude higher than is the case for PMTs. Therefore, the LAAPD is not suitable for single photon detection and VUV-photon spectrometry. Nevertheless, it can be applied to synchrotron radiation in VUV-photon detection and to other areas of optics, where the light levels are adequate for its use.

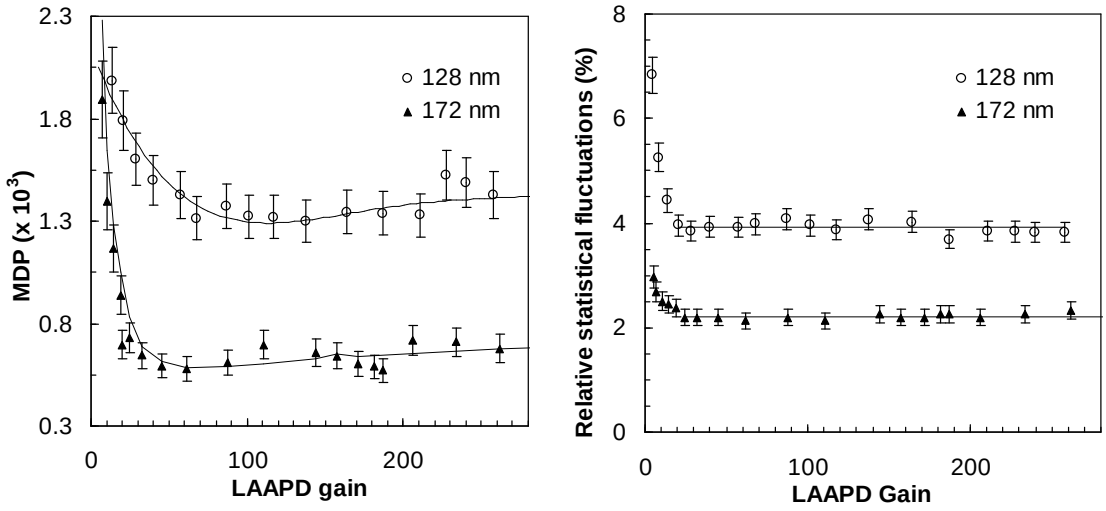

Figure 6.8 - Minimum number of detectable 128-nm and 172-nm VUV-photons as a function of LAAPD gain as well as relative statistical fluctuations associated to VUV detection of 1.4×10^4 photons of ~128 nm and 2.4×10^4 photons of ~172 nm VUV-light pulses as a function of LAAPD gain. The lines serve only to guide the eyes.

The MDP for 172-nm photons is about half of that for 128 nm photons, achieving the lowest values for lower gains. This difference reflects the higher spectral sensitivity of the LAAPD for 172 nm, which is approximately 150 mA/W, corresponding to an average number of 1.1 free electrons produced in the LAAPD per incident VUV-photon, when compared to 50 mA/W that corresponds to an average number of 0.55 free electrons produced in the photodiode per incident VUV-photon for 128 nm [7]. In fact, it is the number of primary charge carriers that defines the corresponding signal amplitude and the signal-to-noise ratio.

Figure 6.8 depicts also the results of the relative statistical fluctuations associated to the VUV detection of $1.4x10^4$ photons of 128-nm and of 2.4×10^4 photons of 172-nm VUV-light pulses. These values are 3.9% and 2.2%, respectively. This difference is consistent with the dependence of the LAAPD resolution on the inverse of the square root of the number of the charge carries produced in the photodiode [8] and it reflects not only the difference in the number of photons involved in each case, but also the difference in the respective quantum efficiency. The numbers of charge carriers produced in the LAAPD are

$2.4 \times 10^4 \times 1.1 = 2.64 \times 10^4$ free electrons for xenon

and

$1.4 \times 10^4 \times 0.55 = 77 \times 10^3$ free electrons for argon,

being

$$2.2 \times \sqrt{\frac{26400}{7700}} \cong 3.9 .$$

This is also consistent with the results for visible (red) light from a LED obtained in [5], with an energy resolution of 7% for 2600 free electrons produced in the LAAPD.

Therefore, the experimental results presented in this chapter show that, both MDP and statistical fluctuations associated to light detection do not depend on photon wavelength, but rather on the number of charge carriers produced by the light-pulse in the LAAPD. This is in opposition to other effects like light-to-X-rays non-linearity and the

amplitude behaviour under intense magnetic fields, where the photon interaction in the first atomic layers of the wafer has a significant influence on these results.

For the present charge carrier quantities, LAAPD gains as low as 30 to 60 are enough to obtain the best performances. However, gains as low as 20 and 30, respectively, are sufficient to achieve a nearly optimum performance, i.e. without presenting significant degradation of MDP and resolution, as can be seen from figure 6.8. For lower light levels, higher gains will be needed to pull the signal of the light-pulse out of the noise and achieve the best possible performance.

6.4. References

[1] L.M.P. Fernandes, J.A.M. Lopes, C.M.B. Monteiro, J.M.F. dos Santos, R.E. Morgado, *Non-linear behaviour of Large Area Avalanche Photodiodes*, Nucl. Instrum. Methods A 478, 395 (2002).

[2] L.M.P. Fernandes, A. Antognini, M. Boucher, C.A.N.Conde, O. Huot, P.E. Knowles, F. Kottmann, L. Ludhova, F. Mulhauser, R. Pohl, J.M.F. dos Santos, L.A. Schaller, D. Taqqu, J.F.C.A. Veloso, *Behaviour of Large área avalanche Photodiodes under intense magnetic fields for VUV, visible and X-ray photon detection,* Nucl. Instrum. Methods A 498, 362 (2003).

[3] J.A.M. Lopes, L.M.P. Fernandes, J.M.F. dos Santos, R.E. Morgado, C.A.N. Conde, *VUV detection in Large Area Avalanche Photodiodes as a function of Temperature,* Nucl. Instrum. Methods A 504, 331 (2003).

[4] T.W. Barnard, M.M.I. Crockett, J.C. Ivaldi, P.L. Lundberg, D.A. Yates, P.A. Levine, D.J. Sauer, *Solid state detector for ICP-OES,* Anal. Chem. 65, 1231 (1993).

[5] L.M.P. Fernandes, J.A.M. Lopes, J.M.F. dos Santos, P.E. Knowles, L. Ludhova, F. Mulhauser, F. Kottmann, R. Pohl, D. Taqqu, *LAAPD low temperature performance in X-Ray and visible light detection,* IEEE Trans. Nucl. Sci. 51, 1575 (2004).

[6] J.M.F. dos Santos, J.A.M. Lopes, J.F.C.A. Veloso, P.C.P.S. Simões, T.H.V.T.Dias, F.P. Santos, P.J.B.M. Rachinhas, L.F.R. Ferreira, C.A.N. Conde, *On the portability of Gas Proportional Scintillation Counters for X-ray Spectrometry,* X-Ray Spectrom. **30,** 373 (2001).

[7] *Windowless Large Area APDs,* Application notes 1999, Advanced Photonix Inc., 1240 Av. Acaso, Camarillo, California, USA

[8] M. Moszynski, M. Szawlowsky, M. Kapusta, M. Balcerzyk, *Large Area Avalanche Photodiodes in scintillation and X-ray detection,* Nucl. Instrum. Methods A 485, 504 (2002).

CHAPTER 7

Conclusions and Future Work

7.1. Conclusions

The absolute reduced electroluminescence yields, defined in terms of produced photons per primary electron per unit of path and per unit of pressure, were determined for xenon and argon and for uniform electric fields below and around the respective gas ionisation thresholds. While the excitation and ionisation thresholds for these gases and the approximately linear dependence of the reduced electroluminescence yield on the reduced electric field, E/p - the electric field divided by the gas pressure - were well established, their absolute values presented either many different values in the literature, as in the

case of xenon, or scarce contradictory values in the literature, as in the case of argon.

For xenon, the differences found for the scintillation amplification parameter, the number of photons produced per drifting electron and per volt, i.e. the slope of the referred to above linear dependence, were attributed mainly to differences in gas purity, which is known to be an important factor for the scintillation processes. This is the reason why only the most recent experimental measurements done at cryogenic temperatures, ~ -90ºC, present the highest values, in agreement with the values obtained by Boltzmann calculation and Monte Carlo simulation for room temperature.

For xenon, a scintillation amplification parameter of 140 photons kV^{-1} was obtained in the present studies, which is in agreement with these latter values. For the first time, it was possible to show that such high electroluminescence yield values can be achieved at room temperature.

For argon, the only experimental set of values for the electroluminescence yield, obtained by the WARP collaboration in a double-phase cryogenic detector, is a factor of ten lower than those obtained by the Monte Carlo simulation, for room temperature. In the present studies, a scintillation amplification parameter of 81 photons kV^{-1} was obtained, which is in good agreement with that predicted by Monte Carlo simulation.

These measurements have shown, for the first time that, even for room temperature, it is possible to achieve a scintillation amplification parameter in argon as high as that predicted by Monte Carlo simulation. The reason for the 10-fold lower scintillation yield presented by WARP may be due to incorrect calibration/normalization procedures, namely in the evaluation of the number of primary electrons that are extracted from liquid argon into the gas phase.

The additional amount of electroluminescence that is produced in the stronger electric fields around the wires of the anode mesh was calculated for the current experimental conditions. It has been demonstrated that this value is only few percent of the total electroluminescence produced in the scintillation gap for reduced electric fields close to the scintillation threshold, decreasing this ratio with increasing reduced electric field and reaching values around 1% for reduced electric fields around the argon ionisation threshold.

The electroluminescence yield, defined in terms of the number of photons produced in the electron avalanches per primary electron resulting from the radiation interaction in the gas, has been determined for GEM and THGEM electron multipliers. This pioneer work demonstrated that a large amount of electroluminescence is produced in the GEM and THGEM avalanches, resulting in overall detector gains that can be few orders of magnitude higher than the charge gain obtained in those avalanches, taking into account the additional gain of the photosensor used for the scintillation readout.

In addition, it was also demonstrated that the gain and the electroluminescence yield achieved in the electron avalanches may be few orders of magnitude higher than the yields attained in uniform electric field gaps. This finding is an asset if alternatives to PMTs, such as LAAPDs and/or G-APDs, are to be considered for the scintillation readout in electroluminescence based detectors. The only exceptions are for GEMs operating in argon and THGEMs operating in xenon at 2.5 bar, where the electroluminescence yield is similar to that produced in a uniform electric field gap.

Table II – Gain and maximum electroluminescence yields for GEMs, THGEMs and 5-mm thick uniform field gap* and for a photosensor gain of 130.

		Xenon		Argon	
		1 bar	2.5 bar	1 bar	2.5 bar
GEM	Gain	1.5×10^5	4×10^4	5×10^3	5×10^3
	Yield	6×10^3	1.5×10^3	3×10^2	3×10^2
THGEM	Gain	1.2×10^6	4×10^4	1.2×10^5	3×10^4
	Yield	7×10^4	2×10^3	1.5×10^4	4×10^3
5-mm uniform field gap *	Gain	7.5×10^3	1.9×10^4	1.9×10^3	4.7×10^3
	Yield	2.3×10^2	6×10^2	1.5×10^2	3.6×10^2

* xenon : E/p = 4.1 kV cm^{-1} bar^{-1}

* argon : E/p = 3.75 kV cm^{-1} bar^{-1}

Table II summarizes the maximum gains and maximum electroluminescence yields of GEMs, THGEMs and 5-mm thick uniform field gap with reduced electric fields of 4.1 and 3.75 kV $cm^{-1}bar^{-1}$ for xenon and argon, respectively. A photosensor gain of 130 was considered. For gas pressures of 1 bar, THGEMs deliver gains and yields that may reach more than one order of magnitude higher when compared to GEMs and two orders of magnitude when compared to the uniform field gap. However, the THGEM gain and yield present a faster decrease with pressure when comparing to GEMs - while for the uniform field gap there is a linear increase with pressure -, reaching only similar gains and yields to GEMs and uniform field gap, for xenon operation at 2.5 bar.

From the experimental setups described in chapters 3 and 4 it was possible to study the minimum number of photons, MDP, that can be detected with the LAAPD from Advanced Photonix Inc, and the associated statistical fluctuations for VUV detection. These LAAPD characteristics had not yet been studied in former works. Considering the setup conditions and the respective number of electroluminescence photons hitting the LAAPD, 2.4×10^4 photons of 172-nm and $1.4x10^4$ photons of 128-nm, the MDP was measured to be about 1300 and 600 for 128- and 172 nm, respectively. The MDP for 172-nm photons is about half of that for 128-nm photons, reflecting the ratio between the respective spectral sensitivities, 1.1 or 0.55 charge carrier pairs per 172-nm or 128-nm photon, respectively. The relative statistical fluctuations associated to the VUV detection of $1.4x10^4$ photons of

128-nm and of 2.4×10^4 photons of 172-nm VUV-light pulses is 3.9% and 2.2%, respectively.

Both parameters do not depend on photon wavelength, but rather on the number of charge carriers produced by the scintillation-pulse in the LAAPD. For the present charge carrier quantities produced in the LAAPD, gains as low as 30 to 60 are enough to obtain the best performances, concerning the above parameters.

7.2. Future Work

The present work triggered many new studies to be performed in our group. Some of these studies have already been done or are ongoing, under the work plan of other Master or PhD programs and/or under the activities of international collaborations in which our group participates, namely:

- Determination of the absolute reduced electroluminescence yield, defined in terms of the number of photons produced per primary electron per unit of path and per unit of pressure, in xenon for uniform electric fields below and around the xenon ionisation threshold and for xenon pressures in the 1 to 10 bar range. These studies have been already concluded, confirming that the xenon scintillation threshold does depend on the pressure and that the xenon scintillation amplification parameter has only a small

dependence on the pressure. These studies were done for the NEXT Collaboration.

- Determination of the quantum efficiency of the Hamamatsu UV-sensitive APD for xenon, krypton and argon electroluminescence. Since the total number of photons hitting the APD can be determined, the number of charge carriers produced in the APD by these photons can be obtained by comparison with direct X-ray absorption in the APD, determining this way the APD quantum efficiency. These studies have been concluded for xenon and a value similar to that presented by the manufacturer was measured. These studies were done for the NEXT Experiment, in collaboration with the group of Barcelona. The studies for argon and krypton are yet to be performed.
- Determination of the electroluminescence yield, defined in terms of the number of photons produced in the electron avalanches per primary electron resulting from the radiation interaction in the gas, in Micromegas electron multipliers operating in xenon. These studies are ongoing in a collaboration between our group and the group of Ioannis Giomataris (Saclay, Paris), the inventor of the Micromegas, under the NEXT Collaboration program.
- Simultaneous charge and scintillation readout produced in Micromegas avalanches for improving the pulse-height distributions obtained with the charge signals. These studies are to be carried out under a bilateral collaboration between our group and the group of Ioannis Giomataris.

- Study of the electroluminescence characteristics of krypton. Krypton was not much studied as a fill gas for radiation detectors. Its high natural radioactivity results in undesirable background, being a drawback in many applications. Nevertheless, its rather low cost, when compared to xenon, and the fact of being heavier than argon, makes it interesting for applications to X-ray spectrometry and medical-imaging instrumentation. Therefore, studies are planned for:

- The performance of a uniform field GPSC with krypton filling; determination of the detector energy resolution in the 1 to 60 keV X-ray energy range and determination of the krypton scintillation and ionisation thresholds.
- Determination of the absolute reduced electroluminescence yield, defined in terms of the number of produced photons per primary electron per unit of path lenght and per unit of pressure, in krypton, for uniform electric fields below and around the krypton ionisation threshold.
- Determination of the electroluminescence yield, defined in terms of the number of photons produced in the electron avalanches per primary electron resulting from the radiation interaction in the gas, produced in GEM, THGEM and Micromegas electron multipliers operating in krypton. The studies for the GEM have already been performed.